August, 1979

LIDS-TH-928

NASA-CR-162140
19790022022

Research Supported By:

NASA Ames Grant NGL-22-009-124
(76265)

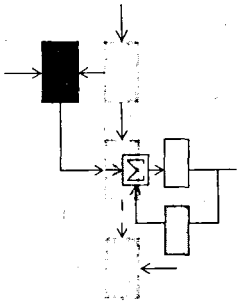

VTOL CONTROLS FOR SHIPBOARD LANDING

Christopher Graham McMuldroch

Laboratory for Information and Decision Systems
Formerly
Electronic Systems Laboratory
MASSACHUSETTS INSTITUTE OF TECHNOLOGY, CAMBRIDGE, MASSACHUSETTS 02139

August 1979 LIDS-TH-928

VTOL CONTROLS FOR SHIPBOARD LANDING

by

Christopher Graham McMuldroch

This research is based on the unaltered thesis of Christopher Graham McMuldroch, submitted in partial fulfillment of the requirements for the degree of Master of Science at the Massachusetts Institute of Technology in June, 1979. The research was conducted at the M.I.T. Laboratory for Information and Decision Systems with support extended by the United States National Aeronautics and Space Administration Ames Research Center under Grant NGL-22-009-124.

Laboratory for Information and Decision Systems
Massachusetts Institute of Technology
Cambridge, MA 02139

VTOL CONTROLS FOR SHIPBOARD LANDING

by

CHRISTOPHER GRAHAM McMULDROCH

B.Sc. (Physics), University of Victoria, Canada 1976

Submitted in partial fulfillment of the

requirements for the degree of

MASTER OF SCIENCE

at the

MASSACHUSETTS INSTITUTE OF TECHNOLOGY

June, 1979

Signature of Author Chris McMuldroch

Department of Aeronautics and Astronautics, May 11, 1979

Certified by Gunter Stein

Thesis Supervisor

Accepted by Harold Y. Wachman

Chairman, Departmental Graduate Committee, Department of Aeronautics and Astronautics

VTOL CONTROLS FOR SHIPBOARD LANDING

by

Christopher Graham McMuldroch

Submitted to the Department of Aeronautics and Astronautics on May 11, 1979, in partial fulfillment of the requirements for the degree of Master of Science.

ABSTRACT

The problem of landing a VTOL aircraft on a small ship in rough seas using an automatic controller is examined. The controller design uses the linear quadratic gaussian results of modern control theory. Performance bounds and control requirements are obtained for two control concepts.

Linear time invariant dynamic models are developed for the aircraft, ship and wave motions. The VTOL is modelled at stationary hover, supported by a lift fan in the nose and a pair of lift/cruise fans at the wing roots. Thrust control dynamics are modelled as first order, while aerodynamic effects are omitted. The ship is modelled at cruising speed in waves typical of sea state five conditions. The wave model, which drives ship motion, is shaped white noise with a theoretical Neumann Spectrum. All states are assumed measurable without reconstruction or noise.

The first control concept is a "hover controller", which commands the aircraft to track position and orientation of the ship deck. An important goal is to use only low levels of control power. Commands for this task are generated by the solution of the steady state linear quadratic gaussian regulator problem. Analytical performance and control requirement tradeoffs are obtained.

The second control concept is a "landing controller", which is designed to command the aircraft from stationary hover along a smooth, low control effort trajectory, to a touchdown on a predicted crest of ship motion. The design problem in this case is formulated and solved as an approximate finite-time linear quadratic stochastic regulator. Performance and control results are found by Monte Carlo simulations.

Thesis Supervisor: Gunter Stein, Ph.D.

Title: Adjunct Professor of Electrical Engineering

ACKNOWLEDGEMENTS

I sincerely thank Professor Gunter Stein for his direction of this thesis. His guidance in the learning of research and communication skills, as well as his patience and encouragement, are greatly appreciated.

I also thank Professor Michael Athans, Director of the MIT Laboratory for Information and Decision Systems (L.I.D.S., formerly ESL) for recommending a thesis topic, arranging financial support, and sponsoring opportunities to present the thesis results at MIT and at NASA/Ames Research Center.

Jim Carrig receives my thanks for the fine drafting he has done in the drawings of this report.

I am very grateful to Sherry Modestino - an excellent typist - for the professional work she has done here.

For their support, interest, encouragement, and friendship, I gratefully thank my parents and brother, my aunt, Mrs. Agnes Buel, and my friend, Dr. Dianne Ripley.

This work was carried out at the MIT Laboratory for Information and Decision Systems with support extended by the United States National Aeronautics and Space Administration Ames Research Center under Grant NGL-22-009-124, and by the Natural Sciences and Engineering Research Council of Canada through a Postgraduate Scholarship.

TABLE OF CONTENTS

PAGE

PAGE

LIST OF FIGURES

LIST OF TABLES

LIST OF ABBREVIATIONS

LP	Landing pad
MARE	Matrix algebraic Riccati equation
rms	Root mean square
SISO	Single input-single output
SLP	Shipboard landing pad
SSLQG	Steady state linear quadratic (regulator)
T/W	Thrust to weight ratio
VTOL	Vertical take-off and landing
V/STOL	Vertical and/or short take-off and landing

LIST OF SYMBOLS

a - scalar constant in ideal wave power spectrum or

- acceleration

A - overall model system matrix or

- system matrix or

- scalar constant

A_A - aircraft system matrix

A_{CL} - closed loop system matrix

A_N - nominal trajectory system matrix

AMPHVE - ship heave motion scale factor

AMPPCH - ship pitch motion scale factor

AMPRLL - ship roll motion scale factor

A_{OW} - ocean wave system matrix for both the pitch-heave and roll models

A_S - ship system matrix

A_{SWPH} - wave to ship coupling matrix for pitch-heave motions

A_{SWR} - wave to ship coupling matrix for roll motion

A_U - system matrix for control state dynamics

A_{WS} - wave-ship system matrix

b - scalar constant in ideal wave power spectrum or

- constant in relation between y_{PW} and y_{HW}

B - overall model control input matrix or

- input matrix

B_A - aircraft control input matrix

B_F - transformation from fan variables to individual fan force

components

B_N - overall model plant noise input matrix or

- nominal trajectory input matrix

B_{OW} - wave model input matrix

B_S - low order ship model plant

B_T - transformation between control states and individual fan variables

B_{WS} - wave-ship system input matrix

$\underline{c}$ - aircraft control dynamics state vector

C - overall model output matrix or

- output matrix or

- root locus gain in wave model transfer function

C_A - aircraft output matrix

C_{A-S} - output matrix for $\underline{y}_{A-S}$ from $[\underline{x}_A^T, \underline{x}_S^T]^T$

C_B^E - coordinate transformation from body coordinates to earth coordinates

C_E^B - coordinate transformation from earth coordinates to body coordinates

C_N - nominal trajectory output matrix

CONST - a scalar constant in $q_{NOM}(t)$

Cov(·) - covariance of (·)

C_{OW} - ocean wave output matrix for both the pitch-heave and roll models

C_{PH} - output matrix from pitch-heave wave models for the output driving ship pitch motion.

C_S - ship output matrix

C_{WS} - wave-ship output matrix

C_1 - output matrix

C_2 - output matrix for ship deck height

DIAG[·] - diagonal matrix with listed elements

exp{·} - exponential of {·}

E {·} - expectation of {·}

$\underline{f}_E$ - force on aircraft in the earth frame

$\underline{f}_{E_i}$ - force on mass i in the earth frame

$\underline{f}_F$ - total fan forces in body frame

$\underline{f}_{RB}$ - ram drag force acting on aircraft in body frame

$\underline{f}_{RBF}$ - ram drag force acting on air mass in body frame

$\underline{f}_{RBF_i}$ - ram drag force acting on air mass at fan or engine i in body frame

$\underline{f}_{REF_i}$ - ram drag force acting on air mass at fan or engine i in earth frame

$f(\omega_w)$ - wave frequency transformation from ω_w to ω_e

F_{GP} - constant in B_T for aircraft pitch control coordination

F_{GP3} - constant in B_T for aircraft pitch control coordination

F_{GNi} - nominal thrust from fan i

F_{GR} - constant in B_T for aircraft roll control coordination

F_{GV} - constant in B_T for aircraft vertical control coordination

F_{GV3} - constant in B_T for aircraft vertical control coordination

$\mathcal{F}\{\cdot\}(\omega)$ - Fourier transform of {·} as a function of (ω)

g - acceleration due to gravity

g_i - gain in low order ship model transfer function for mode i

G - feedback gain matrix

G_A - matrix by which the aircraft states are fedback to the aircraft controls

G_{OW} - ocean wave state vector feedforward matrix to the aircraft controls

G_S - ship state vector feedforward matrix to the aircraft controls

G_V - nominal thrust vector of aircraft in earth coordinates

G_{WS} - wave-ship system state vector feedforward to the aircraft controls

$G(t)$ - state feedback gain matrix

$h_{BS}(t)$ - heave coordinate of the ship in the ship frame; negative of $z_{BS}(t)$

$h_{ES}(t)$ - heave coordinate of the ship in the earth frame; negative of $z_{ES}(t)$

H - output matrix at time t_A

$\underline{H}_B$ - aircraft angular momentum in the body frame

$\underline{H}_E$ - aircraft angular momentum in the earth frame

$\underline{H}_I$ - momentum of the engine cores and fans in the body frame

$H_{1/3}$ - minimum height of the 1/3 largest waves

I_A - partial derivative of aircraft angular acceleration with respect to angular velocity

I_B - aircraft inertia tensor

I_M - partial derivative of aircraft angular acceleration with respect to applied moments

$\dot{I}_M$ - time derivative of inertia tensor for air mass in fans and engines

I_x - aircraft x-axis inertia

I_{xz} - aircraft xz-product of inertia

I_y - aircraft y-axis inertia

I_z - aircraft z-axis inertia

I_1 $= I_x I_z - I_{xz}^2$

$I_{\Omega x}$ - x-axis aircraft inertia due to fan and engine core rotation

$I_{\Omega z}$ - z-axis aircraft inertia due to fan and engine core rotation

J - cost functional

$K_{tp}(t)$ - feedback gain matrix as a function of time tp

$\lim_{T \to a}(\cdot)$ - limit of $(\cdot)$ as T approaches a

L_F - total roll moment due to fan forces

L_p - ram drag roll moment derivative with respect to p

L_r - ram drag roll moment derivative with respect to r

L_v - ram drag roll moment derivative with respect to v

m - aircraft mass

m_i - air mass in fan or engine i

$\dot{m}_i$ - air mass flow rate through fan or engine i

$\underline{m}_B$ - torque acting on the aircraft in the body frame

$\underline{m}_E$ - torque acting on the aircraft in the earth frame

$\underline{m}_{E_i}$ - moment acting on mass i in earth frame

$\underline{m}_F$ - total fan moment in body frame

$\underline{m}_{RBF}$ - ram drag momentum acting on air mass in body frame

M_F - total pitch moment due to fan forces

M_q - ram drag pitch moment derivative with respect to q

M_u - ram drag pitch moment derivative with respect to u

M_v - ram drag pitch moment derivative with respect to v

$\dot{M}_R$ - total air mass flow through aircraft fans and engines

N_F - total yaw moment due to fan forces

N_p - ram drag yaw moment derivative with respect to p

N_r - ram drag yaw moment derivative with respect to r

N_v - ram drag yaw moment derivative with respect to v

$p_v(V)$ - probability density function for velocity

P_F - quadratic cost associated with the end time response

$P(t)$ - solution of the Riccati equation or

- covariance propagation equation

$\underline{P}_{E_i}$ - linear momentum of mass i in earth frame

q - gain between y_{PW} and y_{HW} or

- quadratic weighting ratio

$q_{NOM}(t)$ - nominal trajectory quadratic cost weighting on position error

q_{z_A} - quadratic cost weighting on aircraft position

$q_{z_{A-S}}$ - per unit time quadratic weighting on z_{A-S}

q_{θ_A} - per unit time quadratic weighting on θ_A

$q_{\theta_{A-S}}$ - per unit time quadratic weighting on θ_{A-S}

Q - per unit time quadratic cost associated with response $\underline{y}(t)$

$\underline{r}_{B_i}$ - position of fan or engine inlet i in the body frame

r_{xi} - x-coordinate of fan or engine i inlet

r_{yi} - y-coordinate of fan or engine i inlet

r_{zi} - z-coordinate of fan or engine i inlet

$\underline{r}_E$ - aircraft position in the earth frame

$\underline{r}_{Ei}$ - position of fan or engine inlet i in the earth frame

$\underline{r}_i$ - position of fan or engine inlet i

$r_{\delta z_A}$ - per unit time quadratic weighting on δz_A

$r_{\delta\theta_A}$ - per unit time quadratic weighting on $\delta\theta_A$

R - per unit time quadratic cost weighting matrix for control

$\underline{R}_{\dot{cm}}$ - "Center of air mass flow" through aircraft fans and engines

s - Laplace domain variable

$S_e(\omega_e)$ - ocean wave power spectrum encountered by moving ship

S_{S1} - scaling matrix for ship outputs roll, pitch, and heave

S_{S2} - scaling matrix for ship outputs roll, pitch, and heave rates

S^*_{S1} - S_{S1} with last row set to zero

S^*_{S2} - S_{S2} with last row set to zero

$S\rho_{OW}(\omega)$ - power spectrum of $\rho_{OW}(t)$

$S(\omega)$ - power spectrum

$S(\omega_w)$ - ocean wave power spectrum measured by stationary observer

$S_{OW}(\omega)$ - ocean wave model power spectrum

t - time

t_A - actual touchdown time

t_F - final time

t_{TG} - time-to-go

t_I - initial time

t_M - a constant giving time of maximum $q_{NOM}(t)$

t_T - touchdown time

T - final time

T_{ESC} - transformation between ship center motion and landing pad motion

T_F^F - transformation between individual fan force components and overall x, y, z fan forces in the body frame

T_F^M - transformation from individual fan force components to the resulting moment applied to the aircraft

T_V^F - partial derivative of ram drag forces with respect to aircraft velocity in the body frame

T_V^m - partial deriviative of ram drag moment applied to the aircraft with respect to the aircraft linear velocity

T_W - average apparent wave period

T_θ^F - partial derivative of the force on the aircraft with respect to the out of trim Euler angles

T_ω^F - partial derivative of the ram drag forces with respect to aircraft angular velocity in the body frame

T_ω^m - partial derivative of the ram drag moment applied to the aircraft due to aircraft angular velocity

T_ω^θ - partial derivative of Euler angle rates with respect to the aircraft angular velocity in the body frame

$T(\theta,\omega_B)$ - transformation from aircraft Euler angles and angular velocity to Euler angle rates

$\underline{u}$ - aircraft input control vector

$\underline{u}(t)$ - control vector

$\underline{u}(\underline{x}(t))$ - control vector

$\underline{u}_N(t)$ - nominal trajectory input control vector

$\underline{u}_{NOM}(t)$ - nominal trajectory input control

v_p - gust process fixed field velocity

v_S - ship speed

$\underline{v}_{E_i}$ - velocity of mass i in earth frame

$\underline{v}_B$ - aircraft velocity in the body frame

$\underline{v}_E$ - aircraft velocity in the earth frame

V - noise intensity matrix or

- velocity in $p_v(V)$

$Var\{\cdot\}$ - variance of $\{\cdot\}$

$W(x,t)$ - spatially distributed gust process

$x_{BA}(t)$ - x-coordinate for the aircraft in the aircraft body frame

$x_{BS}(t)$ - x-coordinate for the ship in ship body axes

$x_{EA}(t)$ - x-coordinate of the aircraft in the earth frame

x_{ELP} - x-position of ship landing pad in earth coordinates

$x_{ES}(t)$ - x-coordinate of the ship in the earth frame

x_{Hi} - ith ship heave state

x_i - ocean wave model state i

x_{pi} - ith ship pitch state

x_{Ri} - ith ship roll state

x_{SLP} - x-coordinate of the ship landing pad in the ship frame

x_1 - nominal trajectory deviation from desired vertical end point position

x_2 - nominal trajectory vertical velocity

x_3 - nominal trajectory vertical acceleration

$\underline{x}$ - overall model state vector or

- state vector

$\underline{x}_A(t)$ - aircraft state vector

$\underline{x}_N(t)$ - nominal trajectory state vector

$\underline{x}_{NOM}(t)$ - nominal trajectory state vector

$\underline{x}_{OW}$ - wave state vector

$\underline{x}_{OWPH}$ - ocean wave pitch-heave model state vector

$\underline{x}_{OWR}$ - ocean wave roll model state vector

$\underline{x}_S$ - ship state vector

$\underline{x}_{SHIP}(t)$ - ship model state vector

$\underline{x}_{WS}$ - wave-ship system state vector

$\underline{x}_0$ - initial state vector

x_F - total x-direction fan force

x_q - x-direction ram drag force derivative with respect to q

x_{TL} - x-coordinate of nose lift fan thrust point

x_{TLC} - x-coordinate of lift/cruise fan thrust point

X_u - x-direction ram drag force derivative with respect to u

$y_{BA}(t)$ - y-coordinate of the aircraft in the aircraft body frame

$y_{BS}(t)$ - y-coordinate of the ship in ship body axes

$y_{EA}(t)$ - y-coordinate of the aircraft in the earth frame

y_{ELP} - y-position of the ship landing pad in earth coordinates

$y_{ES}(t)$ - y-coordinate of the ship in the earth frame

y_{HW} - pitch-heave wave model output driving ship heave dynamics

y_{OW} - wave model output

y_{PW} - pitch-heave wave model output driving ship pitch dynamics

y_{RW} - roll wave model output driving ship roll dynamics

y_{SLP} - y-coordinate of ship landing pad in the ship frame

$\underline{y}$ - overall model output vector or

- output vector or

- response

$\underline{y}_A$ - aircraft output vector

$\underline{y}_{A-S}$ - aircraft-ship relative vertical separation and pitch orientation output vector

$\underline{y}_N(t)$ - nominal trajectory output vector

$\underline{y}_{OWPH}$ - ocean wave pitch-heave model output vector

$\underline{y}_{OWR}$ - ocean wave roll model output vector

$\underline{y}_S$ - ship output vector

$\underline{y}_{WS}(t)$ - wave ship system output vector

$\underline{y}_{WSC}$ - pitch-heave and roll wave model output vector driving ship motion

Y_F - total y-direction fan force

Y_p - y-direction ram drag force derivative with respect to p

Y_r - y-direction ram drag force derivative with respect to r

Y_{TLC} - y-coordinate of the righthand side lift/cruise fan thrust point

Y_v - y-direction ram drag force derivative with respect to v

$z(t)$ - vertical position or

- stochastic component of vertical ship position

z_{A-S} - aircraft-ship vertical separation in the earth frame

z_{BA} - z-coordinate of the aircraft in the aircraft body frame

$z_{BS}(t)$ - z-coordinate of the ship in ship body axes

$z_{BA}(t)$ - z-coordinate of the aircraft in the earth frame

z_{ELP} - z-position of ship landing pad in earth coordinates

z_{ES} - z-coordinate of the ship in the earth frame

z_{SLP} - z-coordinate of the ship landing pad in the ship frame

$\underline{z}$ - output at time t_A

$\bar{z}(t)$ - deterministic component of vertical ship position

$\dot{z}(t)$ - stochastic component of vertical ship velocity

$\bar{\dot{z}}(t)$ - deterministic component of vertical ship velocity

Z_F - total z-direction fan force

Z_{TL} - z-coordinate of nose lift fan thrust point

Z_{TLC} - z-coordinate of lift/cruise fan thrust point

Z_w - z-direction ram drag derivative with respect to w

α - acceleration constant in the expression for $\bar{z}(t)$ (acceleration $= (1/2)\alpha$)

α_Y - constant in B_T for aircraft Y control coordination

α_ψ - constant in B_T for aircraft ψ control coordination

$\delta\underline{f}_B$ - deviation from nominal of the forces acting on the aircraft in the aircraft body frame

$\delta\underline{f}_F$ - deviation from nominal of the total x, y, z fan forces

$\delta\underline{f}_R$ - deviation from nominal of ram drag forces

$\delta\underline{m}_B$ - moment applied to the aircraft in the body frame

$\delta\underline{m}_F$ - total moment applied to the aircraft by fans

$\delta\underline{m}_R$ - moment applied to the aircraft in the body frame by the ram drag forces

$\delta\underline{r}_E$ - deviation from nominal of position in the earth frame

$\delta\underline{u}(t)$ - nominal trajectory tracking commands

$\delta\underline{v}_B$ - deviation of aircraft velocity from nominal in the aircraft frame

$\delta\underline{v}_E$ - deviation of aircraft velocity from nominal in the earth frame

δx - x-motion aircraft command input

$\delta\underline{x}(t)$ - aircraft deviation from the nominal trajectory

δx_C - δx command state

δy - y-motion aircraft command input

δy_C - δy command state

δz - z-motion aircraft command input

δz_C - δz command state

$\delta\theta$ - θ-motion aircraft command input

$\delta\underline{\theta}$ - out of trim aircraft Euler angles

$\delta\theta_C$ - $\delta\theta$ command state

$\delta\phi$ - ϕ-motion aircraft command input

$\delta\phi_C$ - $\delta\phi$ command state

$\delta\psi$ - ψ-motion aircraft command input

$\delta\psi_C$ - $\delta\psi$ command state

$\delta\underline{\omega}_B$ - deviation from nominal of aircraft angular velocity in body frame

$\underline{\Delta f}$ - control force components of fans

ΔF_{Gi} - fan i deviation from nominal thrust

ΔF_{xi} - x-control force component of fan i

ΔF_{yi} - y-control force component of fan i

ΔF_{zi} - z-control force component of fan i

ΔS - change in position

$\underline{\Delta u}$ - vector of fan variables

$\Delta z_{A-S}(t)$ - stochastic component of aircraft-ship vertical separation

$\Delta \dot{z}_{A-S}(t)$ - stochastic component of aircraft-ship relative vertical separation

$\Delta z_S(t)$ - stochastic component of vertical ship position

$\Delta \dot{z}_S(t)$ - stochastic component of vertical ship velocity

$\Delta\alpha_i$ - fan i lateral thrust deflection angle ($\Delta\alpha_i = 0$ when vertical)

$\Delta\theta_i$ - fan i longitudinal thrust deflection angle ($\Delta\theta_i = 0$ when vertical)

θ_A - aircraft pitch angle

$\theta_{A-S}(t)$ - aircraft-ship relative pitch orientation

θ_{AW} - heading angle of the wind over the ship deck

θ_S - ship pitch angle

θ_W - wave heading angle

θ_x - constant in B_T for aircraft x control coordination

$\underline{\theta}$ - vector of aircraft orientation : Euler angles θ, ψ, and ϕ

λ_x - frequency of aircraft first order x-command state

λ_y - frequency of aircraft first order y-command state

λ_z - frequency of aircraft first order z-command state

λ_θ - frequency of aircraft first order θ-command state

λ_ϕ - frequency of aircraft first order ϕ-command state

λ_ψ - frequency of aircraft first order ψ-command state

ξ - ocean wave model common damping ratio

ξ_i - damping ratio, low order ship model transfer function for mode i

ξ_H - ship heave damping ratio

ξ_P - ship pitch damping ratio

ξ_R - ship roll damping ratio

π - constant = 3.14159

$\prod_{i=1}^{3}(\cdot)$ - product of $(\cdot)$ for i = 1 to 3

ρ_i - low order ship model white noise input for mode i

ρ_H - low order ship model input for heave mode

ρ_{OW} - wave model input driving noise

ρ_{OWPH} - ocean wave pitch-heave model noise input

ρ_{OWR} - ocean wave roll model noise input

$\underline{\rho}_{OW}$ - ocean wave model driving noise vector

ρ_P - low order ship model input for pitch mode

ρ_R - low order ship model input for roll mode

$\underline{\rho}(t)$ - noise input vector

$\underline{\rho}_S$ - input noise vector for low order ship model

σ - standard deviation or

- width constant in $q_{NOM}(t)$

σ_v - standard deviation of v

$\sigma_{z_{A-S}}$ - rms value of z_{A-S}

$\sigma_{\dot{z}_{A-S}}$ - rms value of $\dot{z}_{A-S}$

$\sigma_{\Delta z_A(t)}$ - standard deviation of $\Delta z_S(t)$

$\sigma_{\Delta \dot{z}_S(t)}$ - standard deviation of $\Delta \dot{z}_S(t)$

$\sigma_{\theta_{A-S}}$ - rms value of θ_{A-S}

$\sigma_{\dot{\theta}_{A-S}}$ - rms value of $\dot{\theta}_{A-S}$

τ - time variable

ϕ_A - aircraft roll angle

ϕ_S - ship roll angle

ψ_A - aircraft yaw angle

ψ_S - ship yaw angle

ω - angular frequency

ω_e - frequency of encounter of ocean waves by moving ship

ω_i - ocean wave model ith natural frequency

ω_{nH} - natural heave frequency of ship

ω_{ni} - ith natural frequency in wave model or

- ith natural frequency in low order ship model transfer function for mode i

ω_{nP} - natural pitch frequency of ship

ω_{nR} - natural roll frequency of ship

ω_W - frequency of ocean waves seen by stationary observer

$\underline{\omega}_B$ - aircraft angular velocity in the aircraft body frame

$d(\cdot)/dt$ - derivative with respect to time of $(\cdot)$

$\partial(\cdot)/\partial[\cdot]$ partial derivative of $(\cdot)$ with respect to $[\cdot]$

$(\cdot)^T$ - transpose of $(\cdot)$

$\dot{(\cdot)}$ - time derivative of $(\cdot)$

$|(\cdot)|$ - absolute value of $(\cdot)$

% - percent

CHAPTER 1

INTRODUCTION

In recent years, interest in vertical take-off and landing (VTOL) aircraft has been demonstrated by a number of studies on potential uses, designs, and technologies required for such vehicles.

Among their many uses, one of the most interesting and significant is the operation of VTOL vehicles from ships at sea. These aircraft could be carried on smaller ships possessing far fewer resources than conventional aircraft carriers. By virtue of combining the hover capability of rotary wing aircraft and the cruise efficiency of fixed wing vehicles, VTOL aircraft would bring the benefits of long range air support to ships previously only capable of carrying helicopters.

Several VTOL aircraft design concepts have been proposed (1,2,3,4,5). One of these is a small lift/cruise fan vehicle supported in hover by three thrust fans: one in the aircraft nose, and the other two at the wing roots. These fans are driven by three gas turbine engines interconnected by shafts or gas ducts in a manner permitting power exchange among the fans without increasing engine power. This provides engine-out safety and rapid vehicle attitude control.

One of the critical problems of ship-borne VTOL operation is the control of landing under severe wave and wind conditions. The vehicles must be capable of achieving soft touchdowns with very limited control authority (thrust to weight capability) under motion conditions as severe as "sea state five" (12). Roughly speaking, this corresponds to wave heights of six feet or more and wind speeds as high as twenty

knots. This thesis investigates two concepts for automatic control of landings under these conditions.

1.1 Background References and Previous Work

A qualitative introduction to recent VTOL ideas is found in references (1, 2, 3, 4, 5). The first four of these describe various V/STOL vehicles and concepts. The last also describes V/STOL requirements including shipboard landings. More detailed papers on a wide range of V/STOL topics are located in reference (6).

The results of a landing controller design and evaluation, which include a manually piloted shipboard landing task, are reported in reference (7), "Design and Evaluation of an Integrated Flight Control System Concept for Manual IFR VTOL Operations", by Vernon K. Merrick and Ronald M. Gerdes. The basic shipboard landing problem in this reference is similar to the one investigated here. In both cases, the goal is to land VTOL aircraft accurately and gently aboard a ship at sea. However, there are some notable differences. First, the reference addresses a manually piloted landing problem, rather than an automatic one as done here. Secondly, the aircraft modelled was a transport aircraft with six thrust fans, not a small vehicle with only three fans as is used in this report. Next, the ship motions modelled in the reference are generated by a combination of sinusoidal components; whereas the ones modelled here are stochastic. Finally, the control design techniques in the reference were classical in contrast to the modern approach followed in this work.

1.2 Objective, Approach and Contributions

The objective of this work is to design a landing controller to guide a VTOL aircraft from stationary hover along a smooth trajectory to a gentle landing on the ship deck. At the same time, the control authority used to follow the trajectory is to be kept small. The intent is to achieve these objectives with design techniques based on modern linear quadratic control. Besides outlining design techniques, the results are also intended to provide design guidelines and performance bounds for eventual practical landing control implementations. It is not a goal of this research to form a detailed engineering design.

Three steps were used to reach these objectives. The first step was to construct mathematical models for each of the system's components, including VTOL aircraft, ship, and ocean waves. The second step was the design of a ship deck chasing "hover controller". The performance of this design motivated the third step, which was the design of a "landing controller". This second controller guides the aircraft to a predicted peak of ship deck motion.

The aircraft modelled is a small VTOL with three lift fans whose thrust magnitude and direction can be varied to control translational and rotational motion. Ship motion is represented by three parallel second order systems for pitch, heave and roll, respectively. These three systems are driven by a pair of sixth order wave models, which in turn are driven by independent white noises. The wave models approximate the theoretical Newmann wave spectrum. Ship model parameters are

chosen to represent a small ship of about 400 foot length in sea state five conditions. To date, pitch-heave dynamics only have been used in the control design studies.

The hover control goal is to make the aircraft track the ship landing deck motion at constant vertical separation. Implemented for automatic landings, the vertical separation command would be replaced by a smoothly decreasing function. The controller design is a steady state linear quadratic regulator chosen to minimize weighted separation error and vertical thrust control effort. Curves of separation error versus vertical thrust control are generated. In addition, a curve for the required vertical sensor and control bandwidths versus control effort is determined.

The thrust to weight requirements of the above controller indicate that an alternative approach is desirable for low control power landings. The approach taken is to predict ship deck motion forward to a peak. Then a smooth nominal trajectory is computed and followed to the predicted peak point and time. The nominal trajectories are generated by a finite end-time linear quadratic regulator using a low order aircraft model. Monte Carlo simulations of this nonlinear landing algorithm show that the required control authority is reduced by a factor of almost two over that required by the hover controller. This demonstrates the potential utility of ship motion prediction.

This study demonstrates how modern control theory can be applied to the VTOL shipboard landing problem. "First iteration" control designs have been generated which provide basic performance trade-off information for shipboard VTOL operation. Low touchdown velocities can be achieved

provided that the control bandwidth exceeds the ship motion spectrum peak at approximately one radian/second. Moreover, ship motion prediction appears to offer a promising way to reduce the control requirements. These findings are tentative, of course, because idealistic modelling and sensing assumptions were made in the design. However, the work has been structured so that more detailed investigations can be made of performance variations with aerodynamic effects, ground effects, sea state conditions, sensor constraints, human piloting considerations, and inclusion of full longitudinal and lateral dynamics.

1.3 Overview of the Chapters

The material in Chapters Two through Five corresponds directly with the synopsis presented above. Chapter Two presents the model. Linear, time-invariant aircraft, wave, and ship models are developed from the nonlinear equations and frequency domain information available in the literature. Chapter Three presents the hover controller design and evaluation. This controller is studied with the initial intention of generalizing it for landing control. The high control authority required there leads to the landing controller in Chapter Four. This more promising controller is developed and then evaluated by Monte Carlo simulations. Chapter Five presents general conclusions, and suggests avenues for further investigation.

CHAPTER 2
MODELLING

2.1 Introduction

The physical system to be modelled has three subsystems: aircraft, ship, and waves. For each of these, a linearized model is derived based on a nominal condition and simplifying assumptions. This chapter discusses the coordinate systems employed and the nominal configuration of aircraft, ship, and waves. Next, the representation of the overall model as the augmentation of its subsystems is presented. Following this general discussion, the model of each subsystem is derived. In Chapter 3, a low order ship motion model is used for comparison of results with the normal wave-ship model. This low order model is also derived in this chapter.

2.2 Coordinate Systems

Figures (2.2.1, 2, and 3) illustrate the coordinate systems used. The aircraft and ship each have two associated coordinate systems. Each of these are standard, orthogonal, right-handed reference frames. They are referred to as "body frames" fixed to the vehicle axes of symmetry and "earth frames" fixed to the earth vertical and horizontal directions. The x-axes all point nominally forward, the z-axes point nominally downward, and the y-axes are oriented to the right completing the right-handed frames. Note the effect of the z-axes definition. Heights above the center of rotation have positive altitude and heave, but negative z-coordinate. For the aircraft, the body fixed coordinate system is centered at the center of mass. For the ship, the corresponding frame

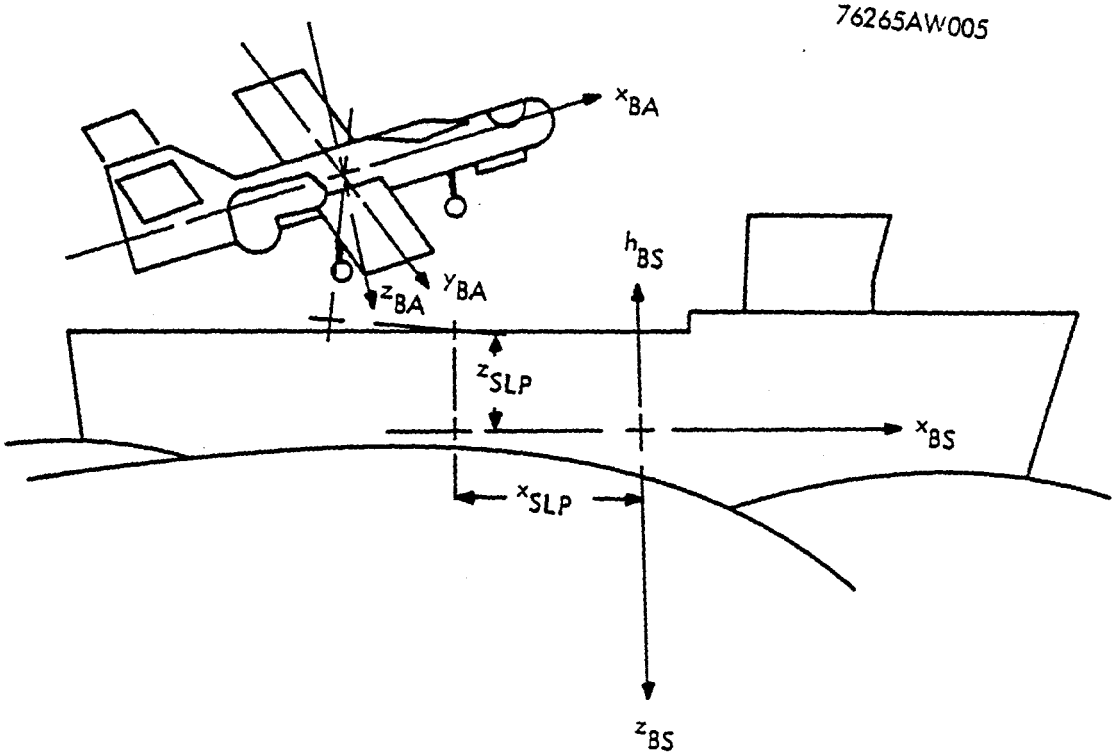

Side View of Aircraft-Ship Configuration

Figure 2.2.1

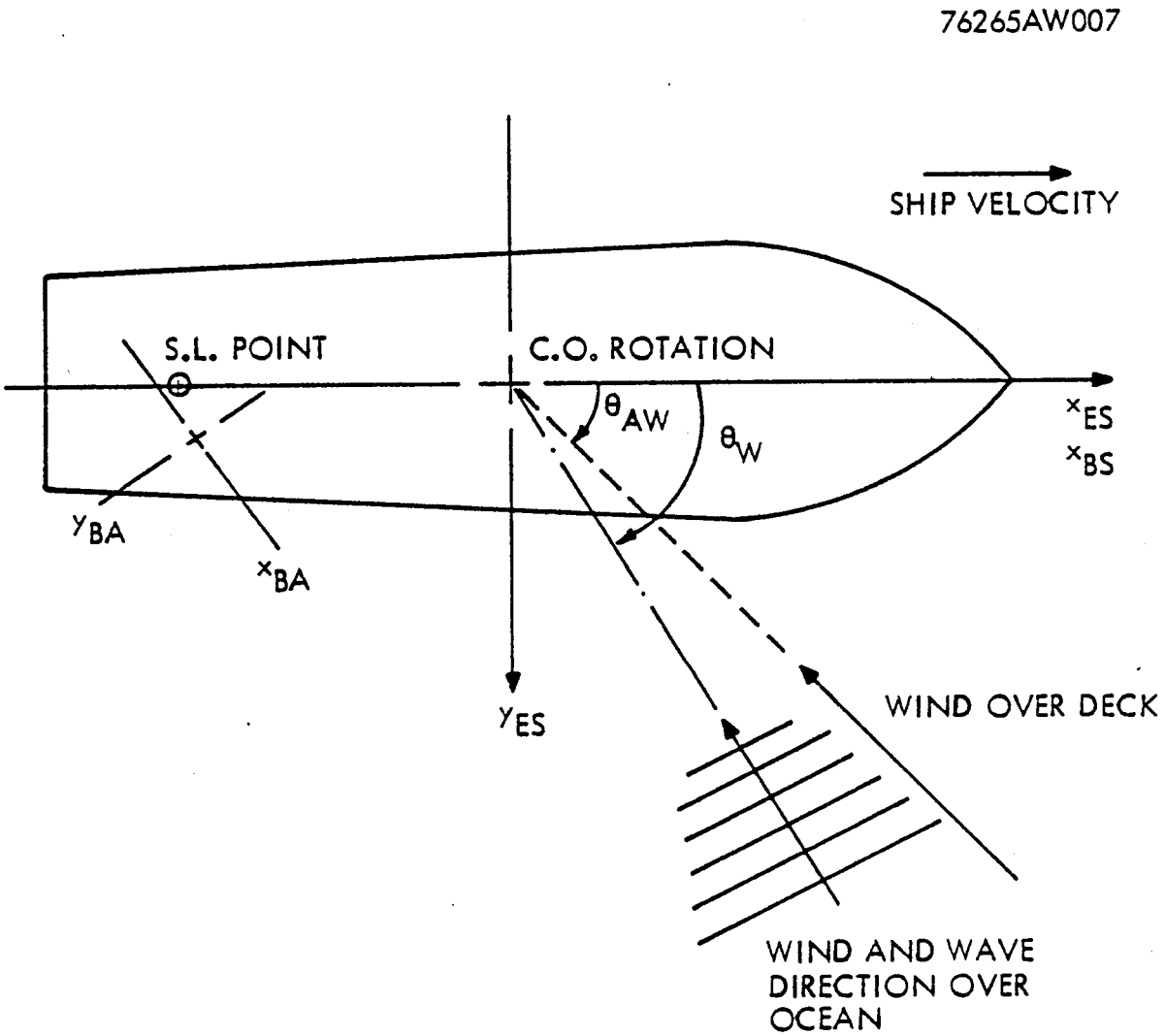

Plan View of Aircraft-Ship Configuration

Figure 2.2.2

76265AW006

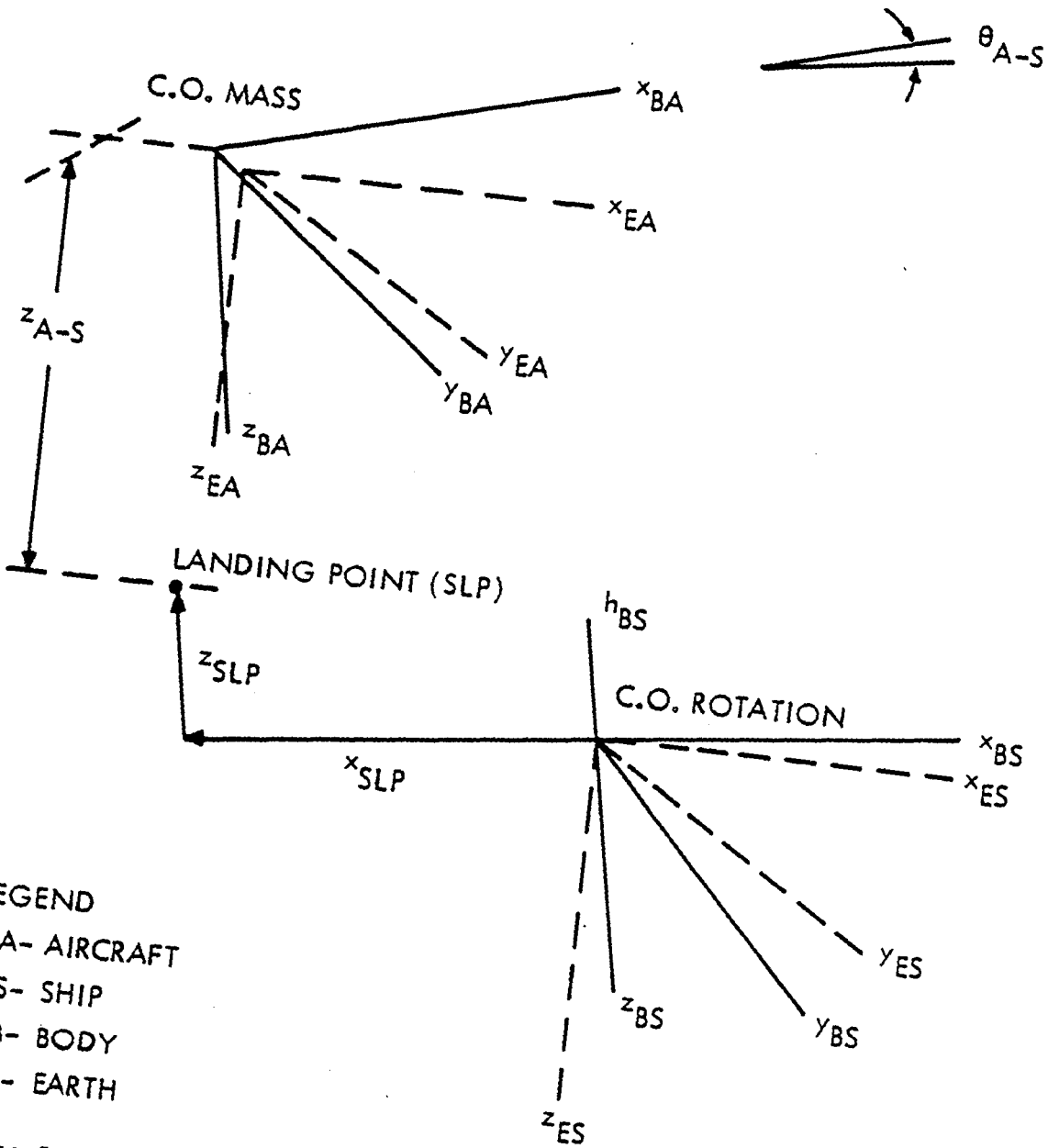

Coordinate Systems

Figure 2.2.3

frame is located at a point approximating the center of rotation. The earth reference frame for the ship moves with the ship center of rotation, but maintains a constant height and a steady orientation with the x_{ES} and y_{ES}-axes locally horizontal, z-axis vertical, and x-axis parallel to the ship velocity vector. The aircraft earth frame is fixed with respect to the ship-earth frame. It is centered at some constant desired height above the nominal position of the ship landing deck.

The following is a summary of the axes labels and other geometry:

Ship body axes x_{BS}, y_{BS}, z_{BS};

Ship earth axes x_{ES}, y_{ES}, z_{ES};

Ship body heave axis h_{BS};

Ship earth heave axis h_{ES};

Ship landing point (SLP) is at ship coordinates $(x_{SLP}, y_{SLP}, z_{SLP})$ where $y_{SLP} = 0$;

Ship pitch angle θ_S;

Ship roll angle ϕ_S;

Ship yaw angle ψ_S, $(\psi_S = 0)$;

Aircraft body axes x_{BA}, y_{BA}, z_{BA};

Aircraft earth axes x_{EA}, y_{EA}, z_{EA};

Aircraft pitch angle θ_A;

Aircraft roll angle ϕ_A;

Aircraft yaw angle ψ_A;

Aircraft position relative to the ship deck in earth coordinates z_{A-S};

Aircraft pitch orientation relative to the ship θ_{A-S};

Heading angle of the wind over the ship deck θ_{AW};

Heading angle of wind and waves over ocean θ_W.

The three drawings above and the notation just introduced are useful in describing the relative position of the vehicles. The ship is steaming into the wind and waves at an angle θ_W, so that the wind over the deck crosses at an angle θ_{AW} ($\theta_{AW} = 0$ in the design work to date). This is the heading angle maintained by the hovering aircraft in order to avoid excessive sideforces. The aircraft position, z_{A-S}, and orientation, θ_{A-S}, relative to the ship landing point (or pad) are quantities to be controlled.

2.3 Overall Model

2.3.1 Augmented Model Dynamical Equation

The overall linearized model of the aircraft, ship and waves is written as an augmented matrix differential equation. This equation is given in Table (2.3.1.1) to indicate the augmented nature of the model. The notation used for this equation is explained below:

$\underline{x}$, $\dot{\underline{x}}$ are the overall model state vector and its derivative;

$\underline{u}$ is the vector of aircraft controls;

$\underline{\rho}_{OW}$ is the vector of noises driving the wave model;

A is the linearized, open loop, augmented or overall system matrix;

B is the overall system control input matrix;

B_N is the overall system plant noise input matrix;

$\underline{x}_A$, $\underline{x}_S$, $\underline{x}_{OWPH}$, $\underline{x}_{OWR}$ are the subsystem state vectors for the aircraft, ship, ocean wave pitch-heave model, and ocean wave roll

THE OVERALL LINEARIZED OPEN LOOP AUGMENTED MODEL EQUATION

$$\dot{\underline{x}} = A\underline{x} + B\underline{u} + B_N\underline{\rho}_{OW}$$

$$A = \left|\begin{array}{c|c|c|c} A_A & 0 & 0 & 0 \\ \hline 0 & A_S & A_{SWPH} & A_{SWR} \\ \hline 0 & 0 & A_{OW} & 0 \\ \hline 0 & 0 & 0 & A_{OW} \end{array}\right|$$

$$B = \left|\begin{array}{c} B_A \\ \hline 0 \\ \hline 0 \\ \hline 0 \end{array}\right| \qquad B_N = \left|\begin{array}{c|c} 0 & 0 \\ \hline 0 & 0 \\ \hline B_{OW} & 0 \\ \hline 0 & B_{OW} \end{array}\right|$$

$$x = \left|\begin{array}{c} \underline{x}_A \\ \hline \underline{x}_S \\ \hline \underline{x}_{OWPH} \\ \hline \underline{x}_{OWR} \end{array}\right| \qquad \underline{\rho}_{OW} = \left|\begin{array}{c} \rho_{OWPH} \\ \hline \rho_{OWR} \end{array}\right|$$

TABLE 2.3.1.1

model, respectively;

ρ_{OWPH}, ρ_{OWR} are the pitch-heave and roll ocean wave model noise inputs;

A_A, A_S, A_{OW} are the aircraft, ship and the ocean wave model system matrices: note pitch-heave and roll waves have the same system matrix;

B_A, B_{OW} are the aircraft and ocean wave model input matrices. Again B_{OW} is shared by the two models;

A_{SWPH}, A_{SWR} are the coupling matrices driving ship motion from the pitch-heave and roll wave models respectively.

The elements of the subsystem matrices are determined in the sections that follow. In the standard model with the standard wave-ship models, there are a total of 36 states. The equation for the overall model using the low order ship model is shown in Table (2.3.1.2). This model is driven by $\underline{\rho}_S$, which acts directly on the ship model. The low order model has 24 states.

THE OVERALL LINEARIZED OPEN LOOP MODEL USING THE LOW ORDER SHIP MODEL

$$\dot{\underline{x}} + A\underline{x} + Bu + B_N\underline{\rho}_S$$

$$A = \left|\begin{array}{c|c} A_A & 0 \\ \hline 0 & A_S \end{array}\right|$$

$$B = \left|\begin{array}{c} B_A \\ \hline 0 \end{array}\right|$$

$$B_N = \left|\begin{array}{c} 0 \\ \hline B_S \end{array}\right|$$

$$\underline{x} = \left|\begin{array}{c} \underline{x}_A \\ \hline \underline{x}_S \end{array}\right|$$

TABLE 2.3.1.2

2.3.2 Overall Model Output Equation

The overall model output is basically the augmentation of all the individual model outputs; however, in addition, other outputs are included. From the aircraft and ship outputs of position and orientation are formed the additional outputs of relative aircraft-ship vertical separation and pitch orientation, as well as their relative rates. This is done by differencing the appropriate outputs of the aircraft and ship. In Table (2.3.2.1), these additional outputs are denoted $\underline{y}_{A-S}$ and are obtained by:

$$\underline{y}_{A-S} = C_{A-S} \left| \begin{matrix} \underline{x}_A \\ \hline \underline{x}_S \end{matrix} \right| \qquad (2.3.2.1)$$

In the table, the following notation is used in addition to that of the previous section:

$\underline{y}$ is the overall model output vector;

C is the output matrix;

$\underline{y}_A$, $\underline{y}_S$, $\underline{y}_{OWPH}$, $\underline{y}_{OWR}$ are the output vectors for the aircraft, ship, pitch-heave, and roll ocean wave models, respectively.

C_A, C_S, C_{OW} are the output matrices of the aircraft, ship, and two identical ocean wave models.

This completes the discussion of the overall system model.

OVERALL MODEL OUTPUTS

OVERALL EQUATION

$$\underline{Y} = C\underline{x}$$

STANDARD MODEL OUTPUT EQUATION

$$\begin{vmatrix} \underline{Y}_A \\ \hline \underline{Y}_S \\ \hline \underline{Y}_{OWPH} \\ \hline \underline{Y}_{OWR} \\ \hline \underline{Y}_{A-S} \end{vmatrix} = \left|\begin{array}{c|c|c|c} C_A & 0 & 0 & 0 \\ \hline 0 & C_S & 0 & 0 \\ \hline 0 & 0 & C_{OW} & 0 \\ \hline 0 & 0 & 0 & C_{OW} \\ \hline C_{A-S} & & 0 & \end{array}\right| \begin{vmatrix} \underline{x}_A \\ \hline \underline{x}_S \\ \hline \underline{x}_{OWPH} \\ \hline \underline{x}_{OWR} \end{vmatrix}$$

LOW ORDER SHIP MODEL OUTPUT EQUATION

$$\begin{vmatrix} \underline{Y}_A \\ \hline \underline{Y}_S \\ \hline \underline{Y}_{A-S} \end{vmatrix} = \left|\begin{array}{c|c} C_A & 0 \\ \hline 0 & C_S \\ \hline C_{A-S} & \end{array}\right| \begin{vmatrix} \underline{x}_A \\ \hline \underline{x}_S \end{vmatrix}$$

TABLE 2.3.2.1

2.4 Aircraft Model

2.4.1 Introduction

The aircraft chosen for this study is a representative small VTOL vehicle with both conventional flight and vertical takeoff and landing capabilities. The model is based on reference (8). Figure 2.4.1.1 illustrates this vehicle type. A lift fan is set in the nose with fore and aft, as well as lateral, thrust deflection louvers. This fan is shut down and doors are closed over it during conventional flight. Two more fans are located at the wing roots, one on each side of the fuselage. Each of these has a nozzle at the outlet for fore and aft thrust deflection and louvers for lateral deflection. In conventional flight, the nozzles are rotated up to produce horizontal forward aircraft motion. The three fans are driven by three turbine engines through shaft interconnections permitting interchange of power among the fans. During hover (the only flight regime discussed here), all the fans are set to generate direct lift forces. The other forces and moments acting on the aircraft are due to aerodynamic and ram drag effects. Each of these effects can be described by nonlinear equations, and linearized for control design and analysis purposes. These nonlinear equations and their linearized counterparts are presented in the next section. Following that, the linearization procedure is outlined.

2.4.2 Model Equations

This section summarizes the original fundamental dynamic and kinematic relationships, the general linearized form, and then the complete

76265AW008

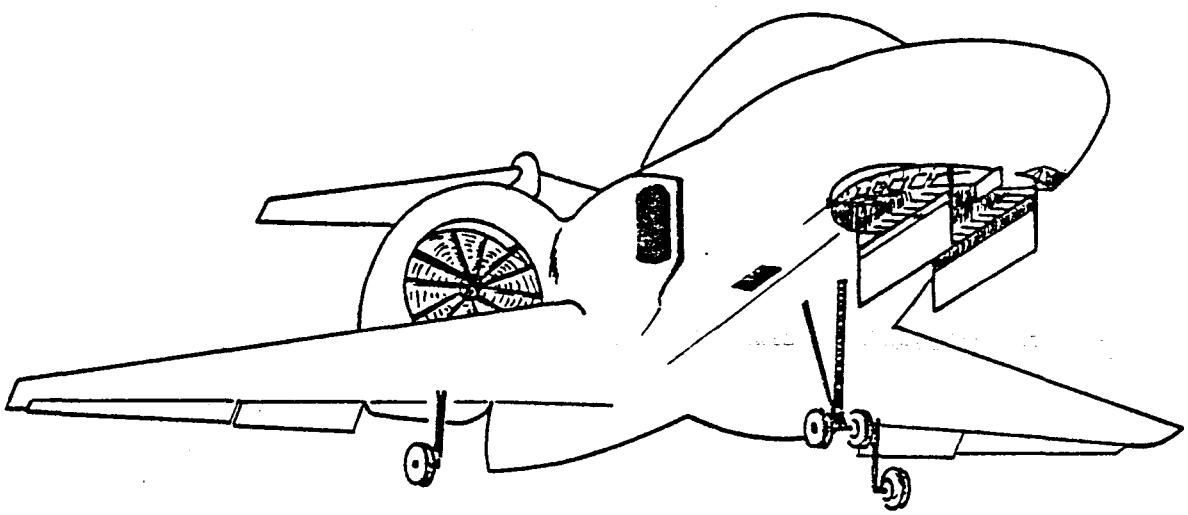

VTOL Vehicle Type: Fan and Louver Locations

Figure 2.4.1.1

linearized aircraft state space model. Section (2.4.3) describes the details of the linearization.

The fundamental dynamic and kinematic relationships are stated in four equations:

Newton's Law:	$m\dot{\underline{v}}_E$	=	$\underline{f}_E$	(2.4.2.1)
Translational kinematics:	$\dot{\underline{r}}_E$	=	$\underline{v}_E$	(2.4.2.2)
Angular momentum:	$\dot{\underline{H}}_E$	=	$\underline{m}_E$	(2.4.2.3)
Rotational kinematics:	$\dot{\underline{\theta}}$	=	$T(\underline{\theta}, \underline{\omega}_B)$	(2.4.2.4)

The force and moment on the aircraft, $\underline{f}_E$ and $\underline{m}_E$, are composed of aerodynamic, ram drag, gravitational, and fan forces and moments. The fan forces are commanded by the aircraft landing controller. They are assumed to be generated in a linear manner about their nominal values from the controller commands.

The fundamental equations are linearized in Section (2.4.3). The results are stated below. Note that the linearization is about stationary hover: $\underline{v}_E = \underline{0}$, $\underline{r}_E = \underline{0}$, $\underline{\omega}_B = \underline{0}$, $\underline{\theta} = \underline{0}$, $\underline{c} = 0$, and $\underline{u} = \underline{0}$. Also note that because aerodynamic forces are proportional to the square of airspeed, they are not small during hover over the ship deck, but they have been neglected to date.

The linearized translational motion equations are stated:

Newton's Law:

$$\delta\underline{v}_E = \frac{1}{m} \left[C_B^E \, \delta\underline{f}_B + T_\theta^F \delta\underline{\theta} \right] \qquad (2.4.2.5)$$

Force summation:

$$\delta\underline{f}_B = \delta\underline{f}_F + \delta\underline{f}_R \qquad (2.4.2.6)$$

Ram drag forces:

$$\delta \underline{f}_R = T_\omega^F \, \delta \underline{\omega}_B + T_V^F \, \delta \underline{v}_B \qquad (2.4.2.7)$$

Fan control forces:

$$\delta \underline{f}_F = T_F^F \, \underline{\Delta f} \qquad (2.4.2.8)$$

Translational kinematics:

$$\delta \dot{\underline{r}}_E = \delta \underline{v}_E \qquad (2.4.2.9)$$

Coordinate transformation:

$$\delta \underline{v}_B = C_E^B \delta \dot{\underline{r}}_E \qquad (2.4.2.10)$$

The rotational motion equations follow:

Angular momentum:

$$\delta \dot{\underline{\omega}}_B = I_M \, \delta \underline{m}_B + I_A \, \delta \underline{\omega}_B \qquad (2.4.2.11)$$

Torque summation:

$$\delta \underline{m}_B = \delta \underline{m}_F + \delta \underline{m}_R \qquad (2.4.2.12)$$

Ram drag torque:

$$\delta \underline{m}_R = T_\omega^M \, \delta \underline{\omega}_B + T_V^M \, \delta \underline{v}_B \qquad (2.4.2.13)$$

Fan control torque:

$$\delta \underline{m}_F = T_F^M \, \underline{\Delta f} \qquad (2.4.2.14)$$

Rotational kinematics:

$$\delta \dot{\underline{\theta}} = T_\omega^\theta \, \delta \underline{\omega}_B \qquad (2.4.2.15)$$

The fan control force components given by $\underline{\Delta f}$ are assumed to be generated as follows from the command $\underline{u}$:

Force components:

$$\underline{\Delta f} = B_F \underline{\Delta u} = B_F B_T \underline{c} \qquad (2.4.2.16)$$

Control state dynamics:

$$\dot{\underline{c}} = A_u \underline{c} + \underline{u} \qquad (2.4.2.17)$$

The complete linearized open loop matrix differential state equation for the hovering aircraft can be written using the above equations. Table (2.4.2.1) presents this equation, which is of the form:

$$\dot{\underline{x}}_A = A_A \underline{x}_A + B_A \underline{u} \qquad (2.4.2.18)$$

The numerical values of A_A and B_A are given in Table (2.4.2.2). A mathematical block diagram of the linearized VTOL aircraft model is shown in Figure (2.4.2.1). This figure presents the model structure graphically.

2.4.3 Linearization of the Equations of Motion

The aircraft equations of motion can be divided into two parts: translational motions and rotational motions. In this section, these motions are derived as functions of fan and ram drag forces and moments. To date, aerodynamic effects are neglected. Next, these forces and moments are derived in terms of fan forces, aircraft velocity, and aircraft angular velocity. Finally, the generation of fan forces from the controls is described.

$$
\begin{bmatrix} \dot{u}_E \\ \dot{v}_E \\ \dot{w}_E \\ \hline \dot{x}_E \\ \dot{y}_E \\ \dot{z}_E \\ \hline \dot{p} \\ \dot{q} \\ \dot{r} \\ \hline \dot{\psi} \\ \dot{\theta} \\ \dot{\phi} \\ \hline \dot{\delta}_{x_c} \\ \dot{\delta}_{y_c} \\ \dot{\delta}_{z_c} \\ \dot{\delta}_{\psi_c} \\ \dot{\delta}_{\theta_c} \\ \dot{\delta}_{\psi_c} \end{bmatrix} =
\left[\begin{array}{c|c|c|c|c}
\frac{1}{m} C_B^E T_V^F C_E^B & 0 & \frac{1}{m} C_B^E T_\omega^F & T_\theta^F & \frac{1}{m} C_B^E T_F^F B_F^B T_T \\
\text{Ram Drag Forces} & & \text{Ram Drag Forces} & & \text{Fan Forces} \\
\hline
I & 0 & 0 & 0 & 0 \\
\hline
I_M T_V^M C_E^B & 0 & I_A + I_M T_\omega^M & 0 & I_M T_F^M B_F^B T_T \\
\text{Ram Drag Moments} & & \text{Internal Momentum + Ram Drag Moments} & & \text{Fan Moments} \\
\hline
0 & 0 & T_\omega^\theta \quad \text{Euler Angles from Body Rates} & 0 & 0 \\
\hline
0 & 0 & 0 & 0 & A_U \quad \text{Control Dynamics}
\end{array}\right]
\begin{bmatrix} u_E \\ v_E \\ w_E \\ \hline x_E \\ y_E \\ z_E \\ \hline p \\ q \\ r \\ \hline \psi \\ \theta \\ \phi \\ \hline \delta_{x_c} \\ \delta_{y_c} \\ \delta_{z_c} \\ \delta_{\psi_c} \\ \delta_{\theta_c} \\ \delta_{\psi_c} \end{bmatrix} +
\left[\begin{array}{c} 0 \\ \hline 0 \\ \hline 0 \\ \hline 0 \\ \hline I \end{array}\right]
\begin{bmatrix} \delta_{x_c} \\ \delta_{y_c} \\ \delta_{z_c} \\ \delta_{\phi_c} \\ \delta_{\theta_c} \\ \delta_{\psi_c} \end{bmatrix}
$$

Table 2.4.2.1

AIRCRAFT LINEARIZED OPEN LOOP MATRIX DIFFERENTIAL STATE EQUATION

LINEAR AIRCRAFT MODEL A MATRIX

$A_A =$

-0.0659	0	0	0	0	0	0	0.05202	0	0	-32.2	0	32.2	0	0	0	0	0
0	-0.0659	0	0	0	0	-0.0520	0	-0.3917	0	0	32.2	0	32.2	0	0	0	0
0	0	-0.0659	0	0	0	0	0.3917	0	0	0	0	0	0	32.2	0	0	0
1	0	0	0	0	0	0	0	0	0	0	0	0	0	0	0	0	0
0	1	0	0	0	0	0	0	0	0	0	0	0	0	0	0	0	0
0	0	1	0	0	0	0	0	0	0	0	0	0	0	0	0	0	0
0	-0.0027	0	0	0	0	-0.1025	-0.1255	-0.0421	0	0	0	0	-4.241	0	4.595	0	0.5346
0.0008	0	0.0062	0	0	0	0.0943	-0.1427	1.0416	0	0	0	1.7037	0	0	0	10.04	0
0	-0.0051	0	0	0	0	-0.0117	0.8273	-0.1471	0	0	0	0	-0.1790	0	0.1939	0	8.046
0	0	0	0	0	0	0	0	1	0	0	0	0	0	0	0	0	0
0	0	0	0	0	0	0	1	0	0	0	0	0	0	0	0	0	0
0	0	0	0	0	0	1	0	0	0	0	0	0	0	0	0	0	0
0	0	0	0	0	0	0	0	0	0	0	0	0	0	0	0	0	0
0	0	0	0	0	0	0	0	0	0	0	0	0	0	0	0	0	0
0	0	0	0	0	0	0	0	0	0	0	0	0	0	0	0	0	0
0	0	0	0	0	0	0	0	0	0	0	0	0	0	0	0	0	0
0	0	0	0	0	0	0	0	0	0	0	0	0	0	0	0	0	0
0	0	0	0	0	0	0	0	0	0	0	0	0	0	0	0	0	0

TABLE (2.4.2.2)

Continued on next page

LINEAR AIRCRAFT MODEL B MATRIX

$$B_A = \begin{vmatrix} 0 & 0 & 0 & 0 & 0 & 0 \\ 0 & 0 & 0 & 0 & 0 & 0 \\ 0 & 0 & 0 & 0 & 0 & 0 \\ 0 & 0 & 0 & 0 & 0 & 0 \\ 0 & 0 & 0 & 0 & 0 & 0 \\ 0 & 0 & 0 & 0 & 0 & 0 \\ 0 & 0 & 0 & 0 & 0 & 0 \\ 0 & 0 & 0 & 0 & 0 & 0 \\ 0 & 0 & 0 & 0 & 0 & 0 \\ 0 & 0 & 0 & 0 & 0 & 0 \\ 0 & 0 & 0 & 0 & 0 & 0 \\ 0 & 0 & 0 & 0 & 0 & 0 \\ 1 & 0 & 0 & 0 & 0 & 0 \\ 0 & 1 & 0 & 0 & 0 & 0 \\ 0 & 0 & 1 & 0 & 0 & 0 \\ 0 & 0 & 0 & 1 & 0 & 0 \\ 0 & 0 & 0 & 0 & 1 & 0 \\ 0 & 0 & 0 & 0 & 0 & 1 \end{vmatrix}$$

TABLE (2.4.2.2) (Continued)

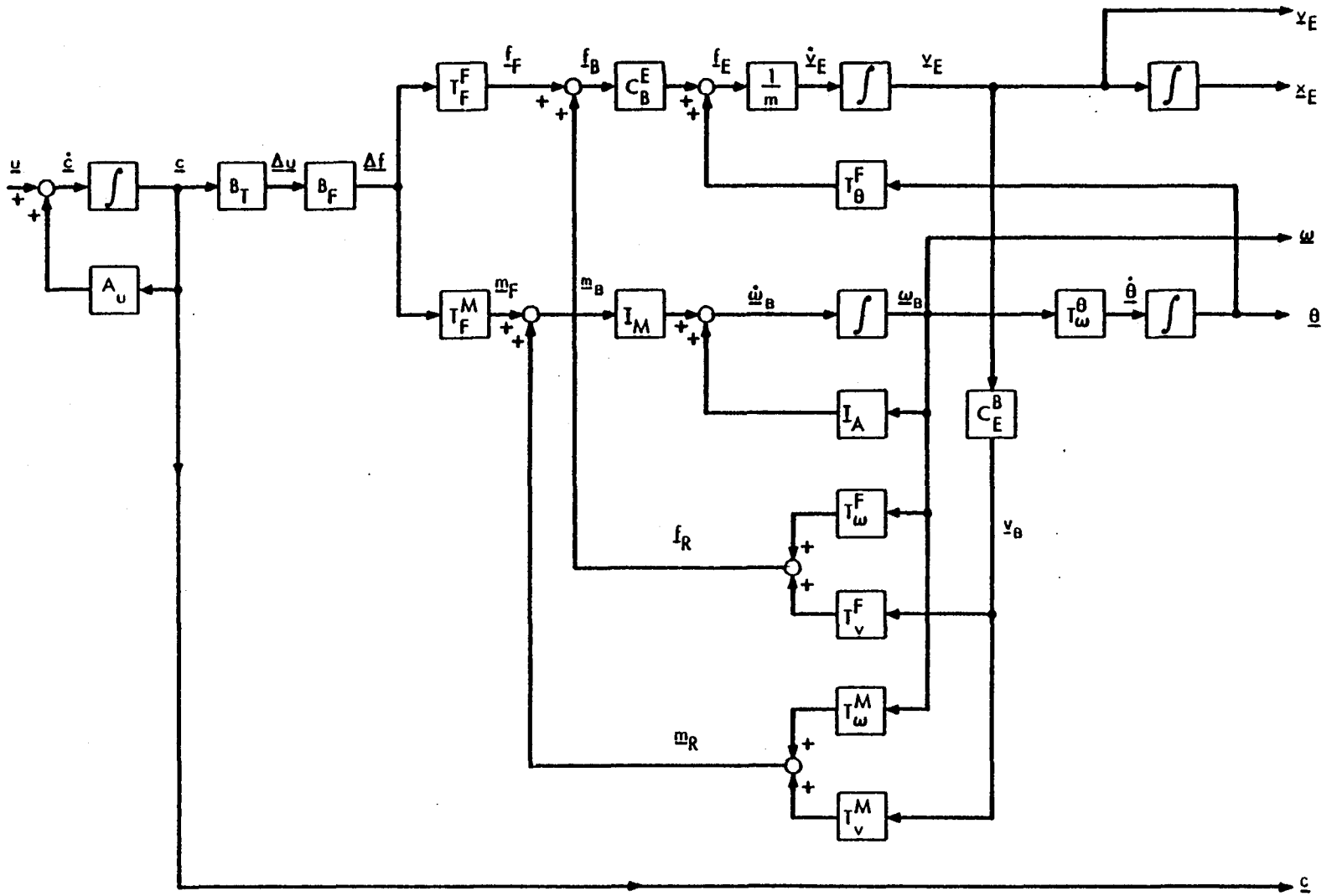

Block Diagram of Linearized VTOL Aircraft Model

Figure 2.4.2.1

A general discussion of equations of motion for an arbitrary system is found in reference (9). The forms and values of the matrices used in the aircraft model linear state equation are presented in Appendix (2.4.3.1).

Translational motions are caused by forces through Newton's Law of motion, which is a statement of momentum conservation:

$$\underline{f}_E = m\dot{\underline{v}}_E \qquad (2.4.3.1)$$

In this equation, m is the mass to which the force $\underline{f}_E$ gives acceleration $\dot{\underline{v}}_E$ in the earth frame E (which is considered as inertial in this derivation). Linearizing this equation and substituting in the nominal values for $\underline{v}_E = \underline{0}$ gives:

$$\delta\dot{\underline{v}}_E = \frac{1}{m}\,\delta\underline{f}_E \qquad (2.4.3.2)$$

Rewriting this equation with the force in the body frame yields the following equation:

$$\delta\underline{v}_E = \frac{1}{m}\left(C_B^E\,\delta\underline{f}_B + T_\theta^F\,\delta\underline{\theta}\right) \qquad (2.4.3.3)$$

where C_B^E is the transfomration from body to earth coordinates for the nominal aircraft trim orientation, and T_θ^F is the transformation between out of trim aircraft orientation $\underline{\theta}$ and the resulting earth frame forces. Note $\delta\underline{\theta} = (\psi, \theta, \phi)^T$. With aerodynamics neglected, $\delta\underline{f}_B$ is composed of fan and ram drag components. $\delta\underline{f}_B$ is given by:

$$\delta\underline{f}_B = \delta\underline{f}_F + \delta\underline{f}_R \qquad (2.4.3.4)$$

The ram drag term $\delta \underline{f}_R$ is a function of linear and angular aircraft velocities as derived in Appendix (2.4.3.2):

$$\delta \underline{f}_R = - \dot{M}_R \underline{v}_B + \dot{M}_R \underline{R}_{cm} \times \underline{\omega}_B \qquad (2.4.3.5)$$

Linearized, this equation is written

$$\delta \underline{f}_R = T_\omega^F \, \delta \underline{\omega}_B + T_V^F \, \delta \underline{v}_B \qquad (2.4.3.6)$$

where $T_\omega^F = -\dot{M}_R$ and $T_V^F = \dot{M}_R \, (\underline{R}_{cm} \times)$. The fan forces term is given by:

$$\delta \underline{f}_F = T_F^F \, \underline{\Delta f} \qquad (2.4.3.7)$$

where $\underline{\Delta f}$ is composed of the fan control force components. The kinematic relationship giving aircraft earth frame position $\underline{r}_E$ is very simple. The nominal value of $\underline{r}_E$ is zero, so the linearized equation is given directly:

$$\delta \dot{\underline{r}}_E = \delta \underline{v}_E \qquad (2.4.3.8)$$

The final translational motion equation required is a velocity transformation:

$$\underline{v}_B = C_E^B \, \underline{v}_E \qquad (2.4.3.9)$$

Linearized about $\underline{v}_E = \underline{0}$, this gives

$$\delta \underline{v}_B = C_E^B \, \delta \underline{v}_E \qquad (2.4.3.10)$$

Rotational motions are caused by torques through the following equation:

$$\dot{\underline{H}}_E = \underline{m}_E \qquad (2.4.3.11)$$

where $\underline{m}_E$ is the torque acting on the aircraft, while $\underline{H}_E$ is the aircraft angular momentum. This equation is a statement of angular momentum conservation. Writing it in the body frame gives:

$$\underline{m}_B = \dot{\underline{H}}_B + \underline{\omega}_B \times \underline{H}_B \qquad (2.4.3.12)$$

The VTOL aircraft angular momentum has two parts: $\underline{H}_I$ is the momentum of the engine cores and fans in the body reference frame. It is assumed to be constant. $I_B\underline{\omega}_B$ is the angular momentum of the aircraft viewed as an entirely rigid body with inertia tensor I_B and angular velocity $\underline{\omega}_B$. The following equation sums these two components:

$$\underline{H}_B = I_B\underline{\omega}_B + \underline{H}_I \qquad (2.4.3.13)$$

Substituting this into equation (2.4.3.12) and then linearizing gives:

$$\delta\underline{m}_B = I_B\,\delta\dot{\underline{\omega}}_B + \delta\underline{\omega}_B \times \underline{H}_I \qquad (2.4.3.14)$$

where the zero nominal angular velocity $\underline{\omega}_B = \underline{0}$ has been inserted. Multiplying this equation by I_B^{-1} and introducing the notation $I_M = I_B^{-1}$, and I_A where

$$I_A\,\delta\underline{\omega}_B = -\,I_B^{-1}\,\delta\underline{\omega}_B \times \underline{H}_I \qquad (2.4.3.15)$$

gives the linearized result:

$$\delta\dot{\underline{\omega}}_B = I_M\,\delta\underline{m}_B + I_A\,\delta\underline{\omega}_B \qquad (2.4.3.16)$$

The linearized moments $\delta\underline{m}_B$ are composed of fan moments $\delta\underline{m}_F$ and ram drag moments $\delta\underline{m}_R$ in the body frame. Again, aerodynamic effects, if modelled, would also contribute moments. The linearized moments sum to give $\delta\underline{m}_B$:

$$\delta \underline{m}_B = \delta \underline{m}_F + \delta \underline{m}_R \qquad (2.4.3.17)$$

The fan moments are a function of the control force components $\underline{\Delta f}$:

$$\delta \underline{m}_F = T_F^M \, \underline{\Delta f} \qquad (2.4.3.18)$$

The ram drag moments, like the ram drag forces, are generated by angular and linear velocities. They are given by the equation derived in appendix (2.4.3.2):

$$\underline{m}_R = -\dot{M}_{R_{cm}} \underline{R} \times \underline{v}_B - \dot{I}_m \underline{\omega}_B \qquad (2.4.3.19)$$

Linearizing this and setting $T_\omega^M = -\dot{I}_m$ and $T_V^M = (-\dot{M}_{R_{cm}} \underline{R} \times)$ gives the following equation for the ram drag moments:

$$\delta \underline{m}_R = T_\omega^M \, \delta \underline{\omega}_B + T_V^M \, \delta \underline{v}_B \qquad (2.4.3.20)$$

To describe the aircraft orientation, Euler angles are used. The nominal aircraft orientation is heading $\psi = 0°$, pitch angle $\theta = 0°$, and roll angle $\phi = 0°$. Euler angle rates are integrated to determine the angles which are written in vector form as $\underline{\theta} = (\psi, \theta, \phi)^T$. Note $\delta \underline{\theta} = \underline{\theta}$ since the nominal $\underline{\theta}$ is zero. Euler angle rates are given by reference (8),

$$\dot{\underline{\theta}} = T(\underline{\theta}, \underline{\omega}_B) \qquad (2.4.3.21)$$

Linearizing this equation yields:

$$\delta \dot{\underline{\theta}} = T_\omega^\theta \, \delta \underline{\omega}_B \qquad (2.4.3.22)$$

This completes the description of the aircraft motion model given the fan forces. The description of the command and actuator, coordination and dynamics follows.

The generation of fan forces and moments from commands is accomplished in four steps. The command $\underline{u}$ is passed through simple dynamics to give the command state vector $\underline{c}$. This is transformed into actuator variables represented by $\underline{\Delta u}$, which in turn are transformed into the force components of the fans, $\underline{\Delta f}$. Finally the total fan forces, $\underline{f}_F$, and moments, $\underline{m}_F$, are obtained by a pair of transformations acting on $\underline{\Delta f}$. An expansion of this description follows.

The command $\underline{u}$ has six components representing the commanded inputs to the x, y, z, θ, ϕ, and ψ motions. In component form it is written as $\underline{u} = (\delta x, \delta y, \delta z, \delta\phi, \delta\theta, \delta\psi)^T$. The dynamics given the command states are uncoupled and first order. For example, δx_c is the state of a first order dynamical system whose only input is δx. The overall command state generator system is described by the equation:

$$\dot{\underline{c}} = A_u \underline{c} + \underline{u} \qquad (2.4.2.23)$$

where $\underline{c} = (\delta x_c, \delta y_c, \delta z_c, \delta\phi_c, \delta\theta_c, \delta\psi_c)^T$. These dynamics are used to model the accumulated dynamics of the control system, control actuators, and thrust generating mechanism. A_u is chosen as a zero matrix so the open loop command states are the integrals of the command components. The next step in the generation of the forces and moments is the transformation from command states to actuator variables. This transformation, shown in the next equation, is chosen to yield uncoupled aircraft motions

from the uncoupled motion commands:

$$\underline{\Delta u} = B_T \underline{c} \qquad (2.4.3.24)$$

$\underline{\Delta u}$ contains longitudinal and lateral thrust deflection angles, and thrust magnitude deviations for each of the three fans. The quantities are $\underline{\Delta u} = (\Delta\alpha_1, \Delta\alpha_2, \Delta\alpha_3, \Delta\theta_1, \Delta\theta_2, \Delta\theta_3, \Delta F_{G1}, \Delta F_{G2}, \Delta F_{G3})^T$. B_T transforms command states into actuator variables by the following scheme. A forward motion command state δx_c is converted to equal aftward deflections in each lift/cruise fan nozzle and in the forward lift fan louvers. Likewise, lateral and vertical command states δy_c and δz_c are converted to lateral thrust deflection and thrust increase respectively. Roll is generated by equal and opposite thrust level variations in the lift/cruise fans. $\delta\theta_c$, the pitch command state, is transformed into increased lift fan thrust and decreased lift/cruise fan thrusts in amounts causing rotation and not translation. Yaw command state $\delta\psi_c$ is similarly transformed into yawing moment by deflecting the lift fan thrust to one side and the lift/cruise fan thrusts to the opposite side. The following equation describes how the actuator variables $\underline{\Delta u}$ transform into fan force components:

$$\underline{\Delta f} = B_F \underline{\Delta u} \qquad (2.4.3.25)$$

where $\underline{\Delta f} = (\Delta F_{x1}, \Delta F_{x2}, \Delta F_{x3}, \Delta F_{y1}, \Delta F_{y2}, \Delta F_{y3}, \Delta F_{z1}, \Delta F_{z2}, \Delta F_{z3})^T$ gives the force components for each of the three fans. These fan components are combined to form the total forces on the aircraft by:

$$\delta \underline{f}_F = T_F^F \underline{\Delta f} \qquad (2.4.3.26)$$

where $\delta \underline{f}_F = (X_F, Y_F, Z_F)^T$. Similarly, the moments are given by:

$$\delta \underline{m}_F = T_F^M \underline{\Delta f} \qquad (2.4.3.27)$$

where $\delta \underline{m}_F = (L_F, M_F, N_F)^T$ has roll, pitch, and yaw moments respectively as elements.

2.5 Wave Model

2.5.1 Introduction

The purpose of the wave model is to generate the stochastic variation of sea surface height at some point along the ship's length. This is used as the disturbance driving the ship motion model. The use of sea surface height to drive ship motion is a commonly used approximation (10). It is a major simplification of the distributed hydrodynamic forces acting on a ship hull, but it does result in an overall wave-ship model whose response is characteristic of actual ship motion. General wave surface and ship motion modelling are described in reference (10).

The Neumann ideal power spectrum for wind generated waves is chosen as the starting point for the wave modelling. Reference (11) gives this spectrum. However, for control design and systems analysis, a linear time invariant dynamic system driven by a gaussian white noise and written in state space form is desired for the wave model. Therefore, the result of the wave modelling is such a state space representation having an output spectrum approximating the Neumann spectrum.

The sea condition, and ship speed and heading are required to specify the wave spectrum encountered by the ship. Ship information is needed in order to transform the wave spectrum from that seen at a stationary point to that seen from the moving ship. The sea and ship are given specifications which provide a realistic, challenging situation for the aircraft landing controller to operate in. The specifications are for a "sea state five" (defined in reference (12)), a ship heading such that the relative wind over the deck is undisturbed by the ship's superstructure, and a ship speed compromising low wind speed over the ship deck and high through the water ship speed. The wind speed generating the sea state five ocean waves is set at 16 knots (10). In steady state over a wide stretch of ocean where the waves will not be fetch limited, the wave heights will reach over 6.5 feet about 30% of the time. (This is generally called the significant wave height, measured from trough to crest.) The corresponding period of these waves will be 7 seconds (10). Ship velocity through the water is chosen so that the wind sweeps the ship landing pad at not more than 20 knots, and at a heading (θ_{AW}) near 45°. This angle avoids air turbulence over the pad due to the ship superstructure. The specification of a low relative wind speed keeps aircraft aerodynamic forces small; and, hence, helps to justify neglecting those forces. In addition, the ship should be cruising at a maneuverable speed. For these reasons, the ship velocity is chosen at about 10 knots, and at an angle (θ_W) of 70° into the wind and waves.

The following section describes the ideal wave spectrum and the

final model. The derivation of the latter is outlined in the subsequent sections.

2.5.2 Model Equations

This section gives the form of the ideal Neumann spectrum for both fixed and moving observers. Then the state space approximation adopted as the stochastic wave model is presented. The following two sections describe how this model is obtained from the ideal spectrum.

The Neumann power spectrum for wind generated ocean waves has the following general form as a function of wave frequency ω_w:

$$S(\omega_w) = a^2\omega_w^{-6}\exp\{-2b\omega_w^{-2}\} \qquad (2.5.2.1)$$

where a and be are constants depending on the wave height and period characteristic of sea conditions as explained in the next section. Transforming this spectrum into the one observed from onboard the ship moving with speed v_s and heading θ_w into the waves gives $S_e(\omega_e)$:

$$S_e(\omega_e) = a^2\omega_w^{-6}\exp\{-2b\omega_w^{-2}\}[1 - (4v_s\omega_e\cos\theta_w/g]^{-1/2} \qquad (2.5.2.2)$$

where:

$$\omega_w = \{-1 + [1 + (4v_s\omega_e\cos\theta_w)/g]^{1/2}\}[(2v_s\cos\theta_w)/g]^{-1} \qquad (2.5.2.3)$$

Note g is the acceleration due to gravity. In figure (2.5.2.1), the amplitude spectrum $(S_e(\omega_e))^{1/2}$ is plotted for comparison with the finite order state space model. Note that due to the exponential factor the

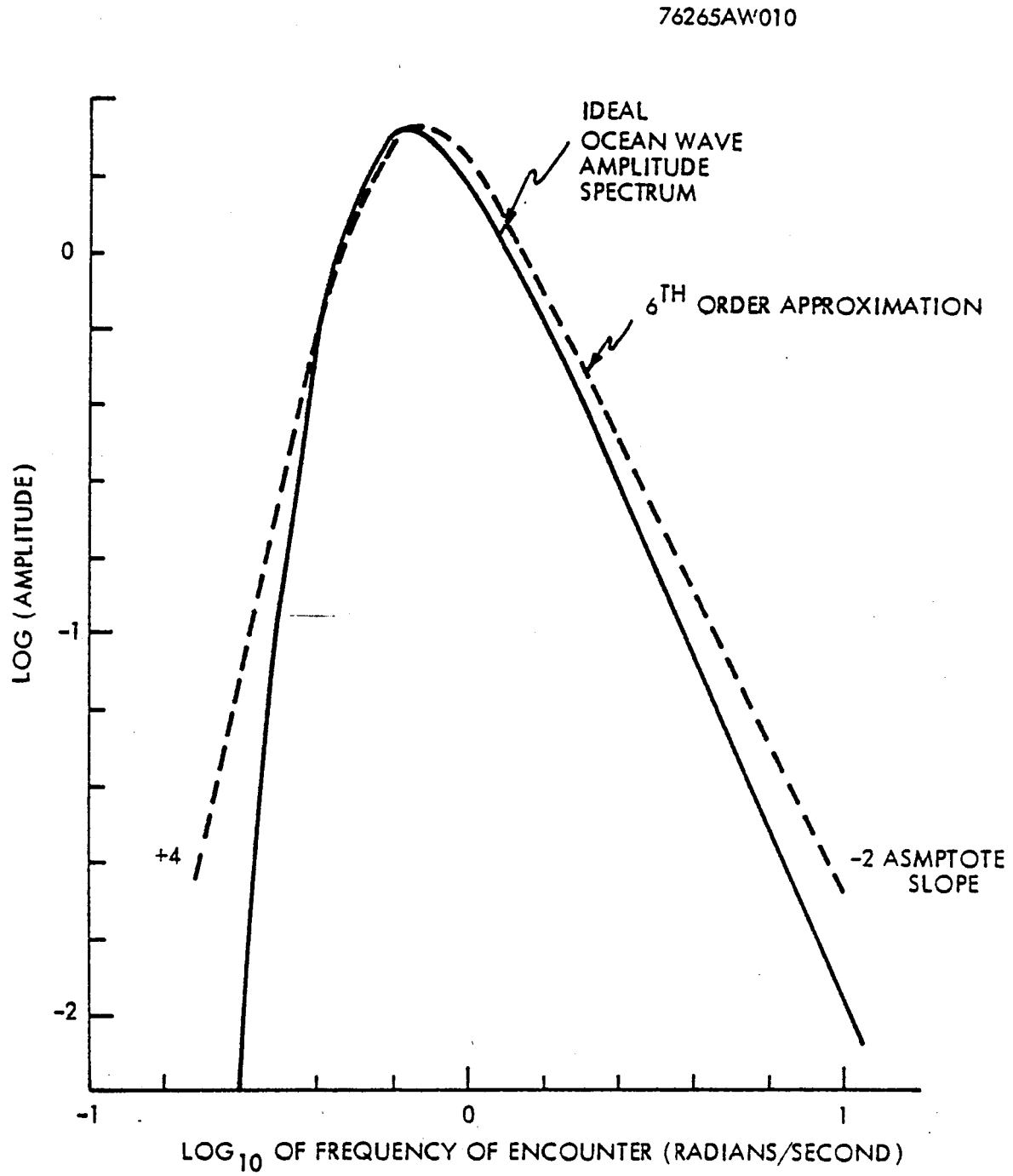

Wave Amplitude Spectra

Figure 2.5.2.1

ideal spectrum drops off faster than any finite order model spectrum at low frequencies.

The finite order model was chosen so that its amplitude spectrum would match the ideal amplitude spectrum, $(S_e(\omega_e))^{1/2}$, closely. This model was formulated with the constraints of finite order, simple structure, and gaussian white noise input. The result is shown in Table (2.5.2.1). The amplitude spectrum of this model is plotted in Figure (2.5.2.1). For the decade of frequencies centered at the peak amplitude, the ideal and model spectra match well. Outside this range the spectra diverge, but the divergence is only significant at low and high frequencies where the amplitudes are very small.

The output of the model, y_{OW}, is extended in the ship modelling sections, where it is used as the ship model input. Ship pitch and heave inputs are related by phase, which can be accounted for in the output vector of the wave model; however, no phase relationship of roll with pitch or heave was determined, so the roll input is generated by a second, identical, independently driven wave model.

In the next two sections, the state space model development is described in more detail beginning in the following section with a more detailed explanation of the Neumann ideal wave spectrum.

2.5.3 Ideal Ocean Wave Spectrum

Various spectral densities for ocean waves are available to naval architects in frequency domain analysis of ship motions (10, 11). Of these spectra, the theoretical Neumann spectrum is chosen here. It is

OCEAN WAVE STATE SPACE MODEL

$$\dot{\underline{x}}_{OW} = A_{OW}\underline{x}_{OW} + B_{OW}\rho_{OW}$$

$$y_{OW} = C_{OW}\underline{x}_{OW}$$

$$\begin{vmatrix} \dot{x}_1 \\ \dot{x}_2 \\ \dot{x}_3 \\ \dot{x}_4 \\ \dot{x}_5 \\ \dot{x}_6 \end{vmatrix} = \begin{vmatrix} 0 & 1 & 0 & 0 & 0 & 0 \\ -\omega_1^2 & -2\xi\omega_1 & 0 & 1 & 0 & 0 \\ 0 & 0 & 0 & 1 & 0 & 0 \\ 0 & 0 & -\omega_2^2 & -2\xi\omega_2 & 0 & 1 \\ 0 & 0 & 0 & 0 & 0 & 1 \\ 0 & 0 & 0 & 0 & -\omega_3^2 & -2\xi\omega_3 \end{vmatrix} \begin{vmatrix} x_1 \\ x_2 \\ x_3 \\ x_4 \\ x_5 \\ x_6 \end{vmatrix} + \begin{vmatrix} 0 \\ 0 \\ 0 \\ 0 \\ 0 \\ \omega_2^6 \end{vmatrix} \rho_{OW}$$

$$y_{OW} = [\, -C\omega_2^2,\ -2C\omega_2\xi,\ 0,\ C,\ 0,\ 0\,]\ \underline{x}_{OW}$$

TABLE (2.5.2.1)

Continued...

OCEAN WAVE STATE SPACE MODEL (CONTINUED)

$$\begin{vmatrix} \dot{x}_1 \\ \dot{x}_2 \\ \dot{x}_3 \\ \dot{x}_4 \\ \dot{x}_5 \\ \dot{x}_6 \end{vmatrix} = \begin{vmatrix} 0 & 1 & 0 & 0 & 0 & 0 \\ -.50126 & -.92040 & 0 & 1 & 0 & 0 \\ 0 & 0 & 0 & 1 & 0 & 0 \\ 0 & 0 & -.50410 & -.92300 & 0 & 1 \\ 0 & 0 & 0 & 0 & 0 & 1 \\ 0 & 0 & 0 & 0 & -.49844 & -.91780 \end{vmatrix} \begin{vmatrix} x_1 \\ x_2 \\ x_3 \\ x_4 \\ x_5 \\ x_6 \end{vmatrix} + \begin{vmatrix} 0 \\ 0 \\ 0 \\ 0 \\ 0 \\ .12810 \end{vmatrix} \rho_{OW}$$

$$y = [\, -8.0555 \quad -14.750 \quad 0 \quad 15.980 \quad 0 \quad 0 \,]\ \underline{x}_{OW}$$

TABLE (2.5.2.1) (Continued)

simple, yet approximates actual sample power spectral densities reasonably well. As presented in reference (11), it has two parameters, T_W and $H_{1/3}$, which characterize average apparent wave period and minimum height of the 1/3 largest waves, respectively. (In the modelling, T_W is assumed to be the period of waves of height $H_{1/3}$.) The Neumann expression for the wave power per unit frequency, ω_W, as seen by a stationary observer is:

$$S(\omega_W) = H_{1/3}^2 T_W (3/8\pi)^{3/2} (\omega_W T_W/2\pi)^{-6} \exp\{(-3/2)(\omega_W T_W/2\pi)^{-2}\} \qquad (2.5.3.1)$$

Travelling on the ship through the waves, a transformed or distorted spectrum is observed. The transformed spectrum can be obtained using a Jacobian transformation. This transformation comes about in the following way. A moving observer sees the same physical waves, as a stationary observer, but at a different frequency and power density, say $S_e(\omega_e)$. The new observed frequency is ω_e called the frequency of encounter. Since both observers must see the same total wave power, the following equality holds:

$$\int_0^\infty S(\omega_W)\,d\omega_W = \int_0^\infty S_e(\omega_e)\,d\omega_e \qquad (2.5.3.2)$$

The Jacobian transformation, or change of variables formula (13), gives:

$$S_e(\omega_e) = S(\omega_W)\Big|_{\omega_e = f(\omega_W)} \cdot \frac{\partial \omega_W}{\partial \omega_e} \qquad (2.5.3.3)$$

To solve this expression for $S_e(\omega_e)$, the frequency tranformation, $\omega_e = f(\omega_w)$, given in reference (10) is required. This reference derives $f(\omega_w)$ from the properties of deep water waves and the frequency-wavelength-velocity of observer doppler shift relationship. The result is:

$$\omega_e = f(\omega_w) = \omega_w \cos\theta_w (\cdot (v_s/g)\omega_w + 1/\cos\theta_w) \qquad (2.5.3.4)$$

or

$$\omega_w = \frac{-1 + (1 + 4\omega_e v_s \cos\theta_w/g)^{1/2}}{2v_s\cos\theta_w/g} \qquad (2.5.3.5)$$

where ω_w is the frequency observed by a stationary observer, v_s is the ship speed, θ_w is the ship heading with respect to the direction of the wind and wave source, and g is the acceleration due to gravity. The final expression for $S_e(\omega_e)$ is:

$$S_e(\omega_e) = \frac{a^2}{\omega_w^6} \exp\{\frac{-2b}{\omega_w^2}\} [1 + \frac{4v_s\cos\theta_w}{g} \omega_e]^{-1/2} \qquad (2.5.3.6)$$

where

$$a = H_{1/3}(3/128\pi^5)^{3/4} T_w^{-5/2} \qquad (2.5.3.7)$$

$$b = 3\pi^2 T_w^{-2} \qquad (2.5.3.8)$$

and ω_w is given by equation (2.5.3.5). This is the power spectral density used to determine the linear finite dimensional stochastic wave model in the next section.

An alternative derivation of $S_e(\omega_e)$ can be accomplished based on the Taylor "frozen field" hypothesis used for wind gust modelling (14).

The frozen field hypothesis assumes that the spatially distributed gust process W(x,t) is a fixed field in time which moves spatially at velocity v_p. Hence, it has the property:

$$W(x,t) = W(0, t - x/v_p) \qquad (2.5.3.9)$$

For ocean waves, the hypothesis would be applied to individual wave frequency components, which may be thought of as fixed in time, but moving spatially with frequency-dependent velocity $v_p(\omega)$.

The next section explains how a state space model of the ocean waves is derived, whose spectrum approximates the Neumann spectrum.

2.5.4 Model Derivation

The purpose of this section is to describe the derivation of a state space ocean wave model having approximately the same spectrum as the Neumann spectrum in the previous section.

The Neumann spectrum of equation (2.5.3.6) represents an infinite order linear system. The reason is that it contains an exponential factor, which at low frequencies causes the spectrum to drop off faster than that of any finite order system. On the other hand, it is desirable to have a simple, low order model for computations and analysis. The construction of such a model follows.

Modelling is a system identification problem: a structure must be hypothesized, and its parameters estimated. The hypothesized structure is a gaussian white noise driven single input-single output (SISO) system. Its dynamics consist of three nearly identical second order damped

oscillators in cascade. This structure has the advantage that it contains only three parameters affecting the output, while satisfactorily matching the ideal spectrum of the previous section. The small variation in the parameters among the three second order systems is to aid numerical algorithms. The model transfer function is:

$$\frac{\text{Ocean surface height}}{\text{noise input}}(s) = \frac{Cs^4}{\prod_{i=1}^{3}(s^2 + 2\xi\omega_{ni}s + \omega_{ni}^2)} \qquad (2.5.4.1)$$

where s is the Laplace variable, C is the root locus gain, ω_{ni} is the ith second order system natural frequency, and ξ is the common damping ratio of the cascaded second order systems. The state space differential equation for this is written in Table (2.5.2.1).

Having chosen a hypothesized structure, its parameters need to be estimated. This is accomplished by matching the square roots of the power spectral densities of the finite order model with the infinite order ideal reference spectrum. If y is the output of a single output system with power spectrum $S(\omega)$, then the quantity under consideration is:

$$(S(\omega))^{1/2} = (\mathcal{F}\{E\,[(y(t) - m(t))(y(t+\tau)-m(t+\tau)]\}\,(\omega))^{1/2} \qquad (2.5.4.2)$$

where

$$m(t) = E[y(t)] \qquad (2.5.4.3)$$

and $\mathcal{F}\{\cdot\}\,(\omega)$ is the Fourier transform, while E is the expectation operator. For single input-single output linear time invariant systems of the model form given in Table (2.5.2.1), the square root of the power

spectrum is:

$$(S_{OW}(\omega))^{1/2} = | C_{OW}(j\omega I - A_{OW})^{-1} B_{OW}| (S\rho_{OW}(\omega))^{1/2} \quad (2.5.4.4)$$

where $S\rho_{OW}(\omega)$ is the power spectrum of the input $\rho_{OW}(t)$. Since $\rho_{OW}(t)$ is white noise, $S\rho_{OW}(\omega)$ is a constant, independent of frequency. $(S(\omega))^{1/2}$ is refered to as the amplitude spectral density.

Four specific features of the ideal and model amplitude spectra are matched. These are: peak amplitude and frequency, peak width, and roll off in the first decade on each side of the peak. The roll off towards low frequencies is obtained by four zeroes at the origin of the root locus plot. Four poles located at the ideal amplitude spectrum peak cancel the effect of the four zeroes at high frequencies, while two more poles at the same location produce the desired high frequency roll off. Thus, the attenuation away from the peak is determined by the model structure itself. Since the peak frequency for a second order system with a zero at the origin is near its natural frequency ω_n, the values of ω_{n1}, ω_{n2}, ω_{n3} are chosen near the ideal spectrum peak at 0.708 radians/second. The values used are: 0.706, 0.708, and 0.710. The damping ratio is set so the width of the model and ideal amplitude spectra roughly match over the first decade of drop from the peak. The value used is $\xi = 0.65$. For comparison, the ideal Neumann and the model amplitude spectra are presented in figure (2.5.2.1). Verification of the model validity is by the close match illustrated in this figure. A further check is made in Section (2.6.5) where a simulation is presented to verify the overall wave-ship model behavior.

The wave model parameter fit was made by eye judgement; however, a better fit might be obtained with a more precise method such as minimum least square error fit. In view of the fact that the ideal wave spectra are themselves only rough approximations of wave behavior, more elaborate fitting methods were not deemed to be justified.

2.6 Ship Motion Model

2.6.1 Introduction

This model represents the dynamics of the ship by transforming ocean surface height into ship motion response. In particular, the landing deck motions are represented. The model has inputs for the roll and pitch-heave dynamics of the ship, and outputs for the resulting orientational and translational landing pad motions. Fore-and-aft sway, yaw and lateral sway are not modelled since it is assumed that their responses are smaller than the others, and so less important to the aircraft landing problem. The ship modelled is a representative small ship like those of the Allen M. Sumner Class. Ships of this class are described in reference (15). They are approximately 400 feet in length and displace roughly 3000 tons. As described in the wave model introduction, the ship is assumed to be cruising at 10 knots, with a heading angle of 70° into the waves. The waves are generated by a 16 knot wind. Ship motion magnitude parameters are sized to produce typical ship roll, pitch, and heave amplitudes of 5 degrees, 2 degrees, and 5 feet, respectively, as suggested by reference (7). The heave amplitude corresponds to about one foot of heave per foot rise in the sea surface;

however, roll and pitch do not appear to correspond with a similar static relationship using wave slope.

The next section describes the linear, time invariant ship model and its origins. The other sections describe the identification of dynamics, the calculation of outputs, and the verification of the overall wave-ship model.

2.6.2 Model Equations

This section presents a brief review of the ship motion modelling, and then gives the model results.

The ship motion analysis techniques used in the modelling are found in reference (10) and in reference (16). The second is the classic paper in the field. In these references, the basic assumption is that the overall ship response is the superposition of responses to the frequency components of the ocean waves. The important result is that to a good approximation, the ship response to irregular seas can be represented by a cascade of the wave model and a shaping filter, where the filter represents the dynamic response of the ship to the waves. Another result is that longitudinal and lateral ship dynamics may be treated as uncoupled for most theoretical and experimental analyses. For the ship modelled here, coupled pitch and heave dynamics data is available from a towing tank experiment (17). However, data on rolling motions has not been located. This lack of roll data is overcome by observing and modifying typical rolling data for other ships (18, 19). Since roll dynamics are not used in the control system design and analysis, the

purpose of including roll is to generate a complete model of the major ship responses. Recall from the introduction that surging, yawing, and swaying are not expected to be as important as pitch, heave, and roll responses, and so are not modelled.

Characteristics of the shaping filter representing ship response are used for the identification of the state space ship model parameters. In this linear time invariant model, pitch, heave, and roll modes are each represented by a separate second order approximation of a pass band filter. To generate the desired phase between pitch and heave, the heave input is lagged behind the pitch input. Since the ship inputs are wave model outputs, the single wave model output is augmented to include a second phase lagged quantity. The two wave output quantities used for ship inputs are y_{PW} and y_{HW}. Since no roll-pitch phase relationship could be determined, roll is driven by a separate identical, but statistically independent wave model. The lack of roll information can be attributed to two factors. Rolling motions are not as critical as pitching and heaving in determining a ship's ability to maintain heading and speed in rough seas; and in those cases where rolling is unacceptable, it can often be reduced to acceptable levels, with the use of roll damping devices.

The end result of the modelling is shown in the tables. The ship model equation with the three independent second order pass band filters representing roll R, pitch P, and heave H dynamics is shown in Table (2.6.2.1). In this equation, ω_n is the natural frequency and ξ the damping ratio of the indicated dynamics. y_{RW}, y_{PW}, y_{HW} are the three ship inputs from the wave models. Next, the output equation is given in Table

SHIP STATE SPACE MODEL DYNAMICS

(The output equation follows in Table 2.6.2.2))

$$\dot{\underline{x}}_S = A_S \underline{x}_S + B_S \underline{y}_{WSC}$$

$$\begin{vmatrix} \dot{x}_{R1} \\ \dot{x}_{R2} \\ \dot{x}_{P1} \\ \dot{x}_{P2} \\ \dot{x}_{H1} \\ \dot{x}_{H2} \end{vmatrix} = \begin{vmatrix} 0 & 1 & 0 & 0 & 0 & 0 \\ -\omega_{nR}^2 & -2\omega_{nR}\xi_R & 0 & 0 & 0 & 0 \\ 0 & 0 & 0 & 1 & 0 & 0 \\ 0 & 0 & -\omega_{nP}^2 & -2\omega_{nP}\xi_P & 0 & 0 \\ 0 & 0 & 0 & 0 & 0 & 1 \\ 0 & 0 & 0 & 0 & -\omega_{nH}^2 & -2\omega_{nH}\xi_H \end{vmatrix} \begin{vmatrix} x_{R1} \\ x_{R2} \\ x_{P1} \\ x_{P2} \\ x_{H1} \\ x_{H2} \end{vmatrix} +$$

$$\begin{vmatrix} 0 & 0 & 0 \\ 1 & 0 & 0 \\ 0 & 0 & 0 \\ 0 & 1 & 0 \\ 0 & 0 & 0 \\ 0 & 0 & 1 \end{vmatrix} \begin{vmatrix} y_{RW} \\ y_{PW} \\ y_{HW} \end{vmatrix}$$

TABLE (2.6.2.1)

(Table continued on next page)

(continuation of Table (2.6.2.1))

$$\begin{vmatrix} \dot{x}_{R1} \\ \dot{x}_{R2} \\ \dot{x}_{P1} \\ \dot{x}_{P2} \\ \dot{x}_{H1} \\ \dot{x}_{H2} \end{vmatrix} = \begin{vmatrix} 0 & 0 & 0 & 0 & 0 & 0 \\ -0.10693 & -0.02616 & 0 & 0 & 0 & 0 \\ 0 & 0 & 0 & 0 & 0 & 0 \\ 0 & 0 & -0.42641 & -0.3265 & 0 & 0 \\ 0 & 0 & 0 & 0 & 0 & 0 \\ 0 & 0 & 0 & 0 & -0.42641 & -0.31344 \end{vmatrix} \begin{vmatrix} x_{R1} \\ x_{R2} \\ x_{P1} \\ x_{P2} \\ x_{H1} \\ x_{H2} \end{vmatrix} +$$

$$\begin{vmatrix} 0 & 0 & 0 \\ 1 & 0 & 0 \\ 0 & 0 & 0 \\ 0 & 1 & 0 \\ 0 & 0 & 0 \\ 0 & 0 & 1 \end{vmatrix} \begin{vmatrix} y_{RW} \\ y_{PW} \\ y_{HW} \end{vmatrix}$$

TABLE (2.6.2.1) continued

(2.6.2.2). $(x_{ELP}, y_{ELP}, z_{ELP})$ is the position of the landing pad in earth coordinates, while $(\phi_S, \theta_S, \psi_S)$ are the Euler angles of the ship orientation. In this equation, C_s is generated by the matrices T_{ESC}, S_{S1}, S^*_{S1}, S_{S2}, and S^*_{S2}. These are described in Section (2.6.4). The coupling structure between the wave output and ship input is presented in Table (2.6.2.3). $\underline{x}_{OWPH}$ and $\underline{x}_{OWR}$ are the state vectors of the wave models associated with the ship pitch-heave and roll dynamics inputs, respectively. ω_2 and ξ_2 are also from the wave model. Finally, the overall wave-ship model is written in Table (2.6.2.4). In the overall structure, note that ρ_{OWPH} and ρ_{OWR} are independent gaussian white noise sources driving the two wave models.

In the next section, the ship dynamics identification is described.

2.6.3 Ship Dynamic Modelling

This section discusses the identification of the structure and parameter values for the ship model. The discussion begins with the important analysis references and sources of data. Then it proceeds to the model structure and parameter estimation.

The modelling approach for the ship was to take the frequency domain response representation of references (16) and (10) and approximate it in the time domain by a low order linear system. The ship motion data for estimating the model parameters came from several sources. For the ship modelled, as for many ships, only pitch-heave information was available. For roll, information on other ships was employed. Data

SHIP MODEL OUTPUT EQUATION

$$\underline{Y}_S = C_S \underline{x}_S$$

$$\underline{Y}_S = \begin{vmatrix} \dfrac{T_{ESC} \cdot S_{S1}}{S^*_{S1}} \\ \dfrac{T_{ESC} \cdot S_{S2}}{S^*_{S2}} \end{vmatrix} \underline{x}_S$$

$$\begin{vmatrix} x_{ELP} \\ y_{ELP} \\ z_{ELP} \\ \phi_S \\ \theta_S \\ \psi_S \\ \dot{x}_{ELP} \\ \dot{y}_{ELP} \\ \dot{z}_{ELP} \\ \dot{\phi}_S \\ \dot{\theta}_S \\ \dot{\psi}_S \end{vmatrix} = \begin{vmatrix} 0 & 0 & -0.16000 & 0 & 0 & 0 \\ 0.29136 & 0 & 0 & 0 & 0 & 0 \\ 0 & 0 & 1.7500 & 0 & -0.12610 & 0 \\ 0.01821 & 0 & 0 & 0 & 0 & 0 \\ 0 & 0 & 0.01000 & 0 & 0 & 0 \\ 0 & 0 & 0 & 0 & 0 & 0 \\ 0 & 0 & 0 & -0.16000 & 0 & 0 \\ 0 & 0.29136 & 0 & 0 & 0 & -1.2610 \\ 0 & 0 & 0 & 1.7500 & 0 & 0 \\ 0 & 0.01821 & 0 & 0 & 0 & 0 \\ 0 & 0 & 0 & 0.01000 & 0 & 0 \\ 0 & 0 & 0 & 0 & 0 & 0 \end{vmatrix} \begin{vmatrix} x_{R1} \\ x_{R2} \\ x_{P1} \\ x_{P2} \\ x_{H1} \\ x_{H2} \end{vmatrix}$$

TABLE 2.6.2.2

WAVE OUTPUT - SHIP INPUT COUPLING

$$Y_{WSC} = C_{WSC} \left| \begin{array}{c} \underline{x}_{OWPH} \\ \hline \underline{x}_{OWR} \end{array} \right|$$

$$\left| \begin{array}{c} y_{RW} \\ \hline y_{PW} \\ \hline y_{HW} \end{array} \right| = \left| \begin{array}{c|c} 0 & C_{OW} \\ \hline C_{OW} & 0 \\ \hline C_{PH} & 0 \end{array} \right| \left| \begin{array}{c} \underline{x}_{OWPH} \\ \hline \underline{x}_{OWR} \end{array} \right|$$

$$C_{OW} = [\ -C\omega_2^2,\ -2C\omega_2\xi_2,\ 0,\ C,\ 0,\ 0\ ]$$

$$C_{PH} = [\ -qC\omega_2^2,\ -2qC\omega_2\xi_2 + qCb,\ 0,\ qC,\ 0,\ 0\ ]$$

$$C_{OW} = [\ -8.0555,\ -1.4750,\ 0,\ 15.980,\ 0,\ 0\ ]$$

$$C_{PH} = [\ -4.0696,\ 3.2535,\ 0,\ 8.0731,\ 0,\ 0\ ]$$

TABLE (2.6.2.3)

OVERALL WAVE-SHIP MODEL STRUCTURE

$$\begin{vmatrix} \underline{x}_S \\ \hline \underline{x}_{OWPH} \\ \hline \underline{x}_{OWR} \end{vmatrix} = \left|\begin{array}{c|c|c} A_S & B_S C_{WSC} & \\ \hline 0 & A_{OW} & 0 \\ \hline 0 & 0 & A_{OW} \end{array}\right| \begin{vmatrix} \underline{x}_S \\ \hline \underline{x}_{OWPH} \\ \hline \underline{x}_{OWR} \end{vmatrix} + \left|\begin{array}{c|c} 0 & 0 \\ \hline B_{OW} & 0 \\ \hline 0 & B_{OW} \end{array}\right| \begin{vmatrix} \rho_{OWPH} \\ \hline \rho_{OWR} \end{vmatrix}$$

$$\begin{vmatrix} \underline{y}_S \\ \hline \underline{y}_{OWPH} \\ \hline \underline{y}_{OWR} \end{vmatrix} = \left|\begin{array}{c|c|c} C_S & 0 & 0 \\ \hline 0 & C_{OW} & 0 \\ \hline 0 & 0 & C_{OW} \end{array}\right| \begin{vmatrix} \underline{y}_S \\ \hline \underline{y}_{OWPH} \\ \hline \underline{y}_{OWR} \end{vmatrix} .$$

TABLE (2.6.2.4)

from the following sources was used for the parameter estimation. Experimental towing tank pitching and heaving data for a model of the 383 foot long Allen M. Sumner Class destroyer was obtained from reference (17). Data was also available from model tests of a similar 500 foot ship in reference (20). Full scale rolling data for a 364 foot destroyer was found in reference (19). In reference (18), model data was found for the pitching, heaving and rolling of an aircraft carrier.

The model structure is now familiar. It is a compromise between simplicity and realism, while taking into account the available data. The response of the ship to ocean surface height is assumed to be linear. Longitudinal and lateral dynamics are decoupled; and, in fact, pitch and heave are decoupled, except for a relative phase relation at their inputs. Qualitatively, the response of the ship to waves is roughly like a pass band over a narrow frequency range. In fact, the three modes behave much like highly tuned second order systems. The references (10), (17) and (21) illustrate this characteristic. In these references, the response amplitude operator is plotted. This is the square of the magnitude of a system's amplitude response. Based on this observation, each mode of response is hypothesized as a second order system. The overall ship model is thus three independent second order systems driven by individual inputs as shown in the previous section, Table (2.6.2.1). The ship state vector, $\underline{x}_S$, is given:

$$\underline{x}_S = (x_{R1}, x_{R2}, x_{P1}, x_{P2}, x_{H1}, x_{H2})^T \qquad (2.6.3.1)$$

where for each mode R, P, and H, the first state is proportional to the orientation or height of the ship in the earth frame, and the second

state is the derivative of the first. Magnitude scaling is accomplished at the output.

Pitch and heave parameters were estimated first. The parameters are the natural frequency and damping ratio of each mode. Reference (17) was the primary source of data here. The first step was to plot amplitude response as a function of frequency of encounter. For a given speed, with the ship heading directly into regular waves, the motion amplitude was recorded for various wavelengths. This information from the report can be plotted as motion amplitude versus wave frequency. A transformation yields a plot of amplitude versus frequency of encounter for the given ship velocity. The transformation from ω to ω_e is the same one used in the wave model derivation.

For the pitching case, it is easy to find the resonant frequency to use as the natural frequency. A value of $\omega_{nP} = 0.65$ radians/second was selected. By comparing the attenuation of the response magnitude at two frequencies, a damping ratio can be determined. The value $\xi_P = 0.25$ was selected.

For heave, the data does not show a peak. From reference (20), however, information was available for a 500 foot destroyer. There, the heave and pitch resonant frequencies were the same. On this basis, ω_{nH} was chosen equal to ω_{nP}. The heave mode damping ratio was set close to the pitch damping ratio since the amplitude responses have about the same attentuation rate near the resonant frequency. The model value is $\xi_H = 0.24$.

A pitch-heave phase relationship was given in reference (17). This was used to generate separate pitch and heave mode inputs to the ship from the wave model output. As shown in Table (2.6.2.3), this was accomplished by giving one wave model two outputs, y_{PW} and y_{HW}. (Note the second wave model drives the roll mode.) The phase relation is as follows. For very low frequency waves, that is ones with long wavelengths, pitch will lead heave by 90 degrees of phase. This is because pitch will be at the maximum positive value when the ship center of rotation heaves upwards through the mean position as the ship climbs a wave to its peak. At the crest of the heave motion, the pitch attitude will return to zero, and so on. At a wavelength corresponding to the frequency of encounter equal to about 0.68 radians/second, the data shows that pitch leads heave by only approximately 60 degrees. These two phases suggest the following frequency domain relation between y_{PW}, the wave output driving ship pitch, and y_{HW}, the output driving ship heave:

$$y_{HW} = q (s + b) s^{-1} y_{PW} \qquad (2.6.3.2)$$

where $q \simeq 0.51$ is set to give the heave and pitch inputs the same magnitude at pitch and heave natural frequency, and $b \simeq 1.3$ gives the desired phase relation. The equation for y_{HW} in the time domain is given in Table (2.6.2.3).

Roll motion data for the Allen M. Sumner Class was not found; however, data from other ships was used as a guide for modelling a second order system to it. From reference (18) and other reports, it was noted that the rolling frequency of a ship is about half the pitching

and heaving frequency. Thus, $\omega_{nR} = 0.33$ was selected. From the same report, an estimate of the roll damping ratio was made. The ship was an aircraft carrier with a length to breadth ratio of 7.7, and its damping ratios were $\xi_H = 0.26$, $\xi_P = 0.20$, and $\xi_R = 0.032$. These values roughly fit the ratio:

$$\frac{\text{length}}{\text{beam}} \simeq \frac{\xi_P}{\xi_R} \simeq \frac{\xi_H}{\xi_R} \qquad (2.6.3.3)$$

Assuming this is also approximately true for the Sumner Class destroyer, where the length/beam ratio is 9.4, the value 0.027 would be chosen for ξ_R. Another report, reference (19), for a 364 foot destroyer gave data from which its damping ratio was calculated at $\xi_R = 0.05$. As a compromise between these two values, the damping ratio for the model was set at $\xi_R = 0.04$.

No phase relation is known for roll with respect to pitch, so the roll mode of the model is driven by an independently excited copy of the wave model, as stated before. The wave model output exciting roll is designated y_{RW} as shown in Table (2.6.2.3).

In the next section, the output equations and the scaling of the motions are discussed.

2.6.4 Ship Model Outputs

This section describes the outputs of the ship model.

The ship responses desired in the output are those of the landing pad (LP) in earth coordinates. The output vector includes the landing pad position, velocity, orientation and angular rate. It is written:

$$y_S = (x_{ELP}, y_{ELP}, z_{ELP}, \phi_S, \theta_S, \psi_S, \dot{x}_{ELP}, \dot{y}_{ELP}, \dot{z}_{ELP}, \dot{\phi}_S, \dot{\theta}_S, \dot{\psi}_S)^T \quad (2.6.4.1)$$

where $(x_{ELP}, y_{ELP}, z_{ELP})$ is the position and $(\phi_S, \theta_S, \psi_S)$ are the Euler angles of the landing pad orientation. Note that $\psi_S = 0$ and $\dot{\psi}_S = 0$, since yawing motion is not modelled.

The ship state vector must first be scaled to the correct magnitude before the output is computed. The desired magnitudes are expressed as root mean square (rms) values. They are 5 degrees, 2 degrees and 5 feet respectively for roll, pitch and heave. To achieve these values, the scale factors AMPRLL, AMPPCH, and AMPHVE are calculated to give the correct corresponding diagonal elements of the steady state, state covariance matrix. The values are shown in Table (2.6.4.1). There, the matrix S_{S1} scales the roll, pitch and heave states, while S_{S2} scales the rates.

The motion at the landing point is found by multiplying the scaled states by T_{ESC}, which is given in Table (2.6.4.2). To retain the properties of linearity, T_{ESC} is evaluated at the nominal orientation of the ship, $\theta_S = 0$, $\phi_S = 0$. The quantities x_{SLP}, y_{SLP}, and z_{SLP} in T_{ESC} are the coordinates of the landing pad in ship coordinates. The values are -175.0, 0.0, and -16.0 feet respectively. X_{SLP} was chosen about half the length of the ship aft of the center of rotation, while the vertical deck position z_{SLP} is estimated at 16.0 feet above the center of rotation. (Note vertical distances are positive downwards in earth and ship coordinate systems.) y_{SLP} is set to zero, directly on the ship center line.

SHIP STATE SCALING MATRICES

S_{S1} Scales roll, pitch and heave states to radians and feet.

S_{S2} Scales roll, pitch and heave derivative states to radians/second and feet/second

$$S_{S1} = \begin{vmatrix} AMPRLL & 0 & 0 & 0 & 0 & 0 \\ 0 & 0 & AMPPCH & 0 & 0 & 0 \\ 0 & 0 & 0 & 0 & AMPHVE & 0 \end{vmatrix}$$

$$S_{S2} = \begin{vmatrix} 0 & AMPRLL & 0 & 0 & 0 & 0 \\ 0 & 0 & 0 & AMPPCH & 0 & 0 \\ 0 & 0 & 0 & 0 & 0 & AMPHVE \end{vmatrix}$$

$$S_{S1} = \begin{vmatrix} 0.01821 & 0 & 0 & 0 & 0 & 0 \\ 0 & 0 & 0.01 & 0 & 0 & 0 \\ 0 & 0 & 0 & 0 & 1.261 & 0 \end{vmatrix}$$

$$S_{S2} = \begin{vmatrix} 0 & 0.01821 & 0 & 0 & 0 & 0 \\ 0 & 0 & 0 & 0.01 & 0 & 0 \\ 0 & 0 & 0 & 0 & 0 & 1.261 \end{vmatrix}$$

TABLE (2.6.4.1)

COORDINATE TRANSFORMATION FROM SHIP STATES TO SHIP LANDING PAD POSITION IN THE EARTH FRAME

Abbreviations: s represents sine

c represents cosine

The subscript S on θ and ϕ is dropped.

$$T_{ESC} = \left| \begin{array}{ccc} s\theta c\phi y_{SLP} + s\theta s\phi z_{SLP} & -s\theta x_{SLP} + c\theta s\phi y_{SLP} - c\theta c\phi z_{SLP} & 0 \\ -s\theta y_{SLP} + c\phi z_{SLP} & 0 & 0 \\ c\theta c\phi y_{SLP} + c\theta s\phi z_{SLP} & -c\theta x_{SLP} - s\theta s\phi y_{SLP} - s\theta c\phi z_{SLP} & -1 \end{array} \right|_{\substack{\text{nominal} \\ \theta = 0 \\ \phi = 0}}$$

$$T_{ESC} = \left| \begin{array}{ccc} 0.0 & -16.0 & 0.0 \\ 16.0 & 0.0 & 0.0 \\ 0.0 & 175.0 & -1.0 \end{array} \right|$$

TABLE (2.6.4.2)

The output matrix C_S is given in Table (2.6.2.2). The first three outputs are the landing pad position, formed by first scaling the position states by S_{S1}, and then transforming them to give the pad coordinates. Similarly, the rates are obtained by scaling the rate states by S_{S2}, and then transforming them to give pad position velocities. The second and fourth triplets of outputs are the angular orientations and rates. S_{S1} and S_{S2} do the scaling. However, the third element for height is zeroed, so the third element represents yaw orientation or rate; hence the notation S^*_{S1} and S^*_{S2}.

2.6.5 Overall Wave-Ship Model Verification

Qualitative features of the ship motion model behavior are verified in this section.

Typical time histories of ship motions in seaways are available for various ships and sea conditions. A typical pitch motion trace for a ship in a seaway is taken from reference (16), and redrawn in Figure (2.6.5.1). No time scale was given for this trace in the reference. Nevertheless, two characteristics may be noted. First, the period is very regular; and second, the pitch amplitude varies quite irregularly. The regularity of the period corresponds to the concentration of power in the ship motion power spectral density almost entirely at the natural frequency. For comparison, a segment of a simulation of the wave-ship model is also shown in the figure. Qualitatively, the simulation trace displays the same two characteristics as the actual ship motion.

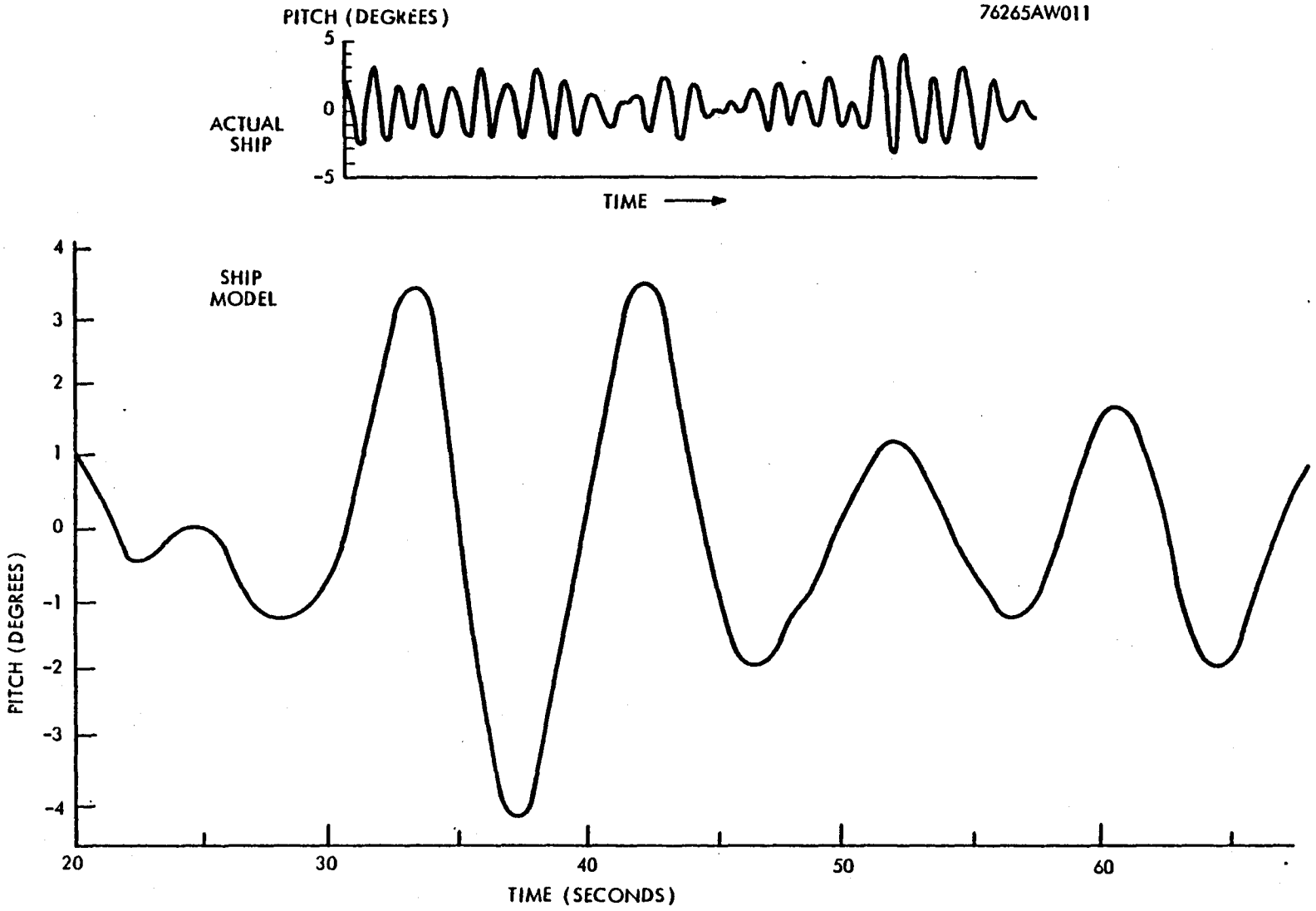

Comparison of Pitch Motion of an Actual Ship in a Seaway and the Ship Model Simulation

Figure 2.6.5.1

2.6.6 Low Order Ship Motion Model

This section describes a simpler model for ship motion. In the hover control chapter, it is used in a comparison demonstrating the effect of modelling accuracy on hover control performance. Historically, this model preceded the separate cascaded wave and ship models of the previous sections. Those models were formulated when the low order model was found to be an insufficiently accurate representation of typical ship motion. The problem with this model is that it provides a relatively broad passband of motion energy, while true ship motion actually occurs in a quite narrow passband. A comparison between the two models is shown in Figure (2.6.6.1).

In the low order model, each mode of ship motion (designated by i), is assumed to be driven directly by an independent, zero mean, gaussian, white noise ρ_i of intensity 1.0. The response i to input i is second order with transfer function:

$$\frac{\text{response i}}{\text{input i}}(s) = \frac{g_i s}{(s^2 + 2\xi_i \omega_{ni} s + \omega_{ni}^2)} \qquad (2.6.6.1)$$

The natural frequency ω_{ni} is chosen as 0.52, 0.97 and 1.0 radians/second for roll, pitch and heave, respectively. These values are according to references (22) and (7). The gain g_i is set so the root mean square output amplitudes would be 5 degrees, 2 degrees and 5 feet, as done in reference (7) and in the standard model. The damping ratio ξ_i is set to a small value, 0.05, to give a highly tuned second order response. The resulting algebraic form is identical to that for the regular ship

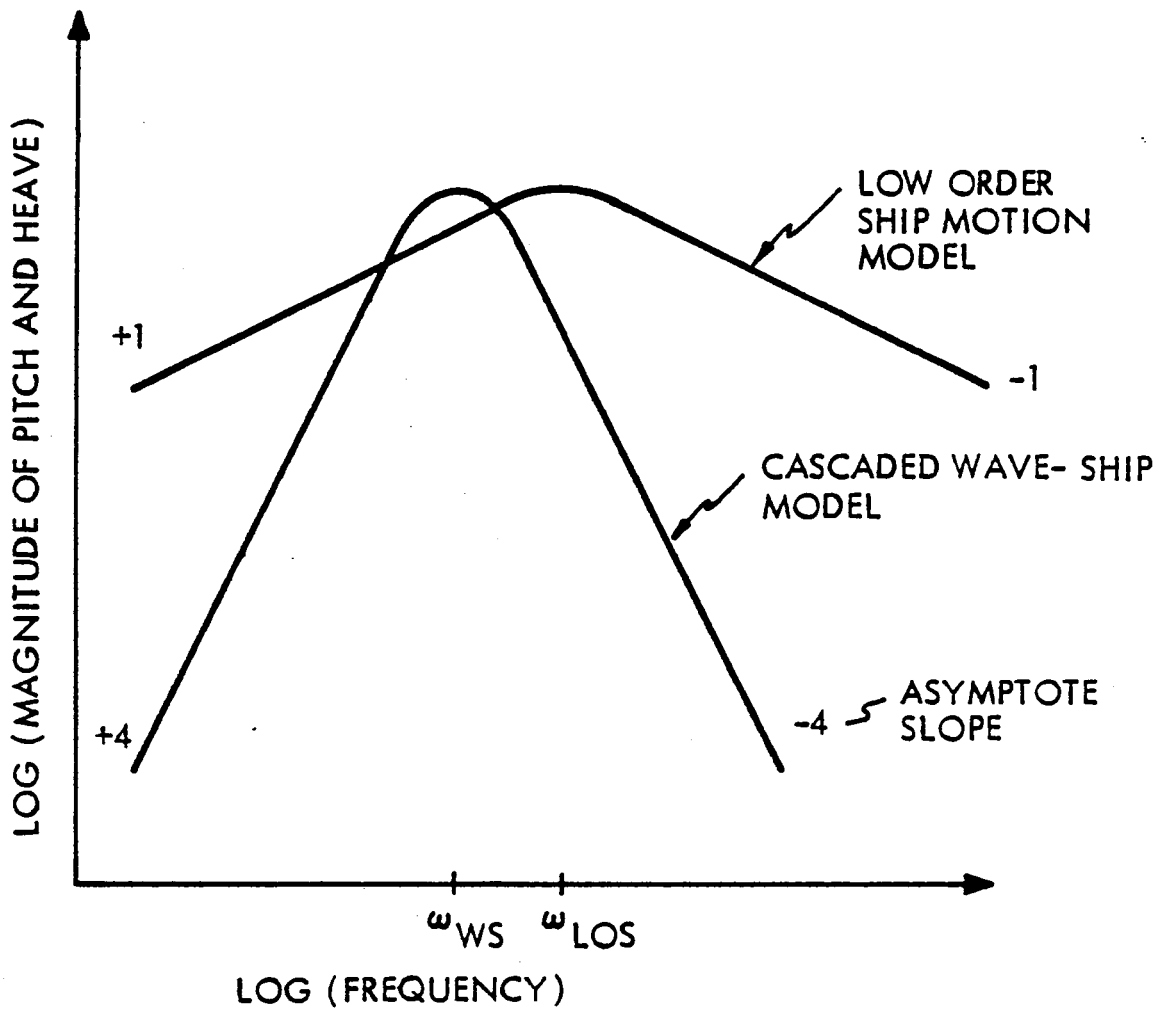

Ship Motion Model Comparison

Figure 2.6.6.1

model shown in Table (2.6.2.1), with the exception that the input is no longer $(y_{RW}, y_{PW}, y_{HW})^T$, but $(\rho_R, \rho_P, \rho_H)^T$. The output equation is also the same. The final low order ship model dynamics are shown in Table (2.6.6.1). Since the output equation is the same as in Table (2.6.2.2), it is not repeated here.

LOW ORDER SHIP MODEL DYNAMICS

$$\dot{\underline{x}}_S = A_S \underline{x}_S + B_S \underline{\rho}_S$$

$$\begin{vmatrix} \dot{x}_{R1} \\ \dot{x}_{R2} \\ \dot{x}_{P1} \\ \dot{x}_{P2} \\ \dot{x}_{H1} \\ \dot{x}_{H2} \end{vmatrix} = \begin{vmatrix} 0 & 1 & 0 & 0 & 0 & 0 \\ -0.275 & -0.0524 & 0 & 0 & 0 & 0 \\ 0 & 0 & 0 & 1 & 0 & 0 \\ 0 & 0 & -0.935 & -0.0967 & 0 & 0 \\ 0 & 0 & 0 & 0 & 0 & 1 \\ 0 & 0 & 0 & 0 & -1.02 & -0.101 \end{vmatrix} \begin{vmatrix} x_{R1} \\ x_{R2} \\ x_{P1} \\ x_{P2} \\ x_{H1} \\ x_{H2} \end{vmatrix} +$$

$$\begin{vmatrix} 0 & 0 & 0 \\ 1 & 0 & 0 \\ 0 & 0 & 0 \\ 0 & 1 & 0 \\ 0 & 0 & 0 \\ 0 & 0 & 1 \end{vmatrix} \begin{vmatrix} \rho_R \\ \rho_P \\ \rho_H \end{vmatrix}$$

TABLE (2.6.6.1)

CHAPTER 3

HOVER CONTROL

3.1 Introduction

In this chapter, a hover controller design for the VTOL aircraft vertical and pitch dynamics is developed. The purpose of the controller is to hover the aircraft at a constant vertical distance above the landing pad of the ship. Both of these vehicles are described in the modelling chapter. The challenge to the controller is the random motion of the ship, which cannot be predicted exactly. For this problem, as it will be defined in this chapter, the derived design is optimal. There is no other design solution whose performance would be better. However, this does not exclude a redefinition of the problem to obtain another more desirable design. A second problem and approach are in fact recommended here, and investigated in the next chapter. The recommendation comes about because the design solution of this chapter is representative of the optimal design under idealistic assumptions, and could easily become unacceptable under realistic conditions

This chapter has three main parts. They are: the design goals, the method to achieve the goal, and the results of the hover controller design. The first part explains the goals of hover control, including the basic assumptions and the theoretical tools available for the controller design. The second part explains how the assumptions and theory are employed in the design method. Finally, the third part discusses the results and how well they achieve the desired goal.

3.2 Control Problem Definition

3.2.1 Design Goals

The design goal is to determine an aircraft, shipboard landing technique based on modern control theory. An important constraint is that the technique should require only a small amount of thrust control authority. In this chapter, the goal is posed as a tracking problem. The aircraft is to hover at a constant separation above the ship deck, as illustrated in figure (3.2.1.1). In this task, it is desired to minimize the deviation of the aircraft from its desired tracking position. The steady state linear quadratic gaussian (SSLQG) regulator gives the optimal solution to this tracking problem when both the aircraft and ship equations of motion are linearized about their nominal operating point; and their separation is defined as an output for which a quadratic cost function is chosen. The SSQLG regulator solution provides a steady state control law which minimizes this cost in the presence of gaussian white plant noise. No other control can reduce the cost further.

3.2.2 Assumptions

Certain assumptions in addition to those made in the linearized model are useful. The model gives linear equations for the aircraft dynamics near stationary hover, and for the ship moving at a constant velocity in ocean waves. To simplify the control design and analysis, the following additional assumptions are made.

The first assumption is complete state measurement. This not

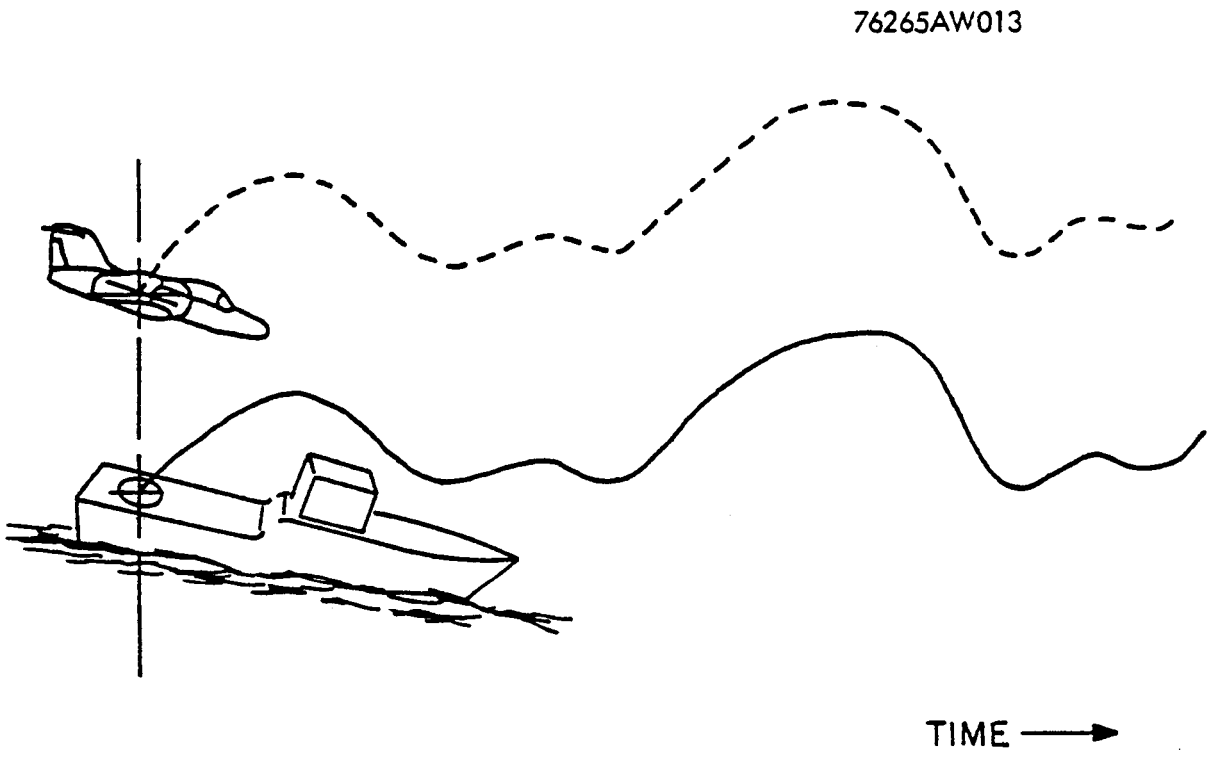

Hover Control Goal: Constant Aircraft-Ship Separation and Orientation

Figure 3.2.1.1

only simplifies the control dynamics, but is an important key to the interpretation of results as being representative of the "best theoretically achievable" performance. Under practical circumstances, measurements are made with noisy sensors of quantities related to, but not necessarily identical with, the ones of interest. For feedback control, the elements of the system state are the desired quantities. Thus, an estimator such as a Kalman filter is generally required to estimate the quantities. The form of the estimator depends on the measurements available. In general, it introduces additional dynamics into the overall system, retarding the overall system response. By assuming that uncorrupted state measurements are directly available, the estimator is not necessary and the best possible performance is achieved. Results presented here should therefore be interpreted as lower performance bounds not necessarily attainable in practice.

The second assumption concerns lateral-longitudinal decoupling. For the ship model, this assumption is justified in Chapter Two, where the ship is represented as two separate decoupled systems, with roll motions entirely separate from pitch and heave motions. As noted in Chapter Two, this is common practice in ship motion modelling. The aircraft model, on the other hand, is not constructed with separate longitudinal and lateral directional dynamics (although that is also common procedure for conventional aircraft (9)). Indeed, the linear aircraft model exhibits some coupling terms between the two types of dynamics. However, these terms are quite weak and can be neglected for most early analysis.

The next level of assumption is that forward horizontal aircraft dynamics do not couple into vertical translation and pitch orientation dynamics. This may also be verified by refering back to the aircraft model. Hence, the aircraft is left with only vertical and pitch motion dynamics for the design and evaluation.

Finally, as an aid to simplifying the design procedure, it is sometimes assumed that vertical and pitch dynamics also decouple. This is a much cruder approximation and is retained only to make certain design decisions and not for the design evaluation.

3.2.3 Optimization Problem

The optimal controller for the tracking problem is presented in this section. Since the system is linear, with additive gaussian white plant noise, and the performance index can be expressed as a quadratic cost function defined over an infinite time interval; the steady state linear quadratic gaussian (SSLQG) regulator is the optimal controller.

The SSLQG optimal controler problem and solution is given in references (23) and (24). It can be stated as follows:

Find a feedback control law $\underline{u}(t) = \underline{u}(\underline{x}(t))$ to minimize the quadratic cost functional,

$$J(u) = E \{ \lim_{T\to\infty} \frac{1}{T} \int_0^T (\underline{y}^T(t)Q\underline{y}(t) + \underline{u}^T(t)R\underline{u}(t)dt \} \quad (3.2.3.1)$$

subject to the constraints ,

$$\dot{\underline{x}}(t) = A\underline{x}(t) + B\underline{u}(t) + B_N\underline{\rho}(t) \quad (3.2.3.2)$$

$$\underline{y}(t) = C\underline{x}(t) \quad (3.2.3.3)$$

where (A, B) is stabilizable,

(A, C) is detectable,

ρ is a gaussian white noise process,

and $E\{\cdot\}$ is the expectation operator.

$Q = Q^T > 0$ is the per unit time quadratic cost associated with the response of y(t),

$R = R^T > 0$ is the per unit time quadratic cost of the control u(t).

The form of the feedback control $\underline{u}(\underline{x}(t))$ is also given in the above references. $\underline{u}(\underline{x}(t))$ follows:

The cost functional J is minimized by,

$$\underline{u}(\underline{x}(t)) = G\underline{x}(t) = -R^{-1}B^TP\,\underline{x}(t) \qquad (3.2.3.4)$$

where P is the unique symmetric positive semidefinite solution of the matrix algebraic Riccati equation (MARE),

$$0 = PA + A^TP - PBR^{-1}B^TP + Q \qquad (3.2.3.5)$$

Note that for given system state and response equations (3.2.3.2) and (3.2.3.3), an SSLQG regulator design is uniquely determined by the response and control vector quadratic cost weighting matrices Q and R. Also note that the control problem formulated above is a special case of the more general one where A, B, B_N, C, Q, and R are time varying.

The implementation of the feedback gains results in a closed loop system whose state equation is written:

$$\dot{\underline{x}} = (A - BR^{-1}B^{T}P)\underline{x} + B_N\underline{\rho} \qquad (3.2.3.6)$$

or using the notation:

$$A_{CL} = A - BG = A - BR^{-1}B^{T}P \qquad (3.2.3.7)$$

the state equation becomes:

$$\dot{\underline{x}} = A_{CL}\underline{x} + B_N\underline{\rho}$$

In the overall system of the aircraft, ship and waves; only the aircraft is controllable. Therefore, the closed loop system matrix, A_{CL} has the form shown in Table (3.2.3.1), where:

A_A is the aircraft open loop system matrix,

A_S is the ship system matrix,

A_{OW} is the ocean wave system matrix,

B_A is the aircraft input matrix,

G_A is the matrix by which the aircraft states are fed back to the aircraft controls,

G_S is the ship state vector feedforward matrix to the aircraft,

G_{OW} is the ocean wave state vector feedforward matrix to the aircraft.

Figure (3.2.3.1) is a block diagram of the hover controller. In the figure, the ocean wave and ship models are combined for compactness. A_{WS}, B_{WS} and C_{WS} represent the combined ocean wave and ship state vector feedforward matrix.

For the hover control problem having only vertical and pitch dynamics, the following correspondences are also made to the general

OVERALL CLOSED LOOP SYSTEM MATRIX

$$A_{CL} = [\, A - BG \,]$$

$$G = [\, G_A \mid G_S \mid G_{OW} \,]$$

$$A_{CL} = \left|\begin{array}{c|c|c} A_A + B_A G_A & B_A G_S & B_A G_{OW} \\ \hline 0 & A_S & A_{WS} \\ \hline 0 & 0 & A_{OW} \end{array}\right|$$

TABLE (3.2.3.1)

76265AW014

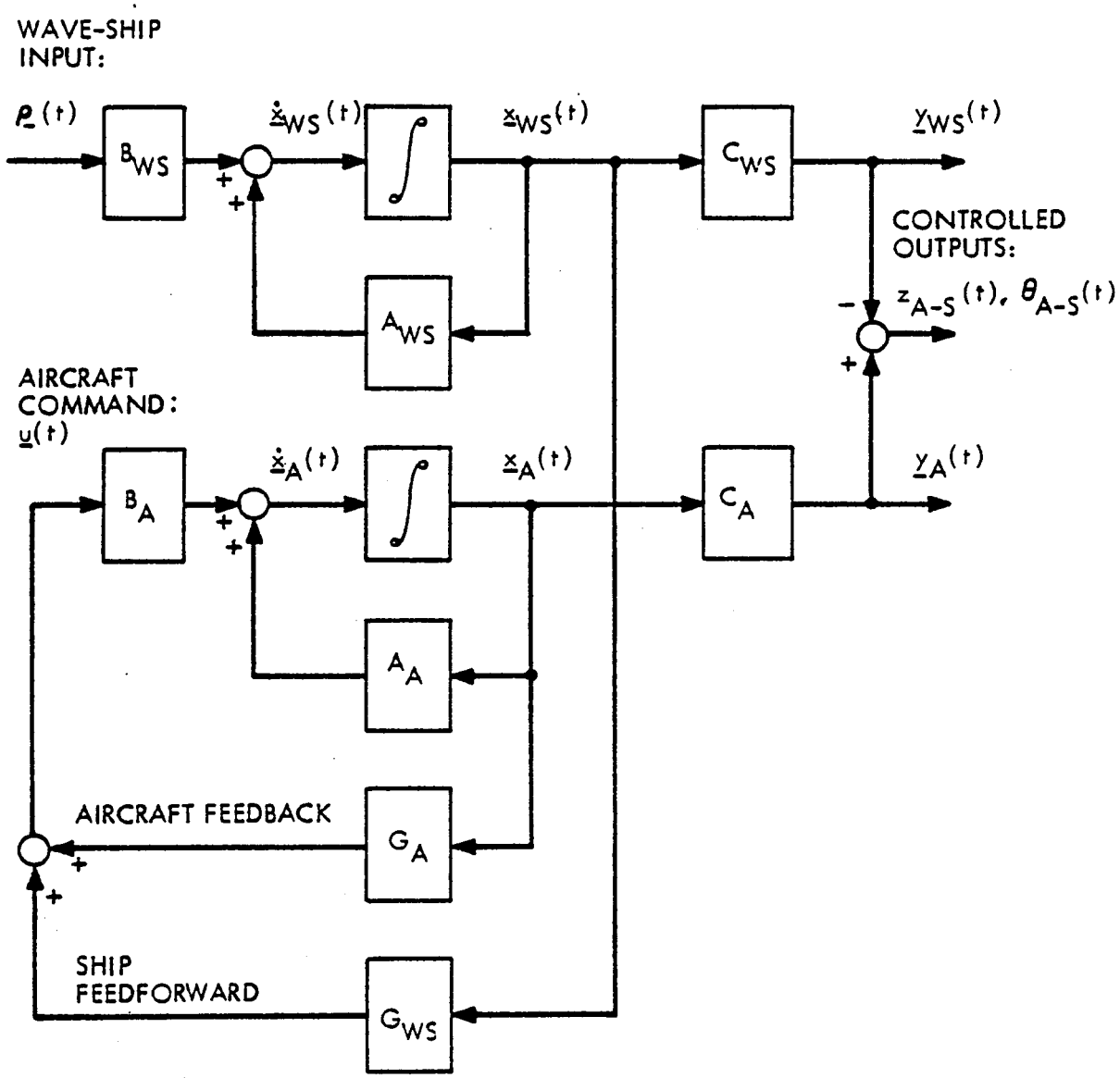

Hover Controller Block Diagram

Figure 3.2.3.1

control problem stated above. $\underline{\rho}$ is the zero mean, gaussian, white noise driving the wave model. $\underline{u}$ is the control vector driving the aircraft. Note, $\underline{u}$ has two elements, altitude control and pitch control. In the quadratic weighting matrix R, these are weighted by $r_{\delta Z_A}$ and $r_{\delta\theta_A}$. The response $\underline{y}$ for ship tracking is chosen as shown:

$$\underline{y} = \begin{vmatrix} z(\text{aircraft}) - z(\text{ship deck}) \\ \theta(\text{aircraft}) - \theta(\text{ship deck}) \end{vmatrix} = \begin{vmatrix} z_{A-S} \\ \theta_{A-S} \end{vmatrix} \qquad (3.2.3.8)$$

Therefore, the controlled variables are the vertical position and pitch orientation tracking errors of the aircraft with respect to the ship. The corresponding diagonal elements of Q are $q_{Z_{A-S}}$ and $q_{\theta_{A-S}}$. The weighting $q_{Z_{A-S}}$ causes the vertical position of the aircraft to match that of the ship. A constant non-zero separation, however, does not change the system dynamics, so Z_{A-S} may be viewed as the deviation of the aircraft from its desired position with respect to the ship. $q_{\theta_{A-S}}$ likewise causes the aircraft to match the ship's pitch attitude.

3.3 Controller Design and Evaluation Method

3.3.1 Design Method

This section discusses how the assumptions and theory are employed in the design procedure. The design procedure begins with the design of a basic hover controller for the case of a stationary ship deck. That is, for the case when the ship has no motion. This design is developed in

two steps. The first step is to get a controller for the pitch dynamics only. The second step is to use this design for pitch, and determine the additional controller structure needed to get a satisfactory controller for coupled pitch-heave dynamics. The basic design's quadratic weightings are then used to handle the ship motion tracking problem. The aircraft model is augmented by the ship and wave models, and the aircraft altitude and pitch quadratic cost weightings are transfered to the aircraft-ship separation and orientation outputs. By varying the two output weightings in unison, controller designs are obtained that reflect the relative importance of tracking performance compared to control effort cost.

Design method details follow. In the basic design, both pitch and vertical control are weighted by unity. For complete design freedom, these could be varied independently. However, since the pitch and vertical dynamics of the aircraft are approximately uncoupled, the pitch-heave control problem can be separated into a vertical control problem and a pitch control problem. In each of these, the important quantity is the relative weighting of output to input. Hence, the choice of unity control weightings. Note that in particular, the vertical dynamics do not affect the pitch dynamics, so the results of step two do not alter those of step one.

The two step design method generates a basic controller that is completely determined by two output and two control weightings. The basic design is for hover control, that maintains the aircraft in a horizontal attitude over a fixed ship deck at a constant vertical separation. The commanded separation is defined to be zero for convenience.

A suitable basic pitch control design is one having a response bandwidth typical of piloted fighter aircraft. Reference (9) gives pilot ratings versus aircraft handling qualities. Bandwidths suitable for manual control were chosen, because aircraft behaving significantly different under automatic and manual control, or unlike conventional aircraft, may receive poor pilot acceptance. In fact, similar manual/automatic behavior may be a safety consideration, required to prevent undesirable transients in situations where the pilot is forced to switch from automatic to manual control. Of course, for good ship motion tracking, the bandwidths must also be at least as large as the dominant ship motion frequencies.

For making bandwidth estimates, the Butterworth pole pattern is useful. An explanation follows. Pitch and heave dynamics are two approximately uncoupled, third order, single input-single output sytems (pitch control input and pitch output and altitude control input and altitude output). (As usual, all states are assumed to be available for feedback control.) Neither has transfer function zeroes, and so the SSLQ regulator produces third order Butterworth pole patterns for each. These patterns are generated by varying the relative quadratic cost weighting magnitudes of the input and output. As the output weighting is increased, the poles approach a common magnitude and move radially outward from the origin along asymptotes. A detailed explanation can be found in reference (23). Since the poles of such Butterworth patterns all have the same magnitude, this magnitude is used as a convenient measure of system bandwidth. In addition, the Butterworth pattern is

useful for design because it indicates that by increasing the output weighting, while holding the input weighting constant, the closed loop system disturbance rejection bandwidth can be made as wide as desired.

To adapt the basic design to track a moving ship deck, the system is first augmented to include the ship and wave states of interest. For the ship, pitch and heave states are required, and for the waves a complete model with the pitch and heave outputs is needed. Secondly, the penalty weightings are transfered to the aircraft to ship relative pitch and vertical separation. They become $q_{\theta_{A-S}}$ and $q_{Z_{A-S}}$. The weightings determined for the basic design now only indicate estimates of the ones required. However, the determination of these basic weightings provides useful experience in estimating the magnitude of weighting changes in the quadratic cost functional and the corresponding performance changes. The final choice of $q_{\theta_{A-S}}$ and $q_{Z_{A-S}}$ is made by scaling them both simultaneously. Since these are the only non-zero elements of the Q matrix, this is just a scaling of Q. Scaling Q to get a final design is an arbitrary, but convenient, choice, since it reduces the design parameters down to one. In addition, by varying all of Q simultaneously, the relative importance of pitch and heave performance is maintained.

Having described the design method, it is appropriate to discuss how designs are evaluated. This is the topic of the next section.

3.3.2 Performance Evaluation Method

Quantities like tracking error, control effort, and bandwidth are of interest in deciding the acceptability of a tracking controller.

Several of these can be estimated from the steady state covariance equation, while bandwidth can be obtained from the system pole locations.

The list of quantities calculated for controller performance evaluation follows:

(1) rms aircraft to ship relative vertical separation:

$$\sigma_{Z_{A-S}} \text{ feet}$$

(2) rms aircraft to ship relative vertical velocity:

$$\sigma_{\dot{Z}_{A-S}} \text{ feet/second}$$

(3) rms aircraft to ship relative pitch orientation:

$$\sigma_{\theta_{A-S}} \text{ degrees}$$

(4) rms aircraft to ship relative pitch rate:

$$\sigma_{\dot{\theta}_{A-S}} \text{ degrees/second}$$

(5) rms aircraft vertical control actuator authority:

percent of nominal

(6) rms aircraft vertical control rate of change:

percent of nominal/second

(7) vertical loop bandwidth: radians/second

The first six of these quantities are calculated from the steady state covariance equation for the outputs and states. In evaluation, three root-mean square (3rms) values are used, since they are rarely exceeded. The last quantity, vertical loop bandwidth is the magnitude of the closed loop system eigenvalues associated with the vertical dynamics. Recall that this bandwidth estimate is by virtue of the Butterworth pole configuration discussed in the previous section. The

pitch loop bandwidth could be determined similarly. However, it is found that the pitch loop requirements of this system are relatively easy to satisfy compared to the vertical loop ones. As a result, only orientation and rate behavior are recorded for the pitch axis.

The steady state root-mean-square deviations of the outputs and states are determined by the following method (23, 25). Let $\underline{y}$ be the vector of quantities whose rms values are desired. Write $\underline{y}$ in terms of the state vector $\underline{x}$ as:

$$\underline{y} = C\underline{x} \tag{3.3.2.1}$$

The the covarinace matrix of $\underline{y}$ is given by:

$$\text{cov}(\underline{y}) = CPC^T \tag{3.3.2.2}$$

where

$$\text{cov}(\underline{x}) = P \tag{3.3.2.3}$$

In turn, P is the steady state solution of the covariance equation:

$$0 = \dot{P} = A_{CL}P + PA_{CL}^T + BVB^T \tag{3.3.2.4}$$

where A_{CL} is the closed loop system matrix, B the noise input matrix, and V the covariance intensity of the driving, zero mean, gaussian, white noise $\underline{\rho}$ of the closed loop system:

$$\dot{\underline{x}} = A_{CL}\underline{x} + B\underline{\rho} \tag{3.3.2.5}$$

The 1rms, 1-sigma, or 1 standard deviation values of $\underline{y}$ are just the square roots of the diagonal elements of cov($\underline{y}$). 1-sigma values, however, are not themselves indicative of the maximum excursions of the elements. From probability theory, it is known, that for a gaussian random variable,

the percentage of outcomes within 1, 2 and 3 standard deviations of the mean is 68.3%, 95.4% and 99.7% respectively (computed using reference (26)). For ergodic stochastic processes, "percentage of the outcomes" can be substituted with "percentage of the time". For the plots presented in the design evaluation, 3rms values are chosen. These values are exceeded only 0.3% of the time, and are therefore conservative estimates of maximum or ultimate levels for design specifications.

3.4 Controller Design and Evaluation

3.4.1 Introduction

The following sections describe the hover controller design and evaluation. The first section discusses the basic controller for hover at a fixed point. As described earlier, this design is developed in two steps. The first step is the choice of a pitch dynamics controller. In the second step, vertical dynamics are included and a correspondingly augmented controller is chosen. The basic controller is converted and used as an initial ship motion tracking controller design in the subsequent section. That section reports on the tradeoff between tracking performance and control cost obtained from scaling the output weighting matrix of the quadratic performance index. Finally, a section is included on the effect of ship modelling accuracy. There, the performance results for a low order ship motion model are compared to the results obtained for the standard wave-ship model.

3.4.2 Quadratic Weights for the Basic Design

The two step scheme outlined in the design method section was used to choose a basic design for the hover control regulator.

Step one is the design of a pitch controller. This is designed as a single input controller with full state feedback by weighting the pitch control input and the pitch attitude output in the quadratic performance index. For each ratio of these weights, a set of feedback gains and closed loop pole locations is determined. The Butterworth pole pattern for this system is shown in Figure (3.4.2.1). The input weighting is unity as explained in the design method section, and the weight q_{θ_A} is 10.0. This gives closed loop pole location magnitudes and bandwidths of about 3 radians/second, which is typical of acceptable piloted aircraft responses (9).

Step two is the inclusion of vertical control. The system is now sixth order, with two inputs and two weighted outputs. However, the coupling between pitch and heave is not strong, so the choice of q_{Z_A}, the vertical position state weighting, does not influence the closed loop eigenvalues of the pitch dynamics. The pole location pattern for the vertical dynamics is shown in Figure (3.4.2.2). The vertical position weighting, q_{Z_A}, is chosen to be 0.01, giving a closed loop vertical response bandwidth of about 1.5 radians/second (Reference (7) suggests similar attitude and flight path dynamic bandwidths at 2.0 and 1.25 radians/second respectively.) The fact that vertical bandwidth is less than the pitch bandwidth reflects physical constraints. Attitude control power of the VTOL aircraft is obtained by rerouting power between the

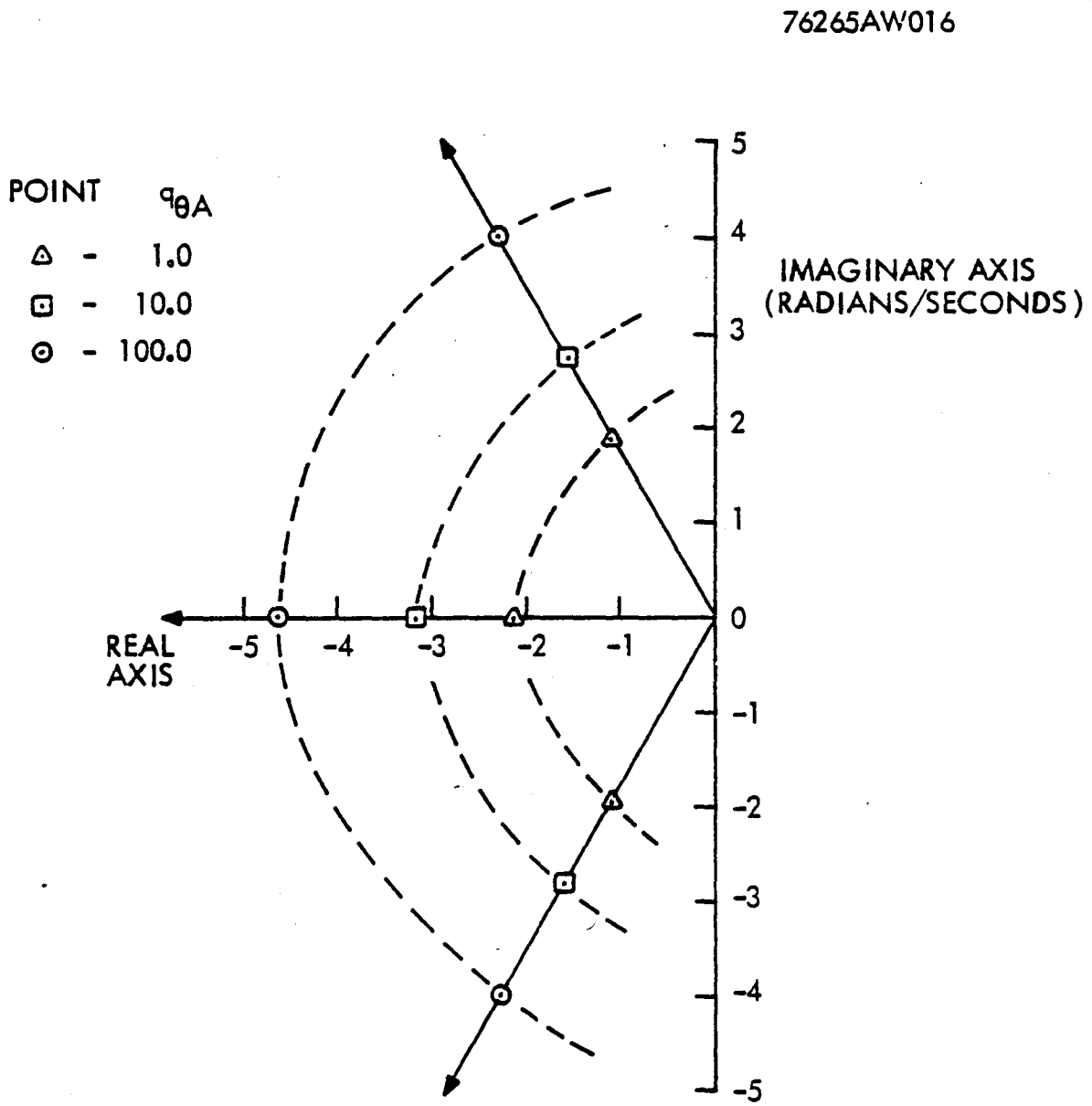

Butterworth Pattern for Aircraft Third Order Pitch Dynamics

Figure 3.4.2.1

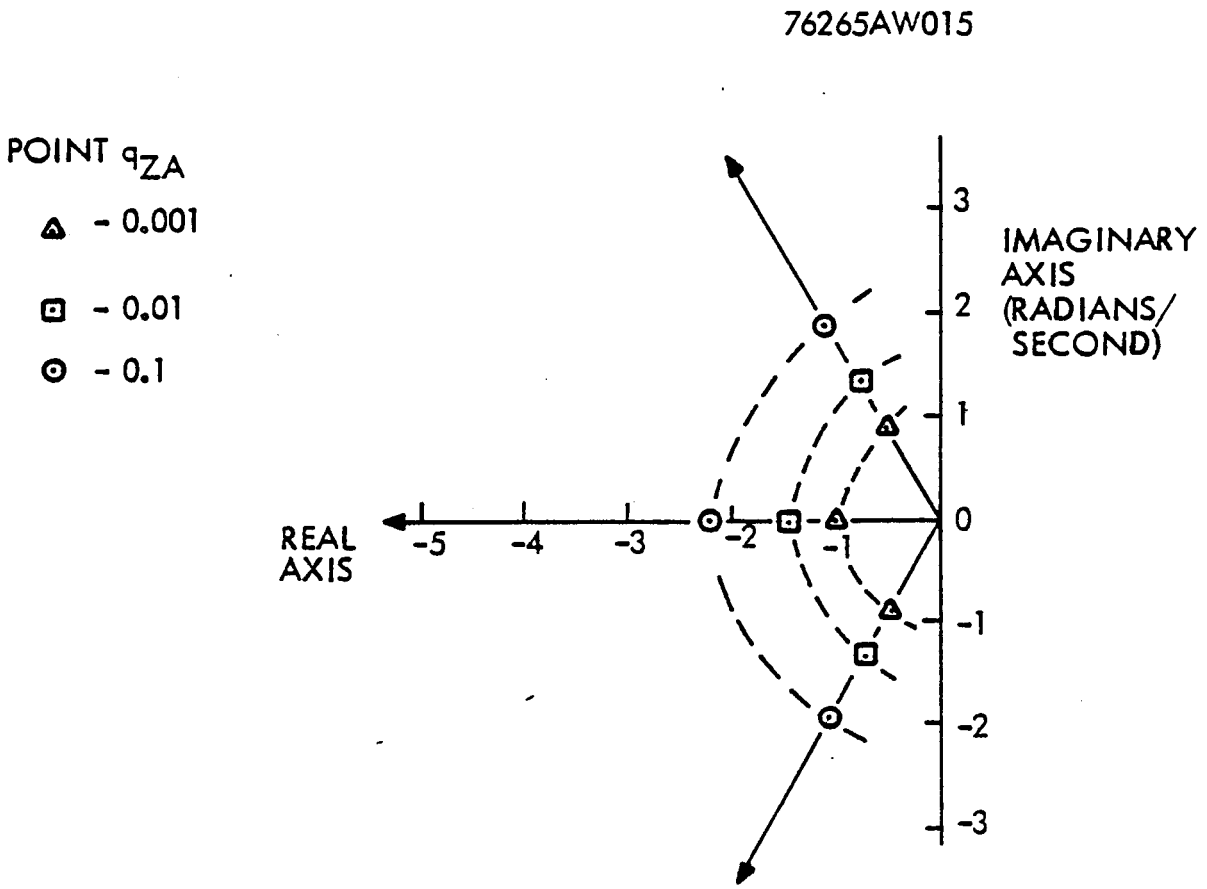

Butterworth Pattern for Aircraft Third Order Vertical Dynamics

Figure 3.4.2.2

fans, without requiring any change in the overall engine output power. This can be done relatively quickly. However, vertical control requires varying the engine output power, which is a slower process. In addition, vertical thrust is limited by the aircraft weight and maximum available engine thrust. This last constraint is expressed as a thrust to weight ratio, T/W. For stationary, undisturbed hover T/W is 1.0. Typically, experimental VTOL vehicles have a maximum T/W capability on the order of 1.05 to 1.3 (27 , 28).

The two weightings chosen above specify the initial point or basic design for the tracking controller. The latter has aircraft-ship relative pitch and vertical separation outputs as controlled responses. Thus, the initial quadratic weightings for the tracking hover controller are $q_{\theta_{A-S}} = 10.0$ and $q_{Z_{A-S}} = 0.01$.

3.4.3 Tracking Controller Performance

This section surveys the performance characteristics of the ship motion tracking hover controller. The basic design of the last section is the starting point for a study of the relation between tracking performance and control cost as quadratic ratios are varied. The covariance analysis and bandwidth estimation scheme described earlier shows how tracking errors go to zero and control effort becomes large, while the bandwidth and the weightings ratio increase.

These results are illustrated in the plots of Figures (3.4.3.1), (3.4.3.2) and (3.4.3.3). Each of these plots has aircraft vertical

76265AW017

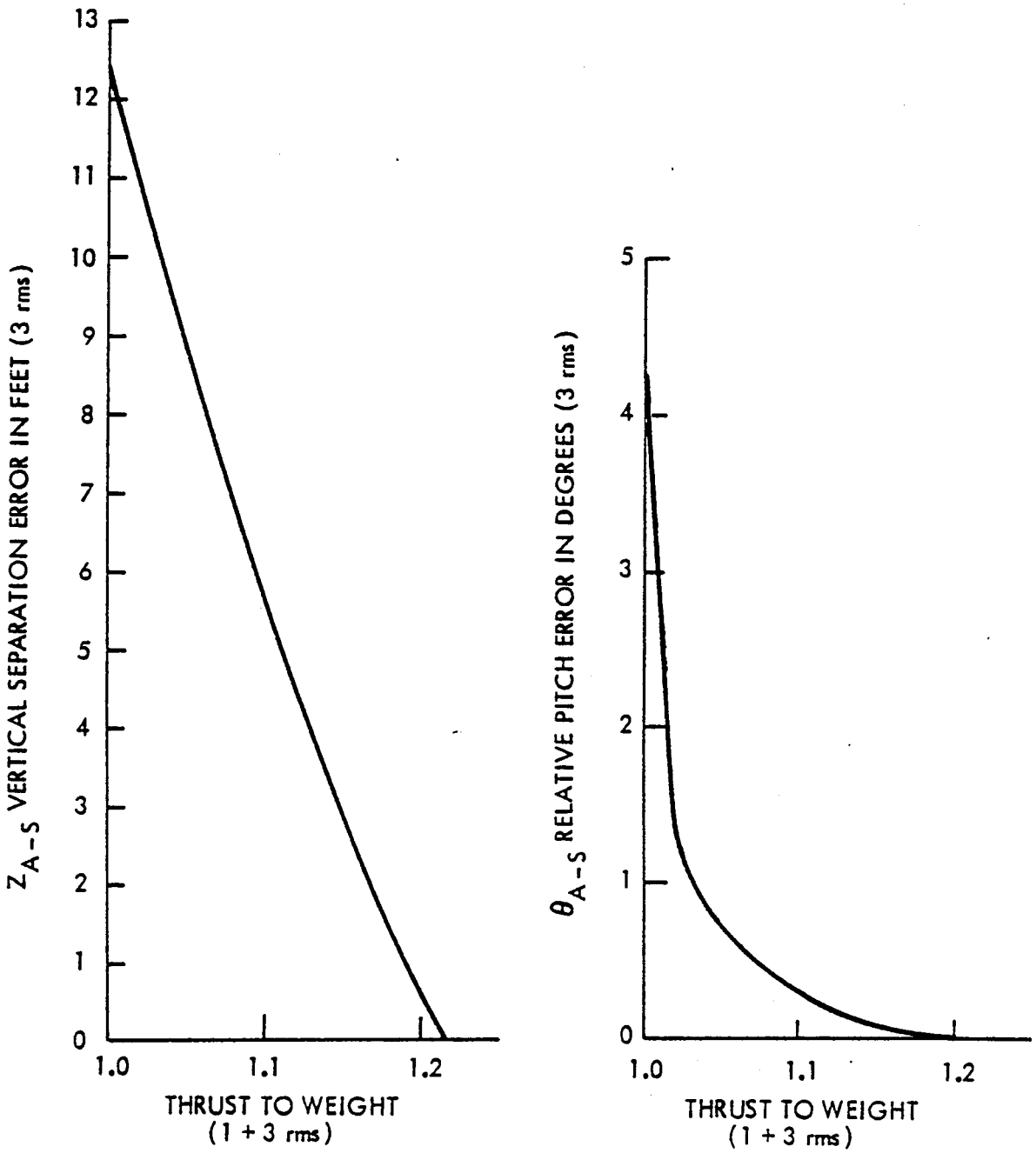

Hover Performance: Separation versus Thrust to Weight

Figure 3.4.3.1

76265AW018

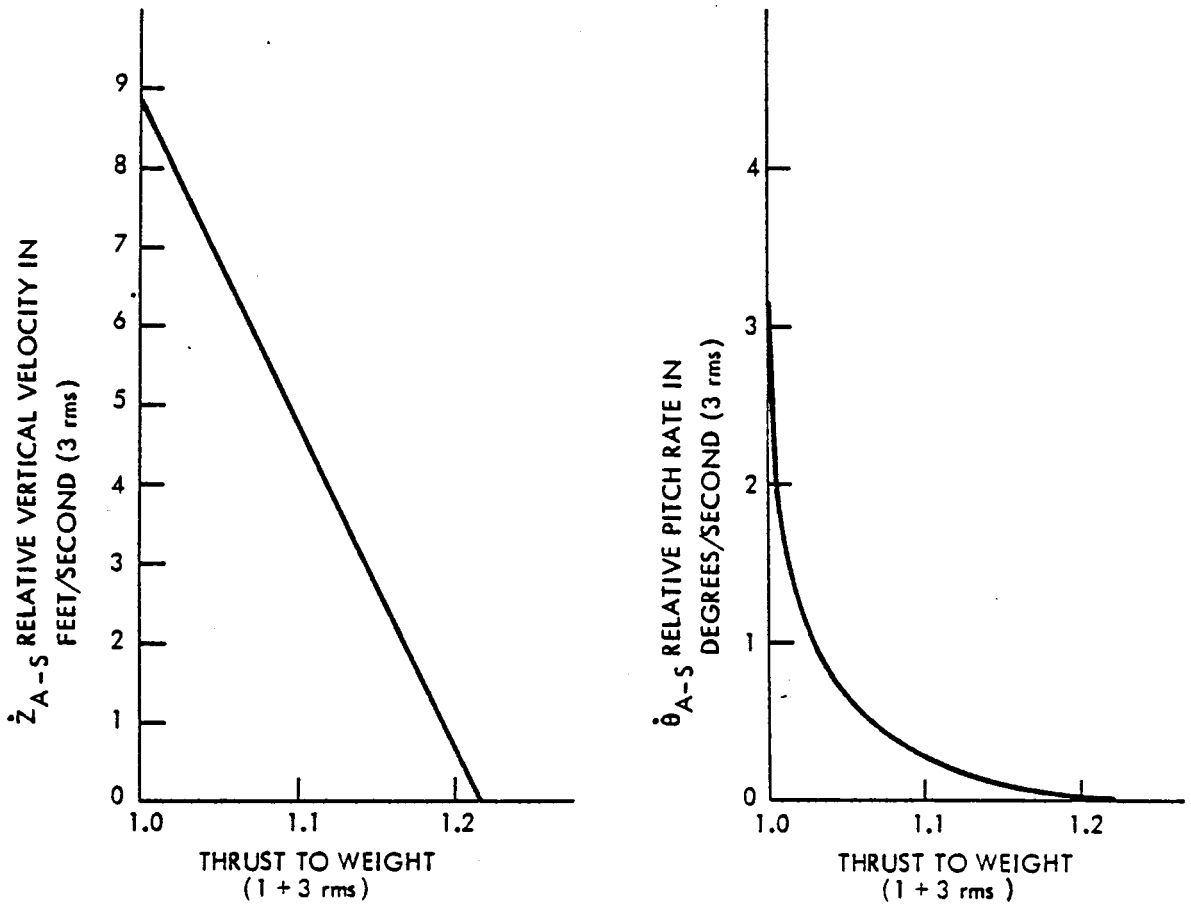

Hover Performance: Relative Velocity versus Thrust to Weight

Figure 3.4.3.2

76265AW019

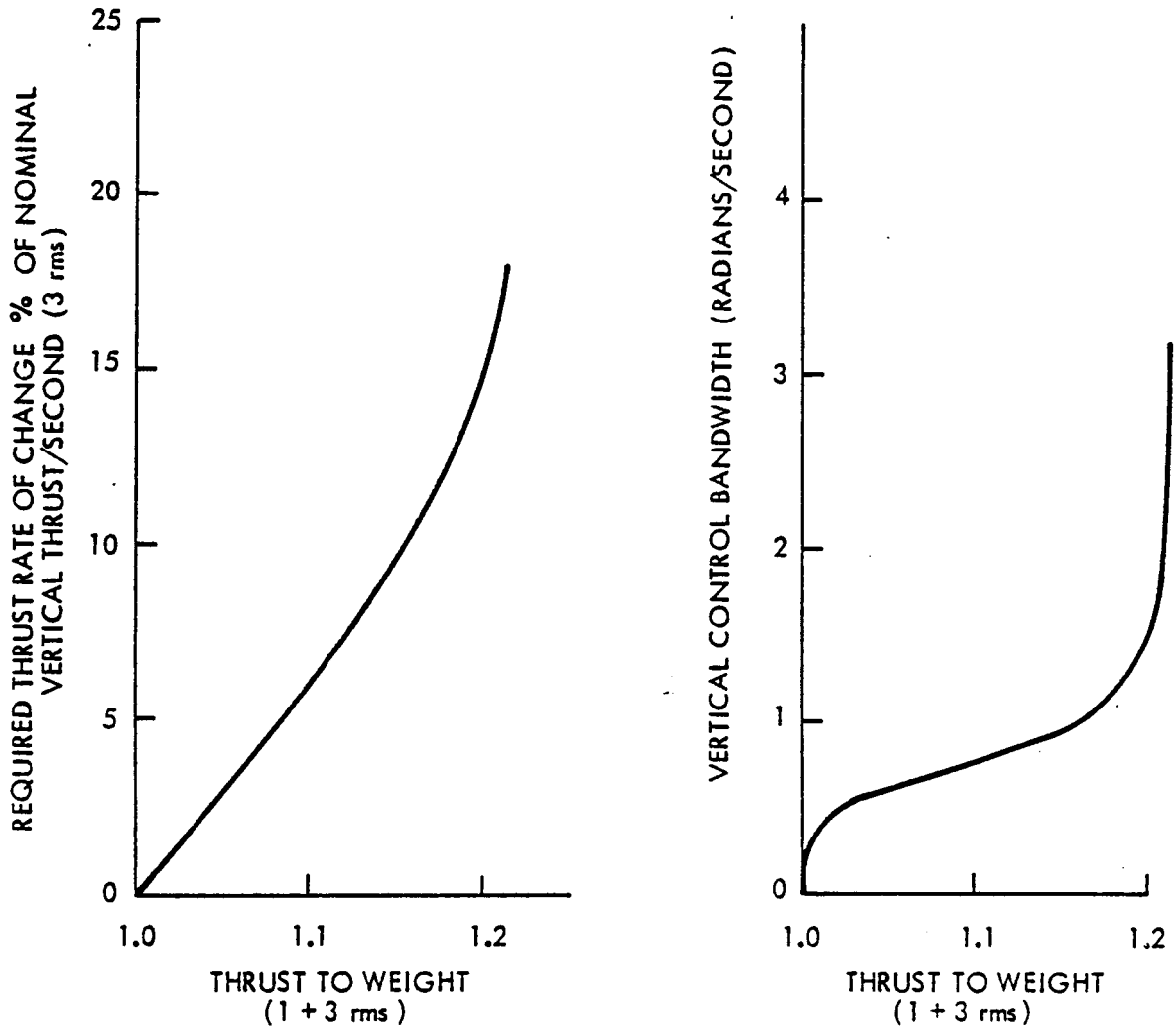

Hover Performance: Vertical Control Rate and Bandwidth versus Thrust to Weight

Figure 3.4.3.3

control actuator authority magnitude as the abscissa, and one of the other six quantities listed in section (3.3.2) as the ordinate. Control actuator authority is presented as aircraft thrust to weight ratio. This is defined as 1.0 (the thrust to weight for stationary, undisturbed hover), plus the 3rms actuator level (in fractions of the amount for stationary hover). The ordinate quantities z_{A-S}, $\dot{z}_{A-S}$, θ_{A-S}, $\dot{\theta}_{A-S}$, and vertical thrust rate of change are plotted as 3rms values. The vertical control bandwidth is taken as the vertical actuator eigenvalue magnitude in radians/second. The index along each curve is q, the ratio q equal to 1.0 gives the basic design. The output quadratic weighting matrix is given:

$$Q = \text{DIAG}\left[\, 0,\ q_{\theta_{A-S}},\ 0,\ q_{z_{A-S}},\ 0,\ \ldots,\ 0 \,\right] \qquad (3.4.3.1)$$

where

$$q_{\theta_{A-S}} = q \cdot 10.0 \qquad (3.4.3.2)$$

$$q_{z_{A-S}} = q \cdot 0.01 \qquad (3.4.3.3)$$

The control input quadratic weighting matrix is given:

$$R = \text{DIAG}\left[\, r_{\delta\theta_{A-S}},\ r_{\delta z_{A-S}} \,\right] = \text{DIAG}[\, 1.0,\ 1.0 \,] \qquad (3.4.3.4)$$

The first four of the plots indicate that as thrust to weight (T/W) is increased, the aircraft hover tracking performance improves. This trend corresponds to increasing the output weighting matrix magnitude q: the more heavily the position and orientation errors are penalized with respect to control, the smaller these errors are kept, and the more control and thus actuator effort is used.

Figure (3.4.3.3) indicates that at the same time tracking errors decrease and thrust to weight increases, the rate of change of thrust to weight (or actuator rates) increases. Similarly, the bandwidths of the aircraft dynamics increase.

The T/W = 1.0 point on the curves represents the condition when the aircraft is hovering at a fixed altitude. Separation errors are not weighted at all at this point, so vertical separation, relative velocity, pitch, and pitch rate are due only to ship motion. Thus, for example, the 3rms ship motion is 12.5 feet (above and below the mean).

The vertical control bandwidth curve has an interesting shape. It is quite flat near T/W = 1.1. In this region, the bandwidth of the aircraft vertical motion is between 0.5 and 1.0 radians/second. To explain this, note that the magnitude of the closed loop pole locations increase with the output weighting. On the other hand, T/W only increases at frequencies where ship motion has significant power. Therefore, bandwidth increases at low frequencies, but T/W does not. At ship motion frequencies, T/W increases significantly causing the curve to flatten. Then at high frequencies, where ship motions are small, T/W increases very slowly; however, bandwidth continues to grow and the curve rises sharply again.

To demonstrate tracking improvement due to increased thrust to weight, simulations are shown in figures (3.4.3.4) and (3.4.3.5) for two different output weighting magnitudes. Table (3.4.3.1) gives the parameters of these simulations. In the figures, the aircraft and ship motions are superimposed, so the difference represents tracking error as usual. (In

Design Parameters for the VTOL Tracking Simulations in Figures 3.4.3.4 and 3.4.3.5

Simulation	Output Weighting		Control Weighting		Thrust to Weight	Tracking error
	$q_{\theta_{A-S}}$	$q_{Z_{A-S}}$	$r_{\delta\theta}$	$r_{\delta Z}$	T/W (1 + 3 rms)	z_{A-S} (3 rms, feet)
1	0.1	0.0001	1.0	1.0	1.08	6.9
2	1.0	0.001	1.0	1.0	1.16	2.4

Table 3.4.3.1

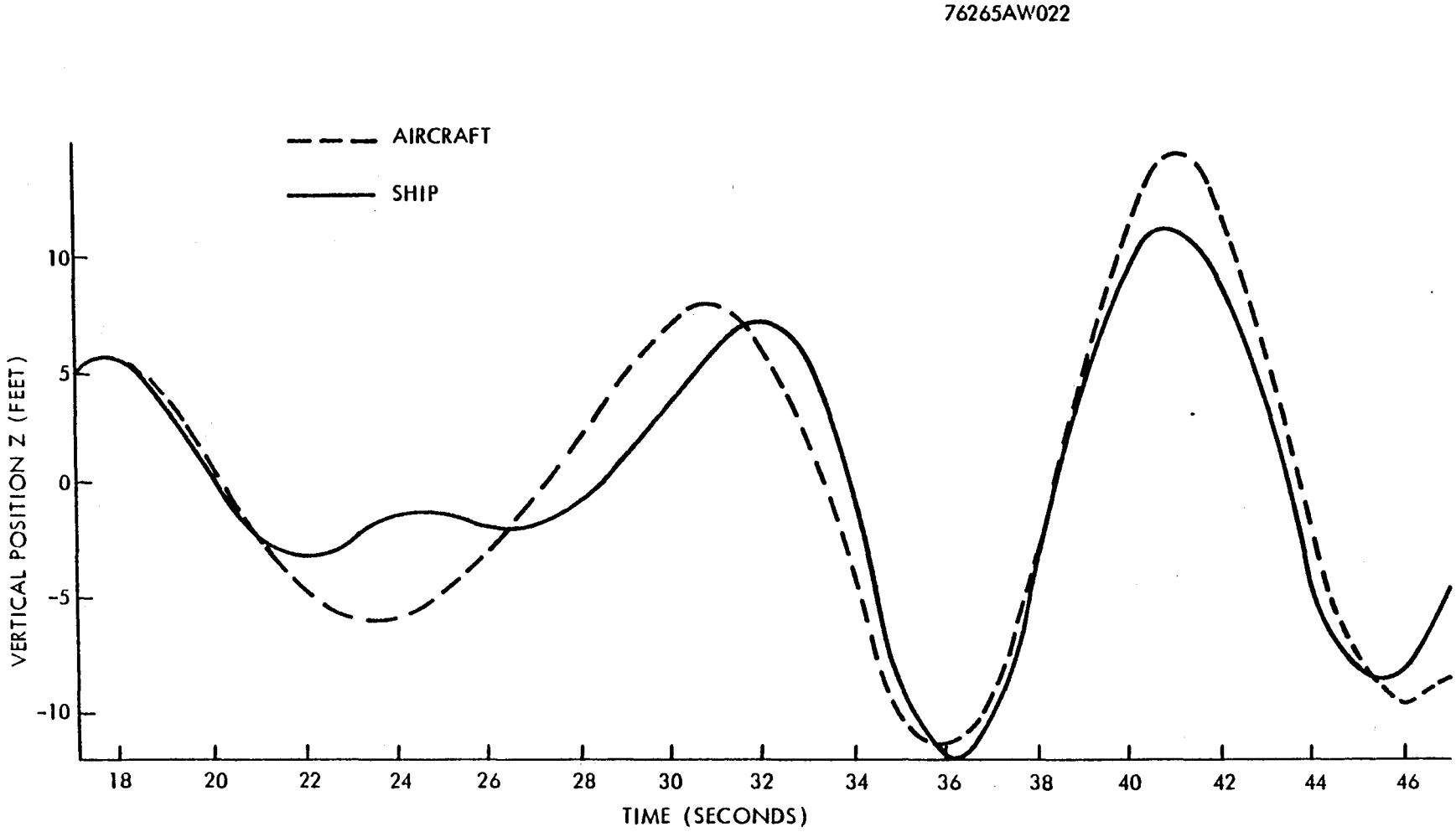

Tracking Simulation 1: Thrust to Weight = 1.08

Figure 3.4.3.4

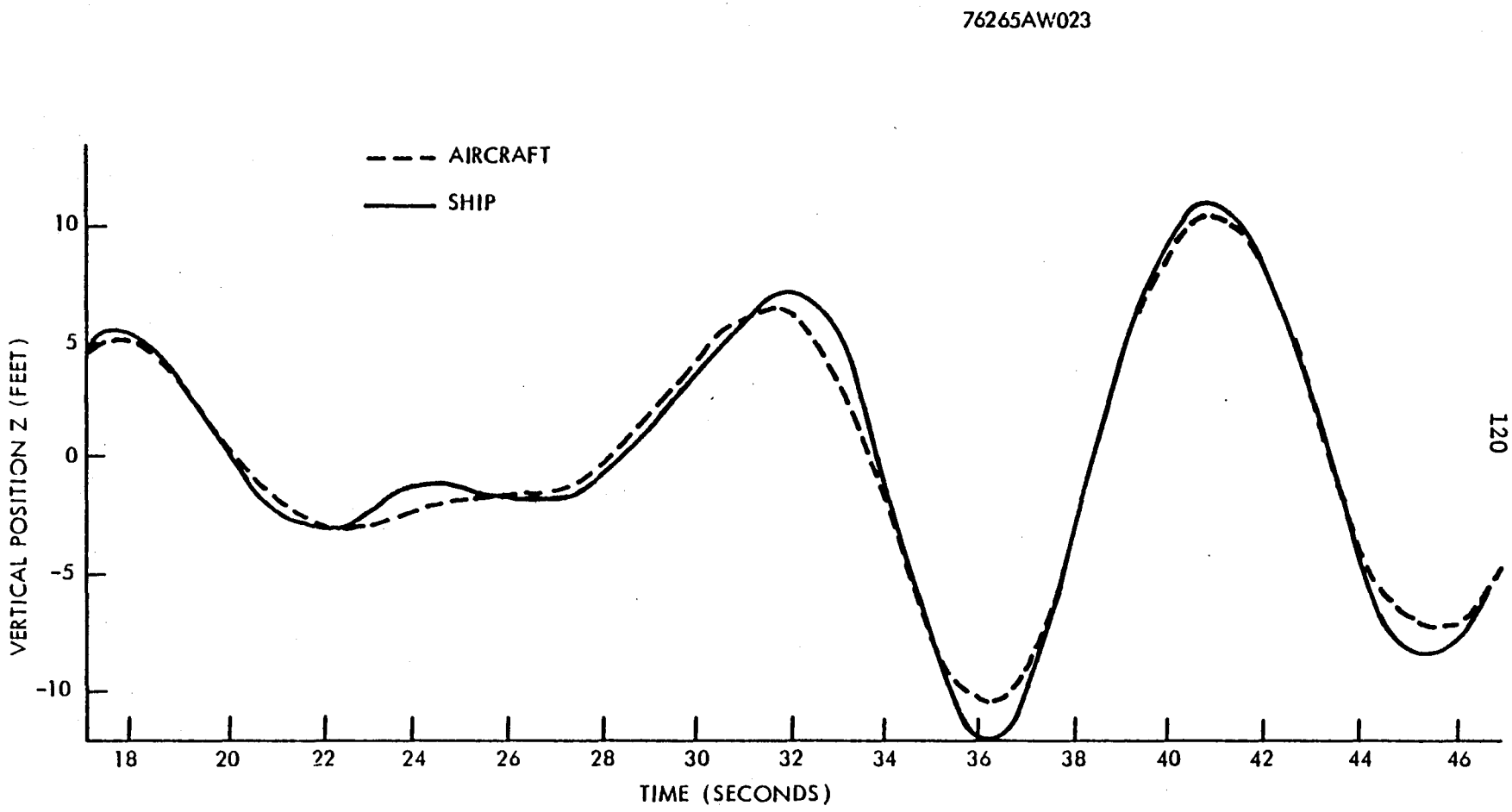

Tracking Simulation 2: Thrust to Weight = 1.16

Figure 3.4.3.5

a physical realization, a non-zero separation would be included, which would be slowly decreased to zero to achieve a landing.) As the table shows, the factor of 10 increase in the output weighting between these two simulations leads to a thrust to weight increase of a factor of 2, from 8% to 16% control authority. At the same time, the corresponding vertical tracking error decreases by a factor of about 3. The simulation plots clearly illustrate this tracking improvement.

3.4.4 Sensitivity to Ship Modelling Accuracy

This section presents evidence that the accuracy of ship motion modelling significantly affects the performance capabilities of the tracking controller.

The performance curves obtained to this point have been for a ship-wave model whose longitudinal dynamics are tenth order, and approximate ship responses to waves having a Neumann ocean wave spectrum. However, before this model was developed, a less sophisticated fourth order model was used. Both the tenth order "standard model" and the fourth order "low order model" are described in Chapter Two.

Figure (3.4.4.1) gives the vertical separation error versus thrust to weight for tracking the low order model. The first difference to be noted is that at T/W = 1.0, the separation, again due to ship motion alone, is almost 17 feet (3rms) rather than the 12.5 feet (3rms) for the standard model. This is because pitch and heave motions in the low order model are independent, and so their effect on the landing deck motion variance is additive. In the standard ship-wave model, these motions

76265AW020

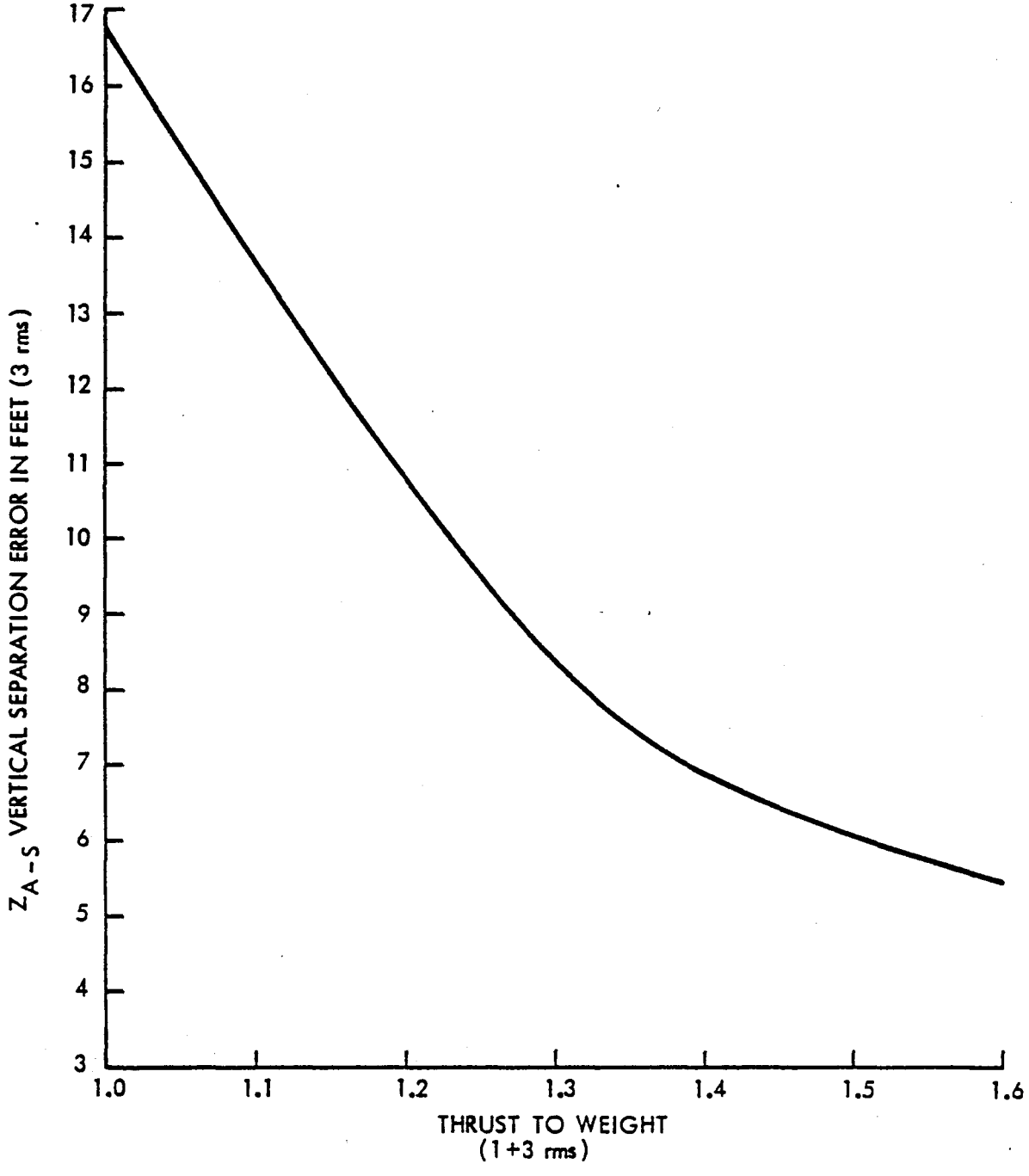

Hover Performance: Separation versus Thrust to Weight for Low Order Ship Model

Figure 3.4.4.1

are correlated in a way that yields less motion at the landing deck. The other difference is the rate at which tracking error is decreased with increased thrust to weight. This rate is very slow for the low order model. The reason for this behavior is that the spectrum of ship motions for the simple model is not nearly so peaked as for the sophisticated model, and so there is a much wider spread of frequencies over which ship motions are significant. Thus, the low order model requires higher values of T/W to arrive at the same level of tracking performance as the standard model. A sketch of the magnitude spectra of the two models was given in Figure (2.6.6.1).

Figure (3.4.4.2) shows the vertical control bandwidth for the low order model. Compared to the corresponding figure (3.4.3.3) for the standard model, the vertical control bandwidth increases much more slowly with thrust to weight, indicating the wide range of frequencies over which the low order model has significant motion energy. In addition, the peak motions now occur near one radian/second. They also have larger amplitude requiring a larger increase in aircraft T/W to track them. Although plots are not given, pitch tracking performance shows similar trends.

These comparisons of the ship tracking performance capabilities of the hover controller demonstrate the importance of accurate ship motion modelling for meaningful assessments of aircraft hovering performance, and associated control system bandwidth and thrust to weight requirements.

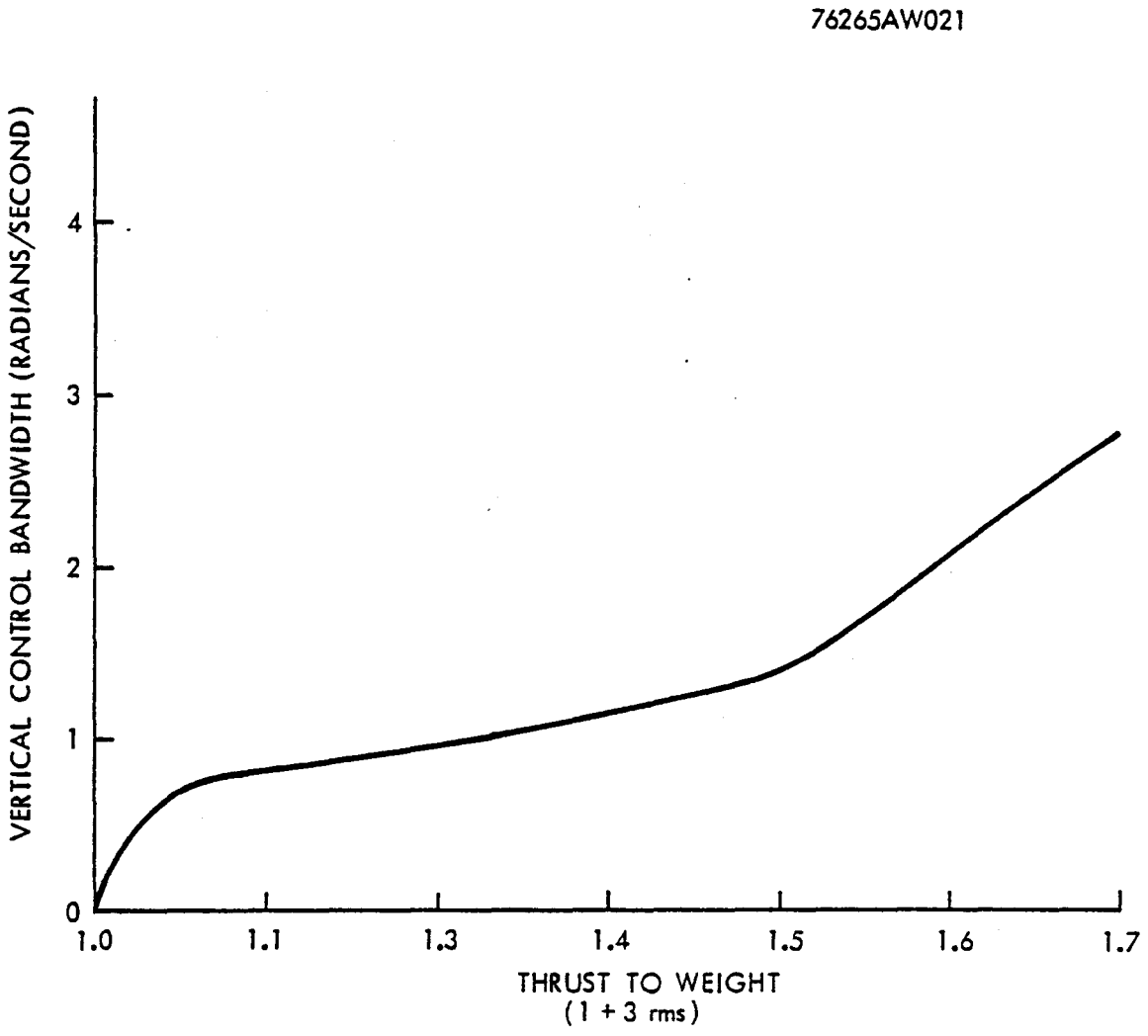

Hover Performance: Vertical Control Bandwidth versus Thrust to Weight for Low Order Ship Model

Figure 3.4.4.2

3.4.5 Conclusions

The goal of the hover controller was to make the aircraft track the ship deck motion as closely as possible, using only a small amount of vertical actuator control authority. The results obtained are performance curves illustrating the trade-off between tracking errors and required aircraft thrust to weight ratio, and the relationship between closed loop system bandwidth for vertical dynamics and the thrust to weight ratio. These curves are indicative of the "best" performance achievable by the VTOL aircraft.

Although only vertical and pitch dynamics are considered, the design method and analysis technique could be used for generating a complete full dynamics tracking controller.

Modelling accuracy was found to be very important in obtaining meaningful results. A low order ship model having a significantly wider power spectrum than the more accurate standard model, required a controller with much higher actuator authority than the standard one.

The results of this chapter motivate the landing controller design in Chapter Four. To meet a goal of reducing touchdown velocities to about one foot per second or less, the hover controller requires a thrust to weight ratio greater than 1.1 (figure (3.4.3.1)). However, the maximum ratio of current VTOL aircraft is only about 1.3 (27 , 28). Thus, the control effort used by the hover controller is a large fraction of the available authority. This motivates the search for an alternative design to achieve good landing performance at lower actuator control levels. Chapter Four discusses one such alternative design.

CHAPTER 4
LANDING CONTROL

4.1 Introduction

In this chapter, a landing controller design for the VTOL aircraft is developed. The purpose of the controller is to land the aircraft on the ship deck beginning with the aircraft hovering at some initial altitude. The design of this chapter is motivated by the performance of the hover controller in the previous chapter. There it was found that simple ship deck tracking requires potentially high levels of control authority to achieve low relative velocities suitable for landings. The objective of the landing controller in this chapter is to reduce this thrust to weight requirement.

This chapter is divided into four main parts. The introduction presents the basic concept of the proposed landing controller. Part two states an optimal control problem whose theoretical solution implements the concept. Only a suboptimal solution has been obtained for this problem. These are developed in part three, the analysis and design. Finally, the last part gives an evaluation of the resulting controller.

The goal of the new controller is to reduce the control actuator levels required to land, below those required by the tracking controller. To achieve this goal, the new controller exploits the predictability of ship motion and lands the aircraft at a peak of vertical ship deck motion, as sketched in Figure (4.1.1). A simple calculation shows how low the required actuator level could be in a situation where the peak is predicted perfectly. The calculation is just the control effort required by a bang-bang controller to move a mass between two points in a given time

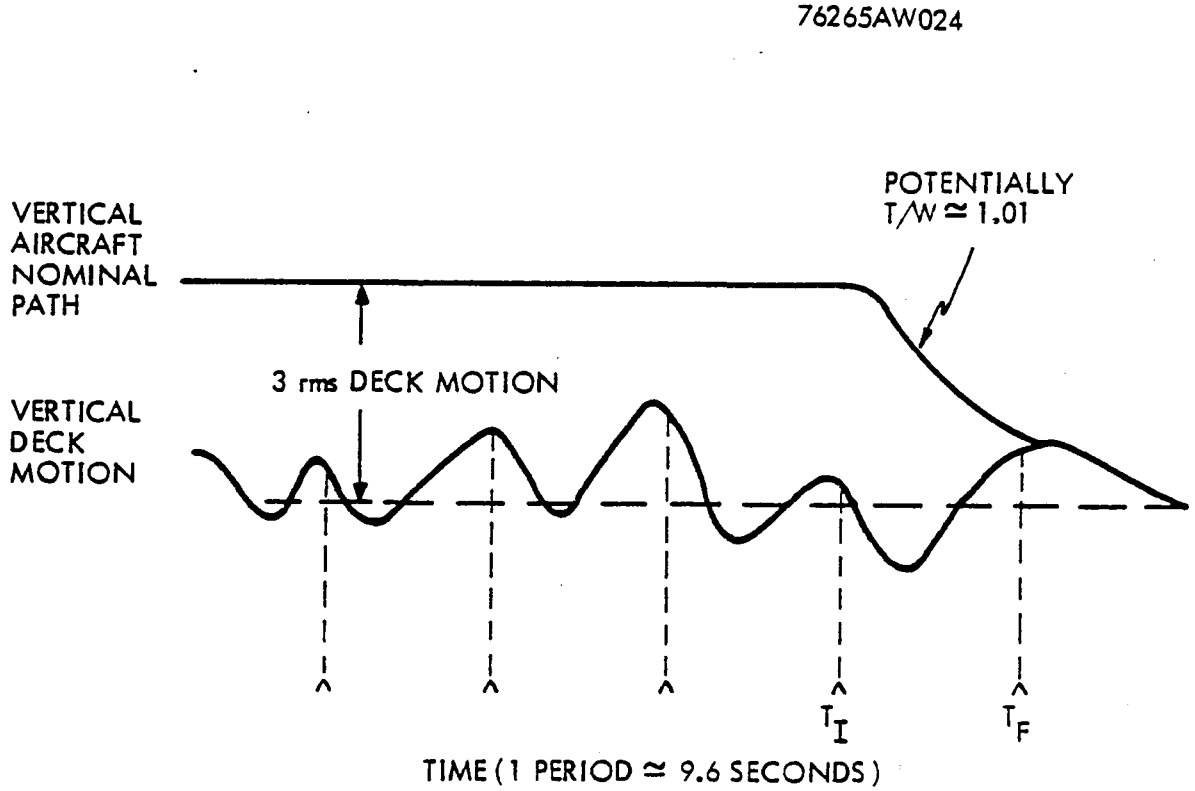

End Point Landing Philosophy

Figure 4.1.1

with zero initial and final velocities. Gravity is not a factor in the calculation, since the aircraft model is linearized about stationary hover. The calculation goes as follows. Denote the initial and final times of the trajectory by t_I and t_F, respectively. During the first half of the trajectory, from time t_I to $\frac{1}{2}(t_F - t_I)$, the acceleration of the mass is +a. At the end of the interval, its position will be $\frac{1}{2}a(\frac{1}{2}(t_F - t_I))^2$. During the last half of the trajectory, the acceleration will be -a, and the mass will have moved an additional distance equal to the first. When the mass comes to rest, the total change in position ΔS will be:

$$\Delta S = \frac{1}{4} a (t_F - t_I)^2 \qquad (4.1.1)$$

The acceleration level to move the mass the distance ΔS is therefore:

$$a = 4\Delta S/(t_F - t_I)^2 \qquad (4.1.2)$$

For $t_F - t_I = 10$ seconds (the natural period of the ship is roughly 9.6 seconds), and $\Delta S = 8$ feet (for hover at 13 feet above mean sea height and descending to a peak 5 feet above the mean height), the acceleration magnitude is $|a| = 0.32$ feet/second^2. This corresponds to a control actuator level of about one percent of the nominal stationary hover requirement. The hover controller of the last chapter required an actuator authority roughly an order of magnitude larger than this value.

In addition to the potentially reduced thrust requirements, other benefits may be realized by this landing control strategy over the hover controller. The first advantage is that ship and wave states are not required aboard the aircraft. The only information needed about the ship is the prediction of the time and position at which the landing pad

will reach a crest. Compared to the ship state vector, this is less complex information to transmit. Furthermore, it may be possible to transmit the information at a lower rate than would be necessary for tracking control. The required update rate remains to be determined however, before the magnitude of this benefit can be ascertained.

4.2 Control Problem

4.2.1 Optimization Problem Statement

The cause of high thrust to weight ratios in the aircraft ship motion tracking controller is the presence of significant power at high frequencies in the motion spectrum of the ship. The goal of the new controller is to eliminate this effect. Ideally this controller commands the aircraft from stationary hover at some initial height along a trajectory of low vertical actuator control levels, towards a height and time when the ship deck motion will reach a crest, ending with zero relative aircraft-ship deck separation and velocity. This ideal behavior can be expressed in terms of the following quadratic optimal control problem.

Find a feedback control law $\underline{u}(t) = \underline{u}(\underline{x}(t))$ to minimize the quadratic cost functional

$$J(u) = E\{ \underline{y}^T(t_F)P_F \underline{y}(t_F) + \int_{t_I}^{t_F} \underline{y}^T(t)Q(t)\underline{y}(t) + \underline{u}^T(t)R(t)\underline{u}(t)\, dt \} \qquad (4.2.1.1)$$

subject to the constraints

$$\dot{\underline{x}}(t) = A\underline{x}(t) + B\underline{u}(t) + B_N\underline{\rho}(t); \quad \underline{x}(t_I) = \underline{x}_0 \qquad (4.2.1.2)$$

$$\underline{y}(t) = C_1\underline{x}(t) \tag{4.2.1.3}$$

where the terminal time is defined by

$$t_F = \underset{\tau}{\text{minimum}} \{\text{argument } [\underset{\tau > t_I}{\text{minimum}} C_2\underline{x}(\tau)]\} \tag{4.2.1.4}$$

$P_F = P_F^T \geq 0$ is the quadratic cost associated with the end time response $\underline{y}(t_F)$, $Q(t) = Q^T(t) > 0$ and $R(t) = R^T(t) > 0$ are the per unit time costs associated with the response $\underline{y}(t)$ and control $\underline{u}(t)$ respectively; and (A,B) is stabilizable and (A,C) is detectable.

In the quadratic cost functional P_F, Q(t)and R(t) should be chosen so the resulting aircraft trajectories use low vertical control effort and have small terminal errors $\underline{y}(t_F)$.

This stochastic control problem is the standard finite terminal time problem, except that the performance index J is a random variable depending upon the ship motion, and thus on $\underline{\rho}(t)$ for $t_0 \leq t \leq t_F$ through the relation of equation (4.2.1.4). While a formal solution to this optimal control problem with random end time is not known, the following heuristic design provides a reasonable approximate solution.

4.2.2 An Approximate Solution

To take advantage of existing results for linear quadratic control problems, the solution of the optimization problem in Section (4.2.1) was approximated by treating the best currently available estimates of terminal time and corresponding deck position as fixed deterministic parameters. An explanation of the resulting algorithm follows.

The aircraft is initially assumed to be at stationary hover a safe distance above the ship landing deck. Ship motion is predicted ahead to the next crest. The time and height of this crest are compared with the current time and aircraft altitude to determine if a landing on the crest is possible. If not, the aircraft is commanded to remain at its original position. Otherwise, a landing is initiated. Using the predicted crest time and height, a nominal aircraft trajectory to the endpoint is computed via the standard time varying linear quadratic regulator problem. This trajectory is then followed by the aircraft using a steady state linear quadratic gaussian (SSLQG) regulator to control trajectory deviations. At certain intervals in time, new predictions of the ship motion peak are made and the nominal trajectory updated.

All the gains used in this design can be calculated prior to the landing. The trajectory following SSLQG gains used for tracking the desired trajectory are, of course, constant and precomputable. Gains for the nominal trajectory itself are precomputable and independent of the vertical height through which the aircraft must move, the initial vertical velocity of the aircraft, and the time required for the maneuver. They are only functions of time-to-go and thus, can be stored as a single time varying set of gains. During a landing approach, these stored nominal gains are used to compute a new nominal trajectory each time an updated estimate of the end point and time are available.

4.3 Analysis and Design

4.3.1 Assumptions

Here the additional assumptions beyond those posed for the modelling and the hover controller are stated. All the previous assumptions leading to the linearized model of the aircraft-ship system, and the design of the longitudinal hover controller in the previous chapters are required. For emphasis, it should be remembered that the ability to decouple aircraft pitch and heave dynamics was used and aircraft states were considered to be perfectly known. In addition, predictions of ship landing pad motion extrema are now required. In the simulations used for evaluation of the controller, peaks are identified via a state space model, but in fact the method of prediction is not important. Ship and wave state measurements are not required as key elements of the algorithm.

4.3.2 Touchdown Prediction Analysis

An approximate analysis of touchdown errors is made in this section. The results are given in Table (4.3.2.1). The expected velocity errors are used in section (4.3.6) to obtain a bound on the nominal aircraft landing trajectory update frequency, and the expected time errors are compared with the simulation results of Section (4.4.1).

A touchdown occurs when the relative aircraft-ship velocity is greater than zero at the first moment t_T when their separation is zero:

EXPECTED TOUCHDOWN ERRORS

PREDICTION TIME t_F seconds	$\sigma_{\Delta z_S}(t_F)$ feet	$\sigma_{\Delta \dot{z}_S}(t_F)$ feet/second	EXPECTED TOUCHDOWN VELOCITY feet/second	EXPECTED TOUCHDOWN TIME ERROR seconds
1.0	0.05	0.14	0.45	0.18
2.0	0.17	0.20	0.80	0.32

Table 4.3.2.1

$$\dot{z}_{A-S}(t_T) \geq 0 \qquad (4.3.2.1)$$

$$z_{A-S}(t_T) = 0 \qquad (4.3.2.2)$$

A touchdown is characterized by its time, the vertical position of the ship deck, and the relative aircraft-ship vertical velocity. The landing controller is designed to generate a near zero velocity touchdown between the aircraft and ship by commanding the aircraft along a trajectory, which terminates with zero velocity and meets the ship deck at its predicted crest height and time. However, the actual touchdown has different values due to uncertainties in the aircraft and ship trajectories. In the present model, the aircraft motion is deterministic once it has been given a commanded trajectory, so all the uncertainties are presently due to ship motion only.

The relative separation and velocity of the aircraft and ship can be written as the sum of their deterministic and stochastic components as follows:

$$z_{A-S}(t) = E\{z_{A-S}(t)\} + \Delta z_{A-S}(t) \qquad (4.3.2.3)$$

$$\dot{z}_{A-S}(t) = E\{\dot{z}_{A-S}(t)\} + \Delta\dot{z}_{A-S}(t) \qquad (4.3.2.4)$$

Equation (4.3.2.3) is illustrated in Figure (4.3.2.1).

Rewriting these equations with the bar notation for mean, noting that the uncertainties are due only to the ship ($\Delta z_{A-S}(t) = -\Delta z_S(t)$, $\Delta\dot{z}_{A-S}(t) = -\Delta\dot{z}_S(t)$), and then dropping the subscripts yields:

$$-z_{A-S}(t) = \bar{z}(t) + \Delta z(t) \qquad (4.3.2.5)$$

$$-\dot{z}_{A-S}(t) = \bar{\dot{z}}(t) + \Delta\dot{z}(t) \qquad (4.3.2.6)$$

76265AW038

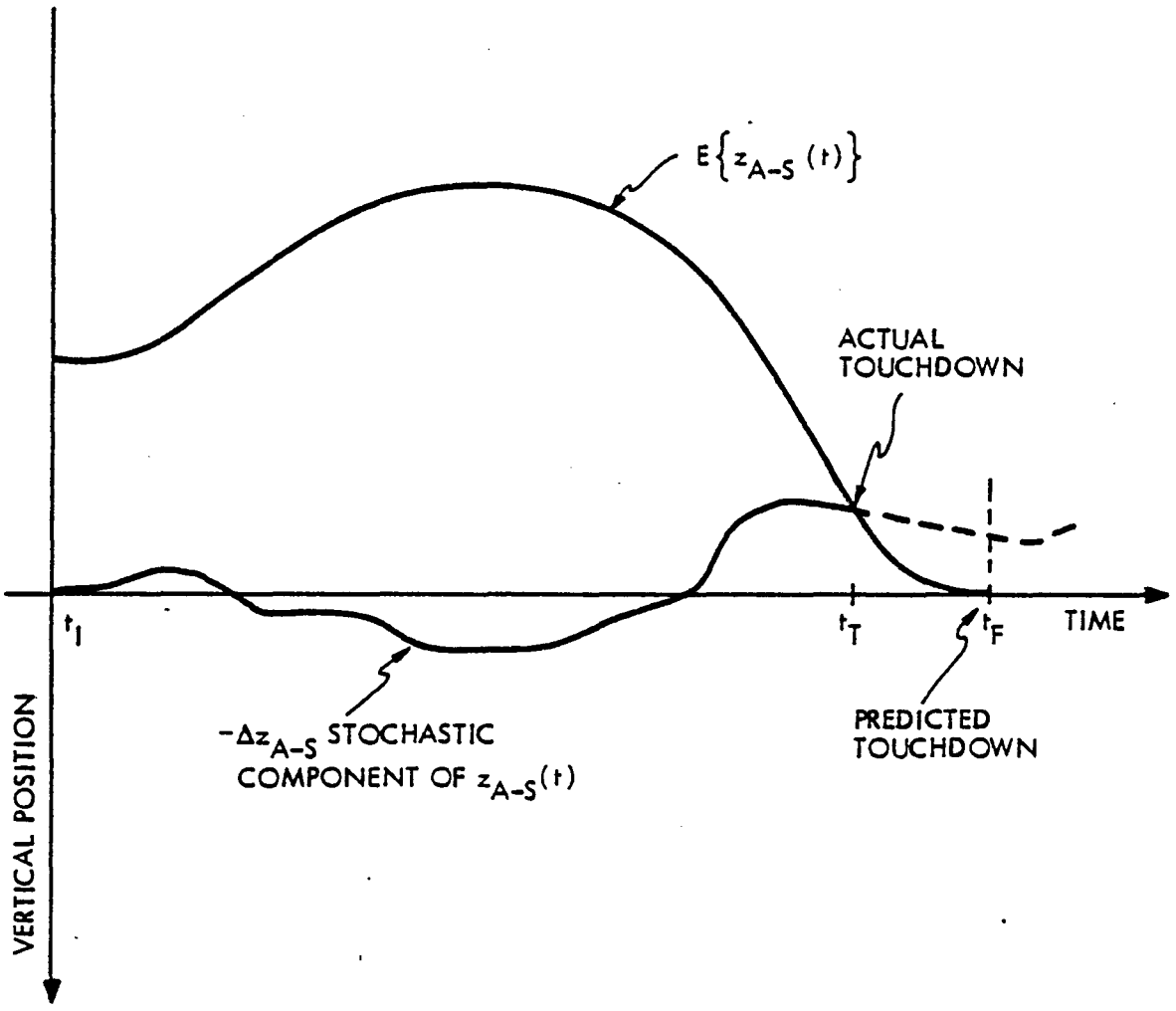

Deterministic and Stochastic Components of a Landing Trajectory

Figure (4.3.2.1)

$\bar{z}(t)$ and $\dot{\bar{z}}(t)$ are approximated by

$$\bar{z}(t) = \alpha(t - t_F)^2 \qquad (4.3.2.7)$$

$$\dot{\bar{z}}(t) = 2\alpha(t - t_F) \qquad (4.3.2.8)$$

where $\alpha = 1.259$. This approximates to second order a cosine wave that peaks at the predicted endtime t_F, and has the same typical period (9.6 seconds) and rms amplitude (4.2 feet) as ship deck motion. For the ideal case where the aircraft has reached the end of its trajectory and is nearly stationary, the approximate $\bar{z}(t)$ and $\dot{\bar{z}}(t)$ represent the total expected aircraft-ship separation and relative velocity. As is clear from Figure (4.3.2.1), actual touchdowns will occur early and at slightly negative positions. The deviations existing at touchdown time t_T can be approximated by the values of t_F that would occur "if the aircraft and ship could pass through each other after touchdown". This is illustrated by the dotted line. If for the interval between t_T and t_F, the velocity deviation $\Delta\dot{z}(t)$ is assumed to be constant, then a reasonable approximation for the touchdown deviations are given in terms of deviations at t_F by:

$$\Delta z(t_F) = \Delta z(t_T) + \Delta\dot{z}(t_F)(t_F - t_I) \qquad (4.3.2.9)$$

$$\Delta\dot{z}(t_F) = \Delta\dot{z}(t_T) \qquad (4.3.2.10)$$

The touchdown time can be found by substituting equation (4.3.2.10) into (4.3.2.9), then substituting the result and equation (4.3.2.7) into (4.3.2.5) with $z_{A-S}(t_T)$ equal to zero:

$$t_F - t_T = (\Delta\dot{z}(t_F) + (\Delta\dot{z}^2(t_F) - 4\alpha\Delta z(t_F))^{1/2}/2\alpha \qquad (4.3.2.11)$$

The touchdown velocity is obtained by substituting this last expression along with equations (4.2.3.8) and (4.3.2.10) into (4.3.2.6):

$$\dot{z}_{A-S}(t_T) = -\Delta\dot{z}(t_F) - 2\alpha(t_T - t_F) \qquad (4.3.2.12)$$

$$= (\Delta\dot{z}(t_F) - 4\alpha\Delta z(t_F))^{1/2} \qquad (4.3.2.13)$$

To second order in $\Delta\dot{z}(t_F)$ this is:

$$\dot{z}_{A-S}(t_T) = (-4\alpha\Delta z(t_F))^{1/2} + \tfrac{1}{4}(-\alpha\Delta z(t_F))^{-1/2}\Delta\dot{z}^2(t_F) \qquad (4.3.2.14)$$

The expected touchdown velocity is found by evaluating:

$$E\{\dot{z}_{A-S}(t_T) \mid \dot{z}_{A-S}(t_T) > 0, \quad z_{A-S}(t_T) = 0\} \qquad (4.3.2.15)$$

The conditions on $\dot{z}_{A-S}(t_T)$ and $z_{A-S}(t_T)$ in this expectation are satisfied by all trajectories such that $\Delta z(t_F) < 0$ (plus some other trajectoreis, which are neglected). Hence,

$$E\{\dot{z}_{A-S}(t_T) \mid \dot{z}_{A-S}(t_T) > 0, \; z_{A-S}(t_T) = 0\}$$

$$\simeq E\{(-4\alpha\Delta z(t_F))^{1/2} + \tfrac{1}{4}(-\alpha\Delta z(t_F))^{-1/2}\Delta\dot{z}(t_F) \mid \Delta z(t_F) < 0\} \qquad (4.3.2.16)$$

The expectation is over $\Delta z(t_F) < 0$ and all $\Delta\dot{z}(t_F)$, which are gaussian random variables with zero means and variances depending on t_F, where t_F is measured with respect to the time when the ship state vector was last updated. Statistics for $\Delta z(t_F)$ and $\Delta\dot{z}(t_F)$ are computed at the end of this section. They are approximately independent with standard deviations $\sigma_{\Delta z_S}(t_F)$ and $\sigma_{\Delta\dot{z}_S}(t_F)$ known as functions of t_F.

The resulting equation for the touchdown velocity can be written as:

$$E_{\Delta z(t_F)} \{ E_{\dot{\Delta z}(t_F)} \{ (-4\alpha\Delta z(t_F))^{1/2} + \tfrac{1}{4}(-\alpha\Delta z(t_F))^{-1/2}\dot{\Delta z}^2(t_F) \,|\, \Delta z(t_F) < 0 \}\} \tag{4.3.2.17}$$

but the expectation of $\dot{\Delta z}^2(t_F)$ with respect to $\dot{\Delta z}(t_F)$ is just $\sigma_{\Delta z(t_F)}$, and the probability density for $\Delta z(t_F)$ over non-positive values is

$$P_{\Delta z|\Delta z<0}(Z|Z<0) = \sqrt{2/\pi}\ (1/\sigma_{\Delta z(t_F)})\ \exp\{ -\tfrac{1}{2}(Z/\sigma_{\Delta z(t_F)})^2\} \tag{4.3.2.18}$$

Therefore the expectation reduces to:

$$E_z \{ (-4\alpha\Delta z(t_F))^{1/2} + \tfrac{1}{4}(-\alpha\Delta z(t_F))^{-1/2}\sigma^2_{\dot{\Delta z}(t_F)} |\ \Delta z(t_F) < 0 \}$$

$$= \sqrt{2/\pi}\ (1/\sigma_{\Delta z(t_F)}) \int_{-\infty}^{0} [(-4\alpha Z)^{1/2} + \tfrac{1}{4}(-\alpha Z)^{-1/2}\sigma_{\dot{\Delta z}(t_F)}]$$

$$\exp\{ -\tfrac{1}{2}(Z/\sigma_{\Delta z(t_F)})^2\}\, dZ \tag{4.3.2.19}$$

The two terms of the integral are given in reference (26). Evaluating the constants gives:

$$E\{ \dot{z}_{A-S}(t_T) \,|\, \dot{z}_{A-S}(t_T) > 0,\ z_{A-S}(t_T) = 0 \}$$

$$\simeq 1.845\sigma^{1/2}_{\Delta z(t_F)} + 0.3832(\sigma_{\Delta z(t_F)})^{-1/2}\sigma^2_{\dot{\Delta z}(t_F)} \tag{4.3.2.20}$$

Numerical values for this expression are given in Table (4.3.2.1).

The expectation of touchdown time error $t_F - t_T$, can be found by noting that the expectation of $\Delta\dot{z}(t_F)$ in equation (4.3.2.11) is zero. The remaining term in (4.3.2.11) is the expectation of the touchdown velocity divided by 2α. Hence,

$$E\{\, t_F - t_T \mid \dot{z}_{A-S}(t_T) > 0,\ z_{A-S}(t_T) = 0 \,\}$$

$$\simeq (1/2\alpha) E\{\, \dot{z}_{A-S}(t_T) \mid \dot{z}_{A-S}(t_T) > 0,\ z_{A-S}(t_T) = 0 \,\} \qquad (4.3.2.21)$$

Table (4.2.3.1) gives these expectations as well.

An expression for the expected ship deck position is not required since in this analysis all collisions occur at $z_s(t_T)$ equal to zero. In actual touchdowns, however, the expected ship deck position is often above the predicted height at touchdown since the aircraft trajectory is designed such that it does not dip below the predicted end point.

The supporting calculation of the variances of $\Delta\dot{z}_S(t_F)$ and $\Delta z_S(t_F)$ follows.

The growth of ship motion prediction uncertainties $(\sigma_{\Delta z_S(t)}, \sigma_{\Delta\dot{z}_S(t)})$ is calculated by solving the time varying covariance equation for the ship deck vertical position and velocity. The state space ship model was used to determine the quantities required in order to solve the covariance equation. The solution $P(t)$ is the state covariance matrix for the ship and wave states at time t. The initial condition for the solution $P(0)$ is equal to the zero matrix. This indicates that all the states are perfectly known at time t= 0. The matrix differential equation (given earlier in equation (3.3.2.4)) is:

$$\dot{P}(t) = AP(t) + P(t)A^T + BVB^T \qquad (4.3.2.22)$$

with initial condition:

$$P(0) = 0 \qquad (4.3.2.23)$$

A, B and V are respectively system, noise input, and noise intensity matrices for the wave-ship model. The output covariance matrix was then found from:

$$Cov(y(t)) = C(t)P(t)C^T(t) \qquad (4.2.3.24)$$

For this analysis, the outputs were ship landing pad vertical position and velocity. The results are shown in Figures (4.3.2.2), (4.3.2.3) and (4.3.2.4). These give rms position and velocity, and the correlation of position and velocity.

Since the output y(t) is the result of a linear system driven by a gaussian process, it too is gaussian, and so 68% of all outcomes are within 1 rms (one standard deviation) of the mean, 95% within 2 rms, and over 99% within 3 rms. (Recall this result was also used in Section 3.3.2).) Thus, in the prediction error plots, 68% of all the times a certain prediction is made, the outcome will actually lie about a predicted mean, within a symmetric band having the half width indicated on the plot.

Note that the regular rising and leveling trand of the prediction error plots is a sinusoidal form superimposed on a smoothly increasing curve. The sinusoid has a period of about 4 or 5 seconds. This is about one half the period of the ship motion. The same phenomenon also occurs for a single second order damped system and in the analysis

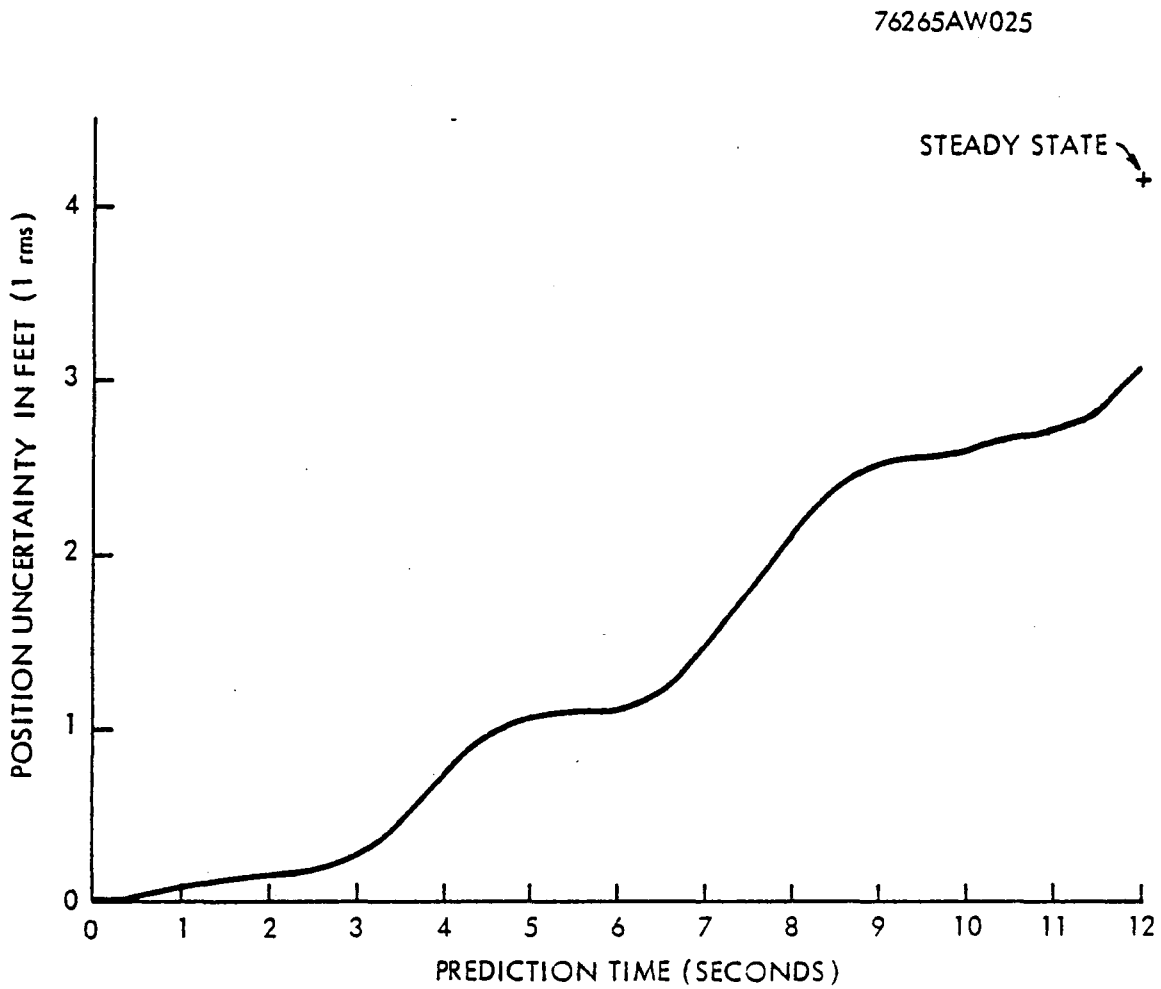

Prediction Errors for Vertical Ship Deck Position

Figure 4.3.2.2

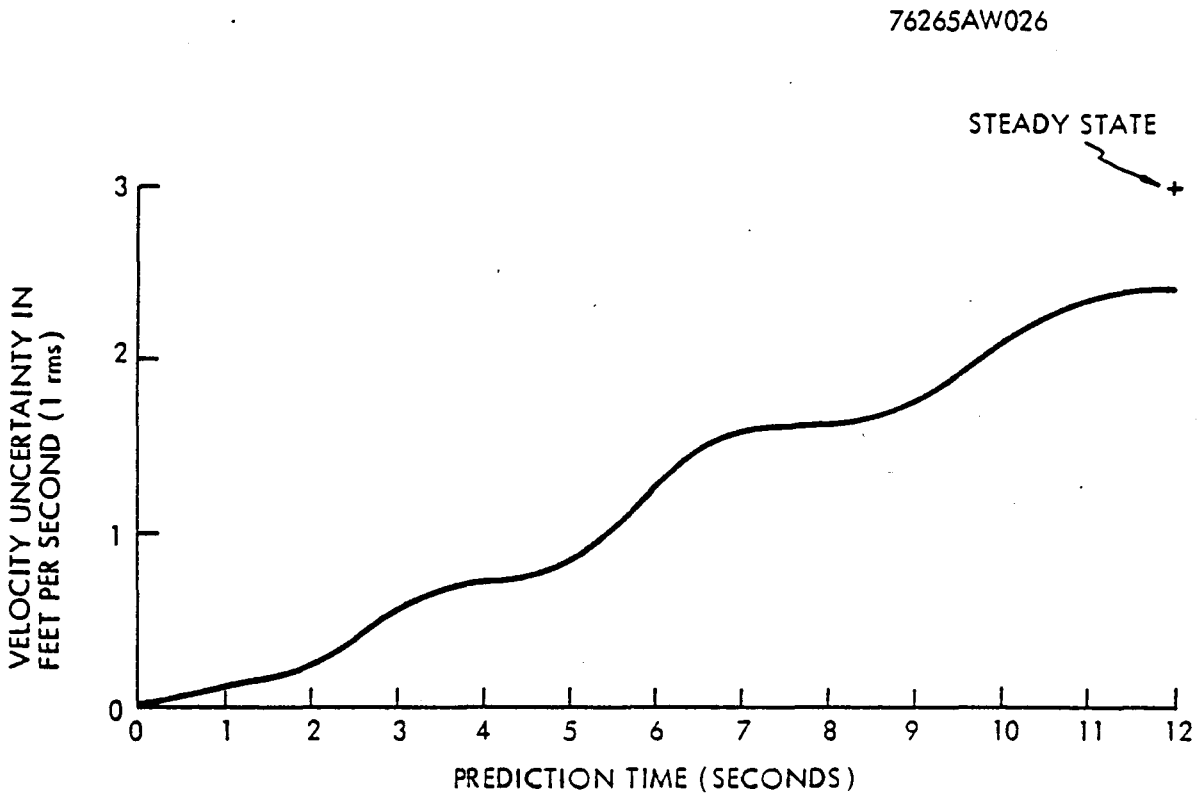

Prediction Errors for Vertical Ship Deck Velocity

Figure 4.3.2.3

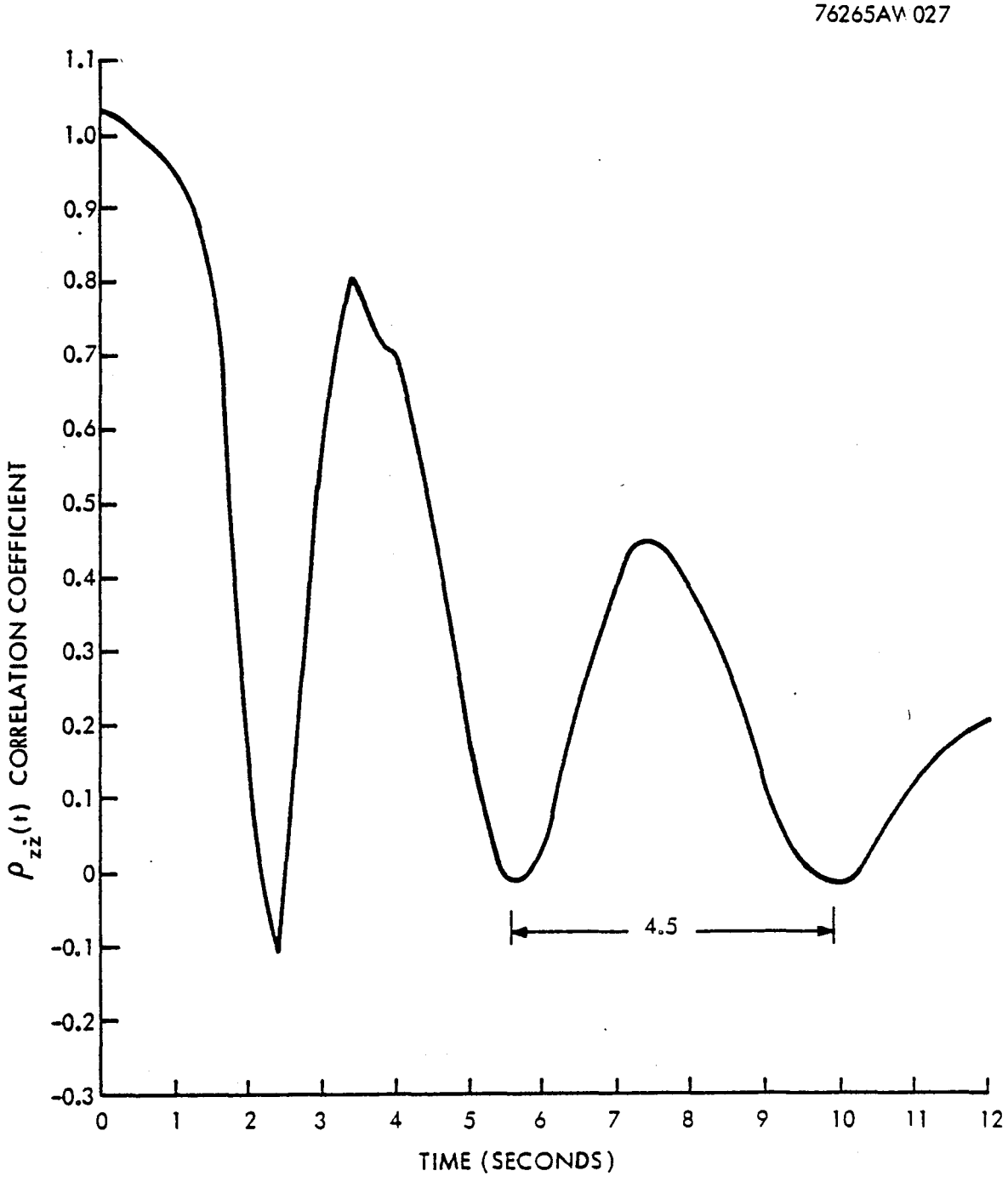

Predicted Correlation Coefficient for Ship Position and Velocity

(Note: Irregularities are Due to Digital Calculation Errors)

Figure 4.3.2.4

of a sinusoidal wave with random amplitude A. The sinusoidal wave covariance result is derived here. Let the sinusoidal wave be given as:

$$y(t) = A \sin(\omega t) \tag{4.3.2.25}$$

where the amplitude A is zero mean gaussian random variable, with variance σ^2. Then:

$$E\{ y(t) \} = \sin(\omega t)\, E\{A\} = 0 \tag{4.3.2.26}$$

$$\begin{aligned} Cov\{ y(t) \} &= E\{ [y(t) - E\{ y(t)\}]^2\} = E\{ y(t)^2 \} \\ &= \sin^2(\omega t)\, E\{A^2\} = \sigma^2 \sin^2(\omega t) \\ &= \frac{1}{2}\sigma^2(1 - \cos 2\omega t) \end{aligned} \tag{4.3.2.27}$$

The squaring of the sinusoidal wave yields a frequency component in the covariance twice that of the original wave form. This corresponds to the observations made above for the ship motion.

The ship vertical position and velocity correlation is shown in Figure (4.3.2.4). The plot shows that position and velocity become less and less correlated in time. This means that knowing position or velocity will not generally help in determining the other. This is an important reason for rejecting landing control strategies that simply command hover at some fixed altitude until the ship rises high enough to contact the aircraft. Because ship position and velocity are uncorrelated in steady state, the conditional distribution of ship velocities given ship height is the same at any height. Therefore, no altitude, even very high ones, will reduce the variation of ship

velocities at impact. Note that a simple second order damped oscillator also has this uncorrelated x, $\dot{x}$ property. For example, write the second order system as

$$\dot{\underline{x}} = A\underline{x} + B\rho \tag{4.3.2.28}$$

where $\underline{x} = [x,\dot{x}]^T$, and ρ is a zero mean gaussian white noise with intensity 1.0. Let the matrices A and B have the form:

$$A = \begin{vmatrix} 0 & 1 \\ -\omega^2 & -2\xi\omega \end{vmatrix} \tag{4.3.2.29}$$

$$B = \begin{vmatrix} 0 \\ q^{1/2} \end{vmatrix} \tag{4.3.2.30}$$

Then the steady state solution of the state covariance equation (equation (4.3.2.22)) is given by:

$$P = \begin{vmatrix} q/4\xi\omega^3 & 0 \\ 0 & q/4\xi\omega \end{vmatrix} \tag{4.3.2.31}$$

where the two zero elements indicate that x and $\dot{x}$ are uncorrelated, as claimed.

4.3.3 Nominal Trajectory Design

The purpose of the nominal trajectory is to guide the aircraft down to a predicted landing position using very little vertical control actuator effort. To accomplish this, a linear quadratic control problem with a finite end time is set up and solved. The gains used to calculate a nominal trajectory during a landing are only dependent

on predicted time-to-go and are stored as a function of that time. With the gains and nominal trajectory dynamics model available, only the initial and final points and times are required to compute a nominal trajectory and its controls.

The general form of the finite end time controller problem and solution are given as references (29) and (23). They are as follows:

Find a feedback control law $\underline{u}(t) = \underline{u}(\underline{x}(t))$ to minimize the quadratic cost functional

$$J(u) = \underline{y}^T(t_F)P_F\underline{y}(t_F) + \int_{t_I}^{T_F} \underline{y}^T(t)Q(t)\underline{y}(t) + \underline{u}^T(t)R(t)\underline{u}(t)\,dt \qquad (4.3.3.1)$$

subject to the constraints of

dynamics $\dot{\underline{x}}(t) = A\underline{x}(t) + B\underline{u}(t)$ (4.3.3.2)

response $\underline{y}(t) = C\underline{x}(t)$ (4.3.3.3)

initial conditions $\underline{x}(t_I) = \underline{x}_0$ (4.3.3.4)

desired final conditions $\underline{y}(t_F) = 0$ (4.3.3.5)

where (A,B) is stabilizable and (A,C) is detectable, $P_F = P_F^T \geq 0$ is the quadratic cost associated with the final response $\underline{y}(t_F)$, $Q(t) = Q^T(t) > 0$ is the per unit time quadratic cost associated with the response $\underline{y}(t)$, and $R(t) = R^T(t) > 0$ is the per unit time quadratic cost associated with the control $\underline{u}(t)$.

The form of the feedback control $\underline{u}(\underline{x}(t))$ is given as follows:

$$\underline{u}(\underline{x}(t)) = G(t)\underline{x}(t) = -R^{-1}(t)B^TP(t)\underline{x}(t) \qquad (4.3.3.6)$$

where P is the unique symmetric positive semidefinite solution of the matrix differential Riccati equation

$$\dot{P}(t) = P(t)A + A^{T}P(t) - P(t)BR^{-1}(t)B^{T}P(t) + Q(t) \qquad (4.3.3.7)$$

with terminal condition $P(t_F) = P_F$.

Note that the Riccati equation is solved backwards in time from the end point, so the solution, and thus the gains can be stored as a function of "time-to-go" to the end.

Using the assumption that aircraft vertical dynamics can be decoupled from all other-degrees of freedom, the nominal trajectory computations are reduced to those for the third order vertical dynamics, which are given in Table (4.3.3.1). The states are deviation from the desired vertical end point x_1, vertical velocity x_2, and vertical acceleration x_3. By the choice of the output matrix C_N, the states are the outputs. The choice of control cost weighting R(t) is made unity as a reference level against which the output weighting Q(t) is compared in the cost functional. Q(t) has only one nonzero element $q_{NOM}(t)$ which weights the position. $q_{NOM}(t)$ has the following form:

$$q_{NOM}(t) = CONST \cdot \exp\{ -\frac{1}{2}(t - t_M)^2/\sigma^2 \} \qquad (4.3.3.8)$$

The characteristic shape of $q_{NOM}(t)$ is shown in Figure (4.3.3.1). This form weights the position more heavily near the end of its trajectory than near the beginning, so that the feedback control solution will cause the deviation from the desired end position to approach zero smoothly. Note, $q_{NOM}(t)$ can be written as a function of time-to-go, t_{TG}, by setting t to t_F minus t_{TG}. $q_{NOM}(t)$ has three parameters. CONST is the scale factor indicating the importance of position error compared to the control effort, σ is the parameter determining the width of the

NOMINAL TRAJECTORY DYNAMICS

$$\dot{\underline{x}}_N(t) = A_N \underline{x}_N(t) + B_N u_N(t)$$

$$\underline{y}_N(t) = C_N \underline{x}_N(t) = \underline{x}_N(t)$$

$$A_N = \begin{vmatrix} 0 & 1.0 & 0 \\ 0 & 0 & 32.2 \\ 0 & 0 & 0 \end{vmatrix}$$

$$B_N = \begin{vmatrix} 0 \\ 0 \\ 1.0 \end{vmatrix}$$

$$C_N = \begin{vmatrix} 1.0 & 0 & 0 \\ 0 & 1.0 & 0 \\ 0 & 0 & 1.0 \end{vmatrix}$$

Table 4.3.3.1

76265AW029

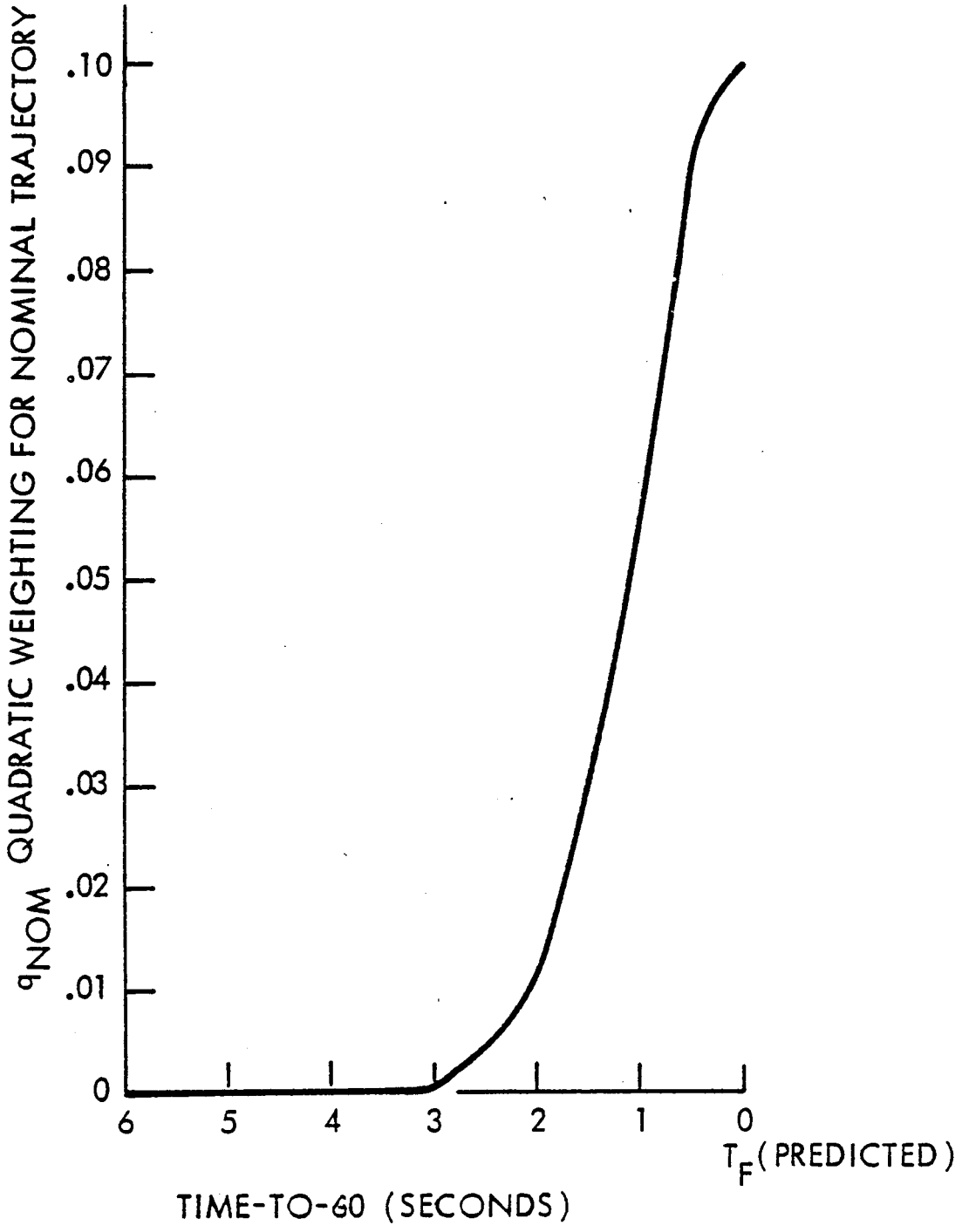

Quadratic Penalty for Nominal Trajectory Calculations

Figure 4.3.3.1

of the weighting in time and so indicates how soon the position error becomes important, and t_M is the time at which the error is weighted most heavily. The effect of making $t_M < t_F$ is to cause the velocity of the aircraft to be small as it reaches t_M, for although position is weighted mostly at t_M, it is also weighted beyond t_M indicating that the position error should remain near zero after t_M. Since this weighting ($t_M < t_F$) causes the aircraft to reach the desired position and approximately zero velocity at t_M, the gains obtained from solving this problem are shifted, so that those at time t_M are considered to be the final gains of a problem ending at t_M. The gains from t_M to t_F are unused. The option of making $t_M < t_F$ is referred to as "shifting the nominal trajectory gains".

Two nominal trajectories are compared in Figures (4.3.3.2) and (4.3.3.3). In these figures the nominal trajectory parameters are:

$$\text{CONST} = 0.1 \text{ feet}^{-2}$$

$$\sigma = 1.0 \text{ second}$$

$$t_F - t_M = 5.0 \text{ seconds}$$

Figure (4.3.3.2) has a trajectory length of 6.0 seconds, while Figure (4.3.3.3) has a trajectory length of 2.0 seconds. The short trajectory is shown to indicate how position errors 2.0 seconds before landing are reduced only partially, while in the longer one they were almost completely eliminated.

The values of CONST, σ and $(t_F - t_M)$ given above provided an initial set of nominal trajectory parameters for the design evaluation. They were selected because they produce smooth trajectories over time

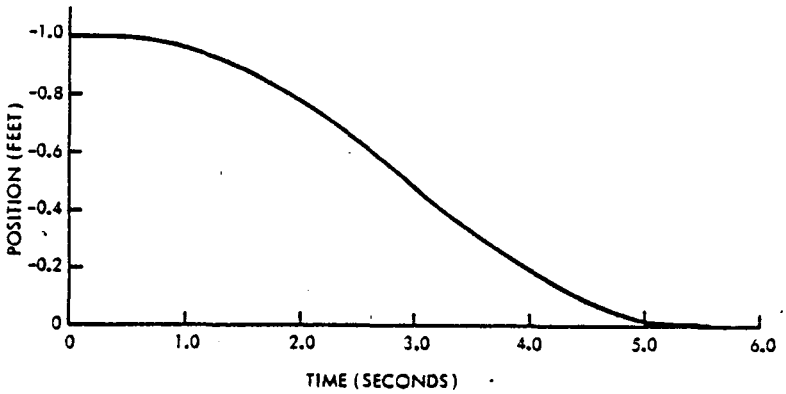

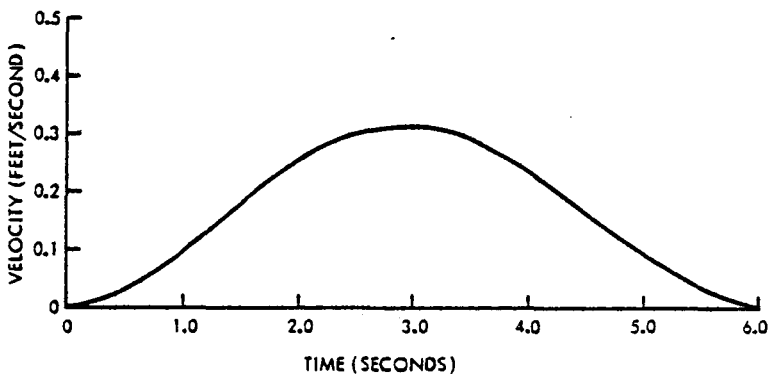

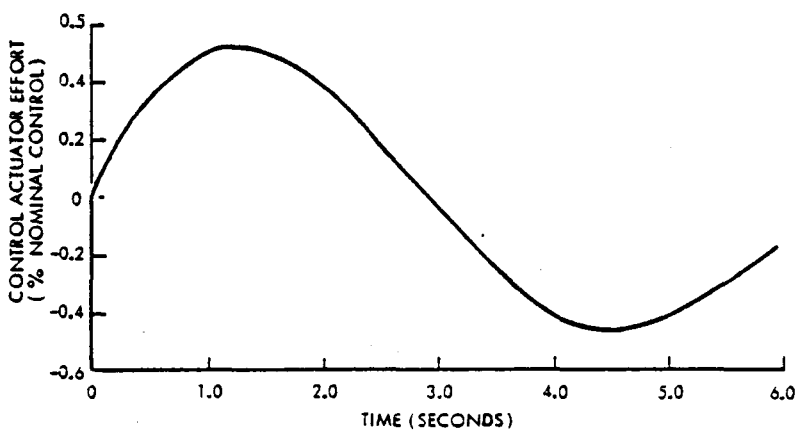

Nominal trajectory for parameters $t_M = 6.0$, $t_F = 11.0$, CONST = 0.1, $\sigma = 1.0$

Figure 4.3.3.2

76265AW031

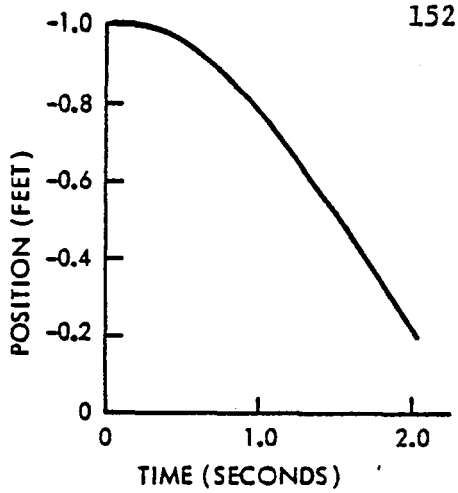

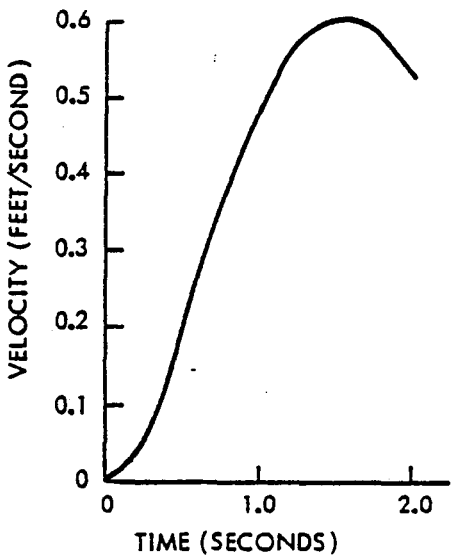

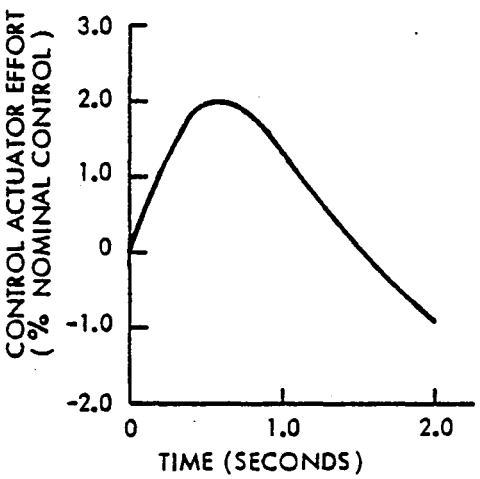

Nominal Trajectory for Parameters $t_M = 2.0$ $t_F = 7.0$ CONST = 0.1 $\sigma = 1.0$

Figure 4.3.3.3

intervals on the order of 6.0 seconds.

4.3.4 Trajectory Follower

This section discusses the purpose of the trajectory follower, and the design used.

The trajectory following controller has the objective of holding the aircraft to the commanded nominal trajectory in spite of any disturbances it may encounter. The corrections it makes to the aircraft trajectory are of higher frequency than those caused by the nominal commands. For this reason, the design of the follower is a steady state linear quadratic regulator with good tracking performance. Besides tracking the commanded vertical trajectory, the follower may also be used simultaneously to track ship orientation, lateral position, and fore-aft position, provided the necessary ship states are available. The control problem solved to get the feedback gains for the trajectory follower is identical to the one solved for the hover controller, with the exception that instead of weighting aircraft to ship vertical separation z_{A-S}, aircraft position alone was weighted by q_{z_A}. The weighting ratio $q_{\theta_{A-S}}$ to q_{z_A} is the same as used previously for $q_{\theta_{A-S}}$ to $q_{z_{A-S}}$. Based on the experience gained with the hover controller, the quadratic weights were chosen as:

$$q_{\theta_{A-S}} = 10.0$$
$$q_{z_A} = 0.01$$

The gains obtained from these weightings are used to feed back vertical trajectory errors and aircraft to ship pitch orientation deviations to

the aircraft control inputs.

4.3.5 End Point Attainability

End point attainability refers to the ability of the controller to bring the aircraft to a given predicted end point using no more than a specified control authority level. Because of the random nature of the ship motions, not all deck motion crests are equally suitable for landing attempts. If a predicted crest is too low or occurs too soon, the nominal trajectory required to reach it may call for excessive control effort. Furthermore, as shown in Figure (4.3.3.3), the nominal trajectory in some cases may not even reach the predicted end point. In other cases it may guide the aircraft to a high velocity impact with the ship. To prevent these situations, all nominal trajectories including ones computed as updates during a landing in progress should be checked for end point attainability. If control authority, miss distance, or impact velocity are unacceptable, a landing should not be initiated (a landing in progress should be aborted).

A crude example of such an attainability check is implemented in the present design. Each initial peak prediction is screened to determine the control effort a bang-bang controller would use to move a point mass from the current aircraft altitude to the predicted height at the predicted time. Any end point requiring more than a specified control effort is skipped in favor of repeating the end point search at a later time.

This simple end point attainability check is implemented with the window shown in Figure (4.3.5.1). Any point initially predicted in the

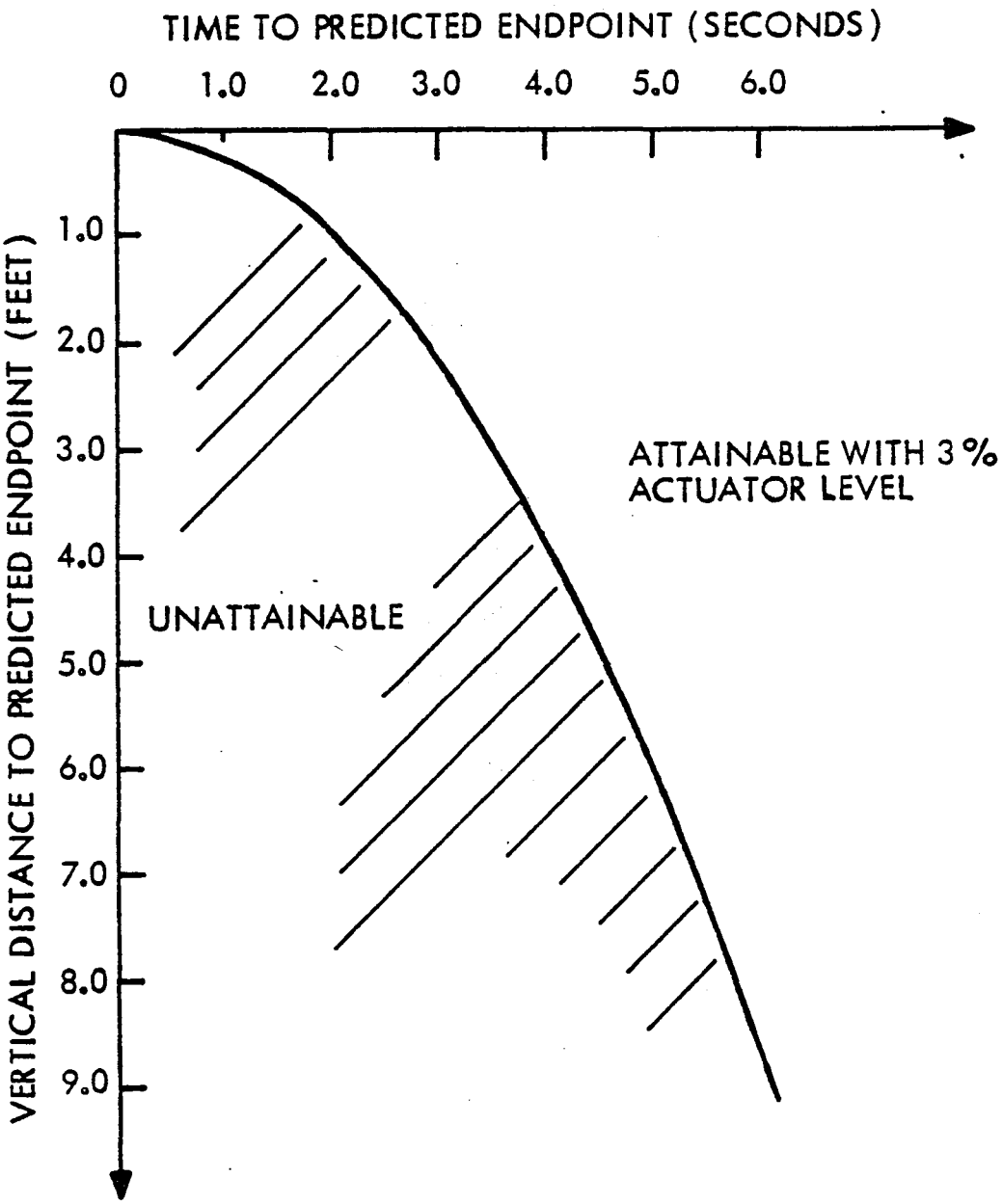

End Point Screen

Figure 4.3.5.1

This Page Intentionally Left Blank

unshaded region is accepted and any outside the region is rejected. This screening is not repeated once a landing is underway.

It should be noted that this screening does not mean the nominal trajectory computation will always use less than the specified actuator level, since the nominal trajectory minimizes a different cost functional than the bang-bang controller trajectory (which minimizes time to the end given a maximum available control level). However, the limit is a useful guide.

This crude attainability check was found to be helpful during the design evaluation, but occasionally it proved inadequate. The algorithm checks only the initial prediction of the end point, and not the subsequent updates, which may be unattainable with the specified control actuator authority. A practical design should include a more complete checking scheme as originally described in this section.

4.3.6 Update Determination

If ship motion were deterministic, the state at the initial time would be sufficient to predict the end point perfectly, and thus the trajectory to reach it. However, this is not the case. Updates must be made to compensate for deviations from the predicted mean ship motion. The rate at which updates are made is a design decision within bounds imposed by two considerations. The upper rate is bounded by the frequency content of ship motion, while the lower rate is bounded by motion uncertainty.

First consider the upper bound on the update rate. This is determined by the highest frequency components of ship motion. The Nyquist sampling frequency theorem, given in reference (30), states that the minimum sampling frequency to retain all the information contained in a band-limited signal is twice the maximum signal frequency. A sampling frequency higher than this is theoretically unnecessary. However, in practical implementations, where signals are not strictly band limited, a factor of ten increase beyond the minimum is often necessary. Since the dominant ship motion period is about 9.6 seconds, its frequency is 0.65 radians/second. The corresponding Nyquist sampling frequency is 1.3 radians/second, and with a factor of ten increase, a reasonable sampling frequency is 13 radians/second or once every 0.5 second. In the design evaluation both 0.5 and 0.2 second sampling periods are tested.

The second consideration follows. The nominal landing trajectory is flat near the end point so any corrections made close to the terminal time can cause the aircraft position to track ship motion. If these corrections are made at a high rate, the landing controller mimics the performance of the hover controller. This performance has already been determined however, and found to be unsatisfactory since it uses high levels of control actuator effort. To avoid this tracking behavior, end point and nominal trajectory updates are suspended a certain time interval before the expected landing. This time is chosen as the largest possible, that does not incur a large ship motion prediction uncertainty. From the analysis of Section 4.3.2 on ship motion prediction, a value of 2.0 seconds was chosen. The value is somewhat

arbitrary, but it keeps the estimated mean ship velocity at touchdown near -0.8 feet/second as listed in Table 4.3.2.1.

4.3.7 Overall Design

The concept of the landing controller, with its main functional components has been described. In this section, the components are assembled in the overall design. The type of evaluation chosen for the system performance is discussed also.

A block diagram of the overall landing control loop is shown in Figure (4.3.7.1). It has three major blocks: one which generates the nominal trajectory $\underline{x}_{NOM}(t)$ and control $\underline{u}_{NOM}(t)$; one which computes the trajectory following feedback control $\delta\underline{u}(t)$; and one which represents the aircraft, ship and wave system.

The nominal trajectory generator has four functions. The first is to determine when endpoint predictions and nominal trajectory updates are to be made. The second is to predict ship motion and identify its peaks. The next is to check end point attainability, and the last is to compute the nominal trajectory and control to the predicted end point. The nominal trajectory $\underline{x}_{NOM}(t)$ and control $\underline{u}_{NOM}(t)$ are the generator outputs, while the actual system state $\underline{x}(t)$ at the update times is the generator input.

The combined aircraft, ship, and wave system has two separate inputs. The wave receives disturbances $\rho(t)$, which drive the wave dynamics, and hence produce stochastic ship motion. The aircraft receives commands $\underline{u}(t)$, which are the sum of the nominal trajectory

76265AW028

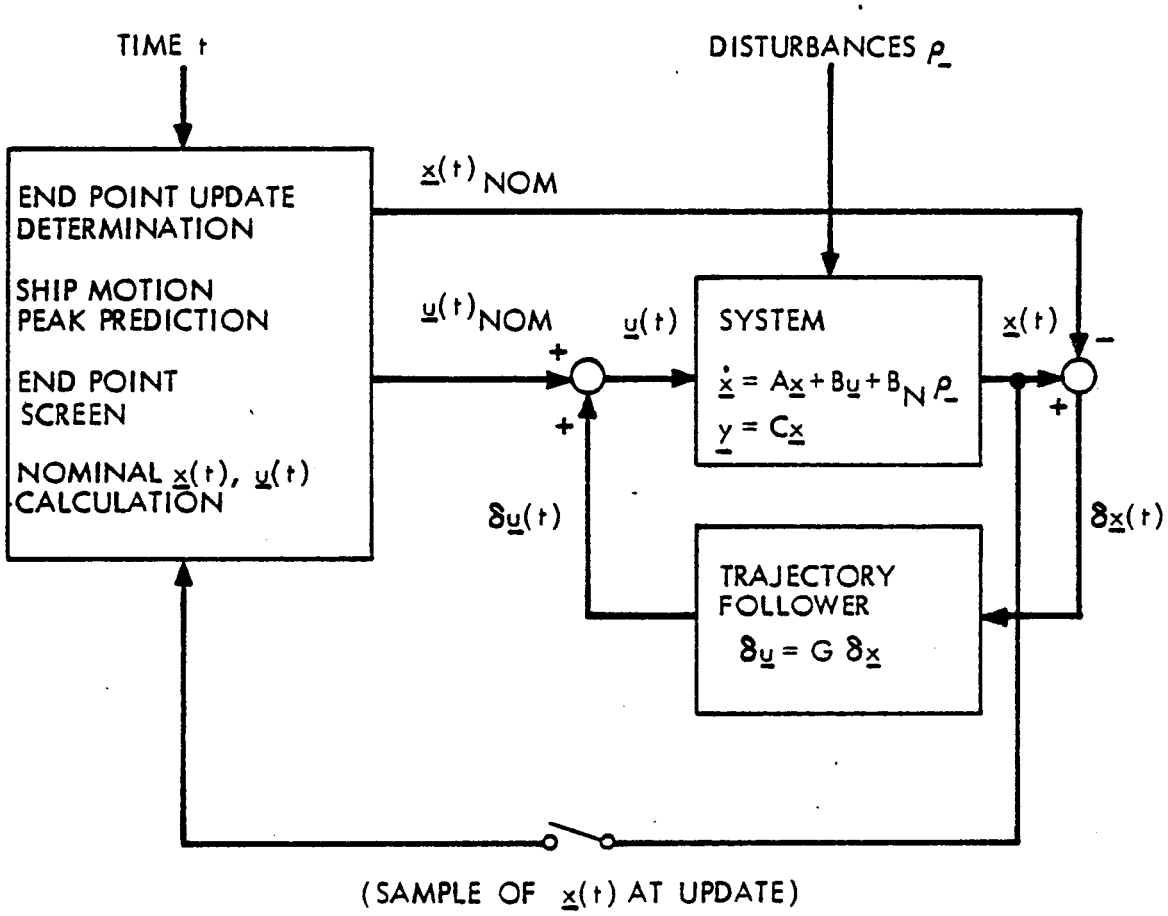

Landing Controller Block Diagram

Figure 4.3.7.1

and nominal trajectory tracking commands $\underline{u}_{NOM}(t)$ and $\delta\underline{u}(t)$ respectively. (Recall from Chapter Two on modelling, that wind disturbances acting on the aircraft have not been included to date.) The state vector $\underline{x}(t)$ and the output vector $\underline{y}(t)$ produced by the combined system contain aircraft, ship, and wave quantities.

Finally, the trajectory follower computes the tracking command $\delta\underline{u}(t)$, from the trajectory deviation $\delta x(t)$, which is the difference between the actual state $\underline{x}(t)$ and the desired state $\underline{x}_{NOM}(t)$.

A sketch of the aircraft and ship tracks during a landing is drawn in Figure (4.3.7.2). For clarity, the update rate in the sketch is only once every 2.0 seconds and the aircraft trajectory deviations are exaggerated.

The evaluation of the overall controller design is discussed in the next section; however, before proceeding, an explanation of the form of the evaluation is appropriate.

The system with the controller is nonlinear. In fact, both the dynamics and the output are nonlinear. First look at the nominal trajectory dynamics,

$$\dot{\underline{x}}_{NOM}(t) = A_N \underline{x}_{NOM}(t) + B_N u_{NOM}(t) \qquad (4.3.7.1)$$

The nominal control $u_{NOM}(t)$ is

$$u_{NOM}(t) = K_{tp}(t)\ \underline{x}_{NOM}(t) \qquad (4.3.7.2)$$

so the closed loop dynamics are

$$\dot{\underline{x}}_{NOM}(t) = (A_N + B_N K_{tp}(t))\ x_{NOM}(t) \qquad (4.3.7.3)$$

76265AW032

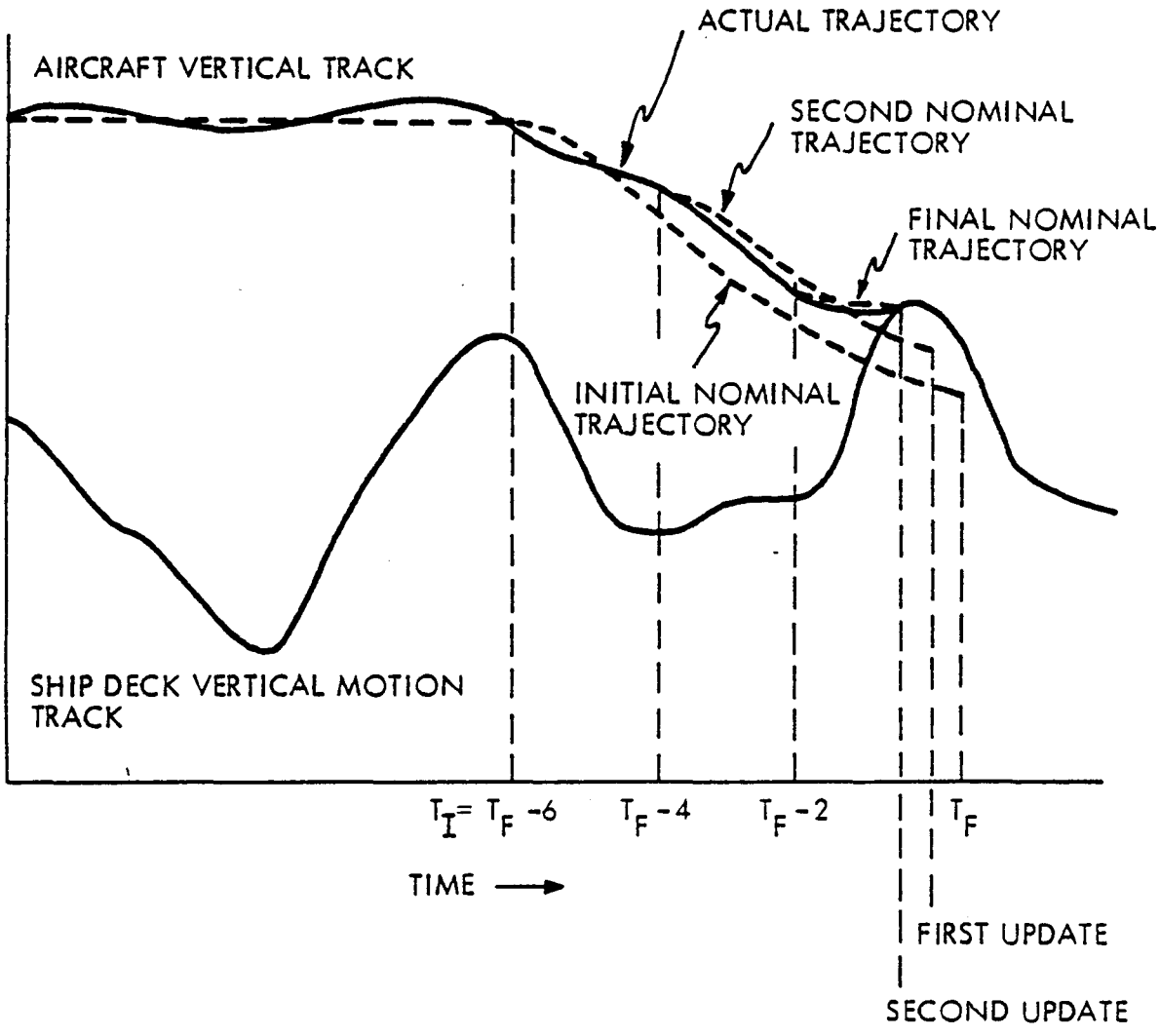

Aircraft and Ship Tracks for Landing Controller Algorithm

Figure 4.3.7.2

where the feedback gain matrix $K_{tp}(t)$ is subscripted to denote that it is determined as a function of the time tp of the predicted ship motion crest. tp is in turn a nonlinear function of the ship and wave initial conditions. Thus, the true trajectory of the aircraft is a nonlinear function of the initial conditions. Secondly, look at the output. This is a vector composed of a linear combination of the system state at the actual time of the touchdown t_A:

$$\underline{z} = H\,\underline{x}(t_A) \qquad (4.3.7.4)$$

t_A is a function of the ship-wave initial condition and its driving noise from the initial time to the landing time. Therefore, $\underline{z}$ is also nonlinear in the initial condition since it depends on $\underline{x}(t)$, which is nonlinear in $\underline{x}_{SHIP}(t_I)$ (through K_{tp} in the nominal trajectory) and on t_A, which is also dependent on $\underline{x}_{SHIP}(t_I)$. Because of these nonlinearities, Monte Carlo simulations are chosen for the evaluation.

4.4 Design Evaluation

As explained above, the landing controller was evaluated by direct Monte Carlo simulations. The following sections discuss its performance under various parameter modifications,and compare its performance with the hover controller of Chapter Three. The last section summarizes the evaluation and comparison results.

4.4.1 Evaluation Parameters

The effects of five parameters on the landing performance were investigated. These were aircraft initial hover height, endpoint and trajectory update rate, nominal trajectory gain shift, update suspension time, and control actuator nominal authority. Table (4.4.1.1) contains the numerical results of the Monte Carlo simulations.

The results for aircraft initial hover heights of 13 and 8 feet above the mean deck height are shown at the top of the table. In this comparison, the update suspension is not implemented. For these heights, the average impact velocity decreases with decreasing height. In addition, the actuator level required decreases by a factor of two.

The decrease in actuator effort is a significant amount and is consistent with the physics of the problem: to displace a mass a long distance in a fixed time, with zero initial and final velocities, requires more effort than to displace it a shorter distance.

The second comparison in Table (4.4.1.1) shows that an increased rate of prediction and trajectory updates has the effect of decreasing impact velocity. This is because updates occur nearer the end time and thus less prediction errors buildup before touchdown. With only an initial prediction and no updates, the impacts have average velocity near 3 feet/second. When updates every 2 seconds are implemented, this velocity is reduced to under 2 feet/second. More frequent updates continue to reduce the impact velocity. At a rate of one update every 0.2 second, the velocity is 1.6 feet/second. Again, this evaluation does not include the update suspension feature.

Evaluation: The Effects of Five Parameters on Landing Performance

Simulation Results for	Initial Hover Height (Feet)	Update Period (Seconds)	Nominal Trajectory Gain Shift (Seconds)	Update Suspension Before Predicted End Time (Seconds)	Control Actuator Nominal Authority (Percent Nominal)	Average Impact Velocity (Feet/ Second)	Standard Deviation of Velocity (Feet/ Second)	Maximum Actuator Effort (Percent Nominal)	Number of Simulations	Better
Initial Hover Height	- 8	0.5	5.0	0.0	3.0	1.45	0.36	2.6	8	↑
	-13					1.70	0.44	5.3	10	
Update Period	-13	0.2				1.63	0.43	5.5	10	↑
		0.5				1.70	0.44	5.3	10	
		2.0				1.82	0.97	4.2	8	
		12.0				2.78	2.01	6.4	10	
Nominal Trajectory Gain Shift		0.2	5.0	2.0		1.98	0.66	4.8	11	?
			0.0			1.53	1.69	6.0	7	
			5.0	0.0		1.63	0.43	5.5	10	?
			0.0			1.02	0.71	6.2	11	
Update Suspension			5.0	2.0		1.98	0.66	0.48	11	↓
				0.0		1.63	0.43	5.5	10	
			0.0	2.0		1.53	1.69	6.0	7	↓
				0.0		1.02	0.71	6.2	11	
Control Actuator Nominal Authority		0.5	5.0	0.0	3.0	1.70	0.44	-5.3	8	↑
					50.0	1.93	0.75	-15.5	10	

TABLE 4.4.1.1

Nominal trajectory gain shifts of 5 and zero seconds are compared next, with and without update suspension. The results show that without a gain shift, the average impact velocity is lowest but the variation of impact velocity about the mean is large. This tradeoff between average performance and variation about the average is independent of update suspension.

Update suspension before the predicted end time yields higher impact velocities than no update suspension does, whether or not nominal trajectory gains are shifted. However, in this comparison shifted gains do reduce the required maximum actuator effort.

The final comparison in Table (4.4.1.1) shows that control actuator nominal authority limitation reduces actuator excursions and the average aircraft-ship impact velocity. The actuator excursion reduction is especially significant. Further reductions appear possible if the nominal trajectory control sequence is assessed at each update rather than at the initial time only.

The set of landing controller parameters, which yielded the lowest impact velocities during the evaluation simulations, are as follows:

initial height	-13.0 feet
update period	0.2 seconds
nominal trajectory gain shift	0.0 seconds
update suspension interval before the predicted time	0.0 seconds
control actuator nominal authority	3.0% of nominal

For this set of parameters, the average impact velocity was about 1.0 feet/second with a standard deviation of about 0.7 feet/second. These

statistics were computed from eleven Monte Carlo simulations. During these eleven simulations, the maximum negative actuator effort was -6.2 percent of nominal. (Note, that the maximum negative value is of interest since this represents a total thrust exceeding the hover level. Positive actuator effort represents a reduction in overall thrust.)

Figure (4.4.1.1) shows time histories of a typical landing using the above controller parameter values. The results obtained are the following:

relative aircraft-ship impact velocity	1.3 feet/second
vertical aircraft velocity	-0.3 feet/second
vertical ship velocity	-1.6 feet/second
vertical ship position	-5.9 feet
maximum actuator effort employed	2.9% of nominal

An examination of the timing and height prediction errors made on the final update before touchdown reveals that landings occur earlier and at more elevated positions than predicted. Figure (4.4.1.2) displays the experimental distribution of errors obtained from eleven simulations using the same controller as in the sample landing above. The figure shows that landings occurred between 0.2 and 0.7 seconds earlier and between 0.0 and 0.8 feet higher than the final predictions made before the touchdowns. These timing errors agree qualitatively with those calculated in the analysis of Section (4.3.2), although they are significantly larger. It is likely that this discrepancy is attributable to the simplifying assumptions and approximations made in the analysis.

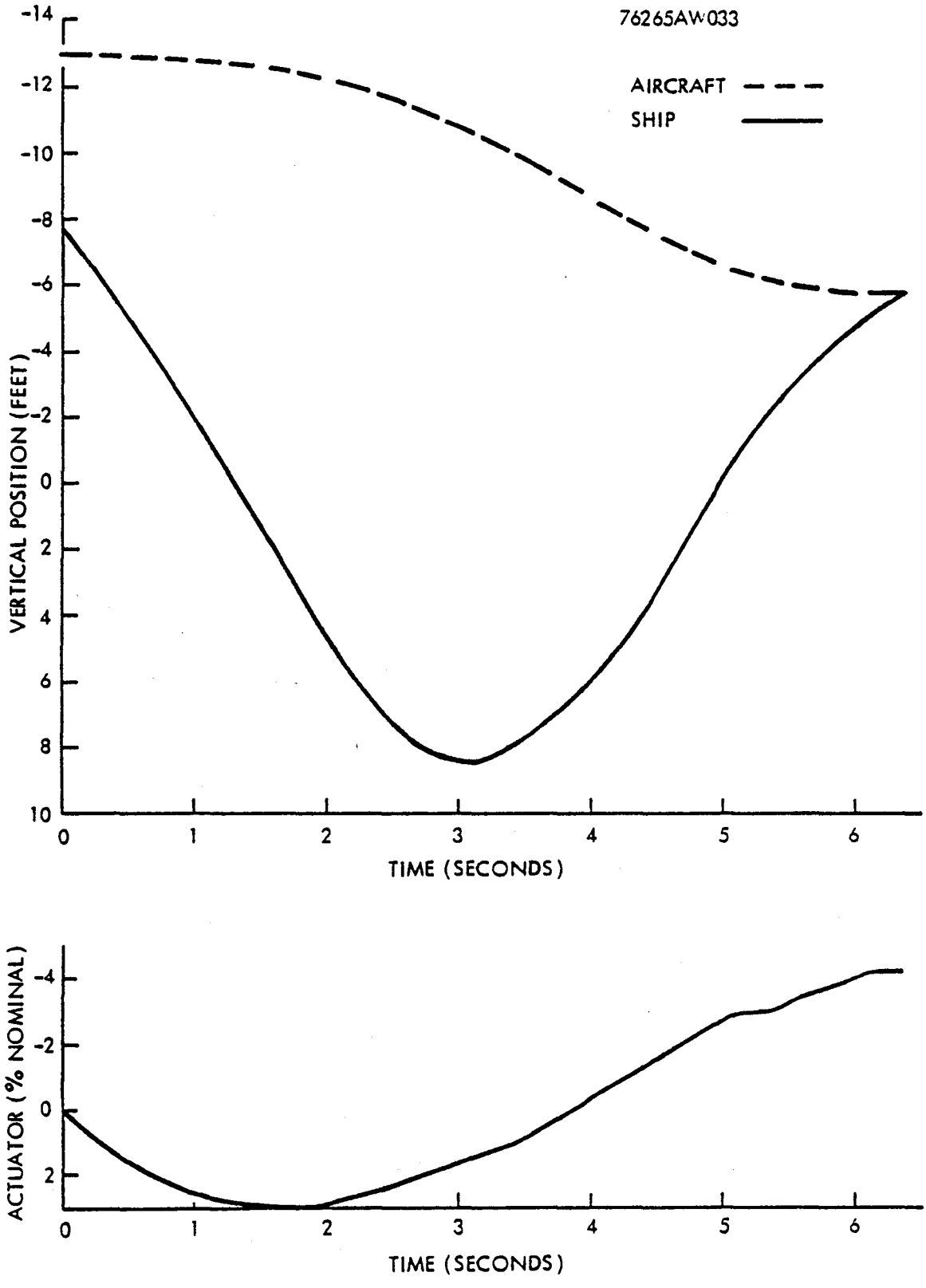

Typical Shipboard Landing Simulation Using Best Design Parameters

Figure 4.4.1.1

76265AW034

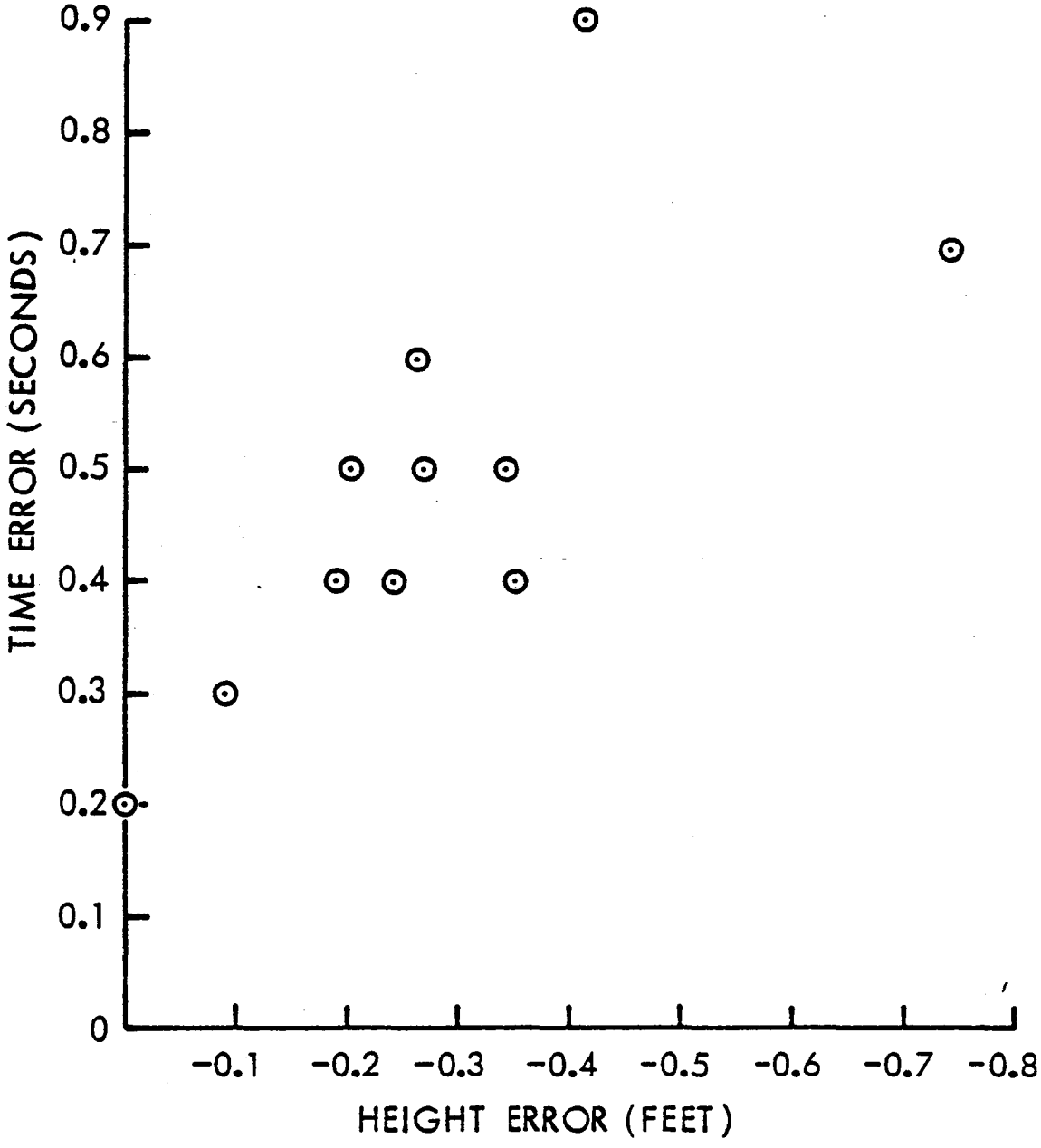

Touchdown Error Distribution for 11 Simulations Using Best Design Parameters

Figure 4.4.1.2

4.4.2 Comparison with the Hover Controller

The results for the landing controller indicate better performance than the hover controller. Using the best set of parameters as indicated in the previous section, the landing algorithm yields an average touchdown velocity of about 1.0 feet/second, whereas the hover controller, which uses the same control actuator effort, yields an average touchdown velocity of about 1.8 feet/second. Alternatively, to obtain the same average impact velocity as the landing controller, the hover controller must use about twice as much control authority as the landing controller.

This comparison does not take into account the practical considerations required for implementation. These additional considerations also favor the landing controller since it requires less ship motion data and actually computes the controls necessary to bring the aircraft from stationary hover, along a nominal trajectory, to a shipboard landing.

The comparison is presented graphically in Figure (4.4.2.1). The figure shows the distribution of impact velocity and extreme negative excursions of the vertical control actuator (in terms of thrust to weight ratio) obtained for the simulations. For comparison with the hover controller, the figure includes the mean and one rms bands for the hover controller impact velocity. The computation of the mean and standard deviation for the hover controller is described below.

Aircraft-ship touchdown only occurs when the relative separation $z_{A-S}(t)$ is zero and the relative velocity $\dot{z}_{A-S}(t)$ is positive. For

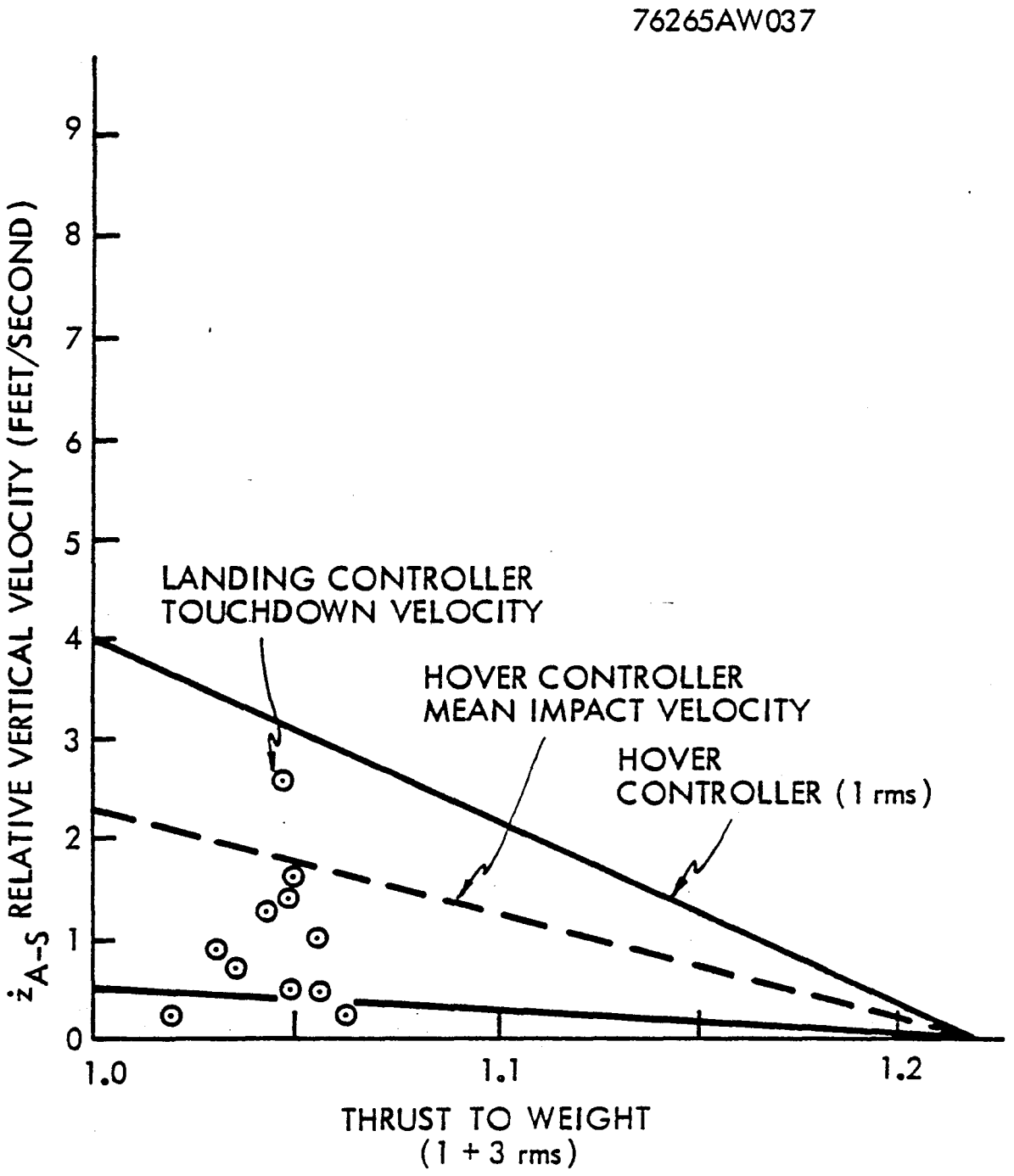

Controller performance comparison: Hover Controller versus Landing Controller

Figure 4.4.2.1

the hover controller these quantities are stationary, independent gaussian random processes with zero means, and standard deviations $\sigma_{z_{A-S}}$ and $\sigma_{\dot{z}_{A-S}}$, respectively. (In figure (3.4.3.2), the three-sigma values are plotted as functions of thrust to weight.) The expected touchdown velocity is given by:

$$E\{\dot{z}_{A-S}(t) \mid z_{A-S}(t) = 0,\ \dot{z}_{A-S}(t) \geq 0\} \tag{4.4.2.1}$$

but the distributions of $z_{A-S}(t)$ and $\dot{z}_{A-S}(t)$ are independent of time, and also statistically independent of each other, so the expectation reduces to:

$$E\{\dot{z}_{A-S} \mid \dot{z}_{A-S} \geq 0\} \tag{4.4.2.2}$$

The probability density function for the velocity $v = \dot{z}_{A-S}$ is:

$$P_v(V) = (1/\sqrt{2\pi})(1/\sigma_v)\ \exp\{-\tfrac{1}{2}(V/\sigma_v)^2\} \tag{4.4.2.3}$$

for $-\infty < V < \infty$. Hence, the conditional density is:

$$P_{v|v \geq 0}(V|V \geq 0) = (\sqrt{2/\pi})(1/\sigma_v)\ \exp\{-\tfrac{1}{2}(V/\sigma_v)^2\} \tag{4.4.2.4}$$

for $0 \leq V < \infty$. The resulting mean and standard deviation of the impact velocity are:

$$E\{\dot{z}_{A-S} \mid \dot{z}_{A-S} \geq 0\} = (\sqrt{2/\pi})\,\sigma_{\dot{z}_{A-S}} \tag{4.4.2.5}$$

$$(\mathrm{Var}\{\dot{z}_{A-S} \mid \dot{z}_{A-S} \geq 0\})^{1/2} = (\sqrt{1-2/\pi})\sigma_{\dot{z}_{A-S}} \tag{4.4.2.6}$$

Using the conversion between $\sigma_{\dot{z}_{A-S}}$ and thrust to weight available from Figure (3.4.3.2), this mean and standard deviation are plotted in Figure (4.4.2.1) for comparison with the landing controller simulation results.

4.4.3 Conclusions

The goal of the landing controller was to decrease the thrust to weight ratio required to attain low aircraft-ship relative touchdown velocities compared to the value required by the tracking hover controller. This goal was achieved in Monte Carlo simulations of the controller.

The landing controller achieved touchdown velocities near one foot/second. These were obtained with a 0.2 second sampling rate and a thrust to weight control authority approximately half the magnitude required by the hover controller yielding the same average impact velocity. The extreme values of thrust to weight were 5 or 6 percent above the stationary hover value of 1.0. High initial hover positions required higher thrust to weight ratios. The nominal trajectory gain shift did not yield the expected softer landings that the earlier nominal trajectory analysis predict. Similarly, update suspension before touchdown did not reduce impact velocity or thrust to weight requirements. Finally, control acutator nominal authority limitation proved to be beneficial by significantly reducing the control levels used.

These observations indicate that the best performing landing controller is one using unshifted nominal trajectory gains, no update suspension, minimum safe initial hover height and update rates of 5 per second or higher.

The biases between the actual and predicted touchdown itmes and heights that were found analytically and also observed in the simulations, result in significant touchdown velocities.

Unlike the hover controller, the landing controller performance is not necessarily the "best" possible. Other landing algorithms may yield better performance, either by using lower control power or obtaining lower touchdown velocities. This is because the landing controller algorithm is only an approximate solution of its defining optimization problem in Section (4.2.1). On the other hand, physical implementation of the algorithm probably would not perform as well as the simulation results indicate, since the simulations were based on idealistic modelling assumptions. In this sense, the landing controller results presented in this chapter can still be viewed as lower performance limits for VTOL systems.

CHAPTER 5

CONCLUSIONS

5.1 Introduction

The primary objective of this research has been to design a shipboard landing controller for a hovering VTOL aircraft. The major problems faced in such a landing, especially aboard a small ship in heavy seas, are the limited control authority and the severe ship motions. When these difficulties are overcome, VTOL operations from small ships will be considerably closer to realization than they are currently. The results of this research are basic performance characteristics and requirements for VTOL controllers. They are not intended as detailed engineering designs.

5.2 Achievements

Aircraft dynamics, wave motions, and ship motion were modelled. The resulting overall model was then used in the design and analysis of the hover and landing controllers. The hover controller demonstrates that good shipboard landing performance is possible. The landing controller exhibits similar performance levels, but with reduced control power requirements.

The aircraft considered is a representative lift/cruise fan VTOL modelled near stationary hover. Each of the six degrees of freedom associated with the rigid vehicle motion are controlled by a separate actuator with assumed first order dynamics. Aerodynamics were not modelled. However, the model is structured to accommodate changes and

additions such as aerodynamics for future studies. Sea state five ocean wave conditions were modelled as shaped white noise with a theoretical Neumann spectrum, modified to account for ship speed and heading. The ship itself is a small destroyer of 400 foot length. Its pitch and heave, and roll motions are driven by two identical, but independent wave models. Each of the three motion responses was modelled as a second order system, with parameters estimated from available frequency response data of similar ships.

Two VTOL control concepts were designed and analyzed. The first is a "hover controller", which commands the vehicle to track ship landing pad motions with small control actuator thrust levels. A steady state linear quadratic regulator design was used for this controller. The tracking errors, control effort, and required sensor bandwidth were determined analytically. For 3 rms tracking errors on the order of one foot, thrust to weight ratios near 1.2 are required by this controller. These results represent ultimate (lower) performance bounds, since not all the dynamics, disturbances, and measurement constraints are accounted for. The second design is a "landing controller". Its goals are to land the vehicle onboard the ship with a low touchdown velocity and small control thrust levels. The "landing controller" commands the aircraft from stationary hover along a smooth, low control effort trajectory, to a touchdown on a predicted crest of ship motion. Performance analysis was by Monte Carlo simulations since the overall system is nonlinear; and hence, incompatible with linear covariance analyses. The effect of five algorithm parameters were studied. With "optimized" parameters,

the landing controller uses about a half of the control authority required by the hover controller, which has comparable touchdown velocities. For average touchdown velocities of one foot per second, the thrust level requirements are about six percent of the nominal hover amount. These landing controller results are subject to the same performance bound interpretation as the hover controller results since the same aircraft-wave-ship system model assumptions were used.

5.3 Further Research

As this work stands, several open questions remain. These concern the influence of the following:

(1) the inclusion of full longitudinal and lateral dynamics,

(2) noisy and incomplete sensor measurements,

(3) human piloting considerations,

(4) ship and ocean conditions,

(5) aerodynamic disturbances, and

(6) ground effects.

The first of these is of considerable interest in the light of the low levels of lateral control that have been displayed by VTOL aircraft, which limits their maneuverability (31). The influence of sensor measurements should be examined, since it is improbable that all system states will be available for feedback. Particularly, it is improbable that wave states can be measured. Therefore, the problem of predicting ship motion based only on practical measurements is an important research question. Pilot dynamics representing human tracking

of ship motion or of a commanded trajectory can be incorporated into the overall model. A comparison of the subsequent results with those obtained here would indicate the performance degredation associated with inserting a pilot into the loops of the automatic hover and landing controllers. It was found in the hover controller performance analysis, that ship motion has a strong effect on performance. Hence a parametric study of controller performance versus different ship types, speeds, headings, and sea states could yield useful guidelines for controller design and general operating procedures for VTOLs at sea. Aerodynamic forces and moments on the aircraft are unlikely to be negligible at the high wind speeds crossing the ship deck. As a result, their effects should be evaluated. VTOL vehicles are also susceptible to ground effects such as fountain and suck-down phenomena. In the past, these have not been reliably predicted (4). However, by making a simple model of the force and moment magnitudes they exert on the aircraft as a function of, say, aircraft to landing deck separation and orientation, helpful parametric information relating controller requirements to ground effect magnitude may be obtained. A study of this effect is strongly recommended, since it is critical to VTOL aircraft operating in ground proximity.

This work has laid a foundation for these studies. A versatile model and promising modern control design and analysis approach have been developed for shipboard landing of VTOL aircraft. From this point, more accurate and more complete models may be used with the same design and analysis techniques, or better performing control algorithms may be

developed, analyzed and compared with the current model and results established in this report.

APPENDIX 2.4.3.1

MATRICES USED IN THE AIRCRAFT MODELLING

$$
C_B^E = \begin{vmatrix} \cos\theta\cos\psi & -\cos\phi\sin\psi + \sin\phi\sin\theta\cos\psi & \sin\phi\sin\psi + \cos\phi\sin\theta\cos\psi \\ \cos\theta\sin\psi & \cos\phi\cos\psi + \sin\phi\sin\theta\sin\psi & -\sin\phi\cos\psi + \cos\phi\sin\theta\sin\psi \\ -\sin\theta & \sin\phi\cos\theta & \cos\theta\cos\phi \end{vmatrix}
$$

at nominal $\phi\ \theta\ \psi$

$$
= \begin{vmatrix} 1 & 0 & 0 \\ 0 & 1 & 0 \\ 0 & 0 & 1 \end{vmatrix}
$$

$$T_{\theta}^{F} = \left| \frac{\partial C_B^E}{\partial \psi} C_E^B G_V \right| \left| \frac{\partial C_B^E}{\partial \theta} C_E^B G_V \right| \left| \frac{\partial C_B^E}{\partial \phi} C_E^B G_V \right|_{\text{nominal orientation}}$$

$$G_V = \begin{pmatrix} 0 & 0 & -gm \end{pmatrix}^T$$

$$\frac{\partial C_B^E}{\partial \psi} = \begin{vmatrix} 0 & -1 & 0 \\ 1 & 0 & 0 \\ 0 & 0 & 0 \end{vmatrix}$$

$$\frac{\partial C_B^E}{\partial \theta} = \begin{vmatrix} 0 & 0 & 1 \\ 0 & 0 & 0 \\ -1 & 0 & 0 \end{vmatrix}$$

$$\frac{\partial C_B^E}{\partial \phi} = \begin{vmatrix} 0 & 0 & 0 \\ 0 & 0 & -1 \\ 0 & 1 & 0 \end{vmatrix}$$

$$C_E^B = \begin{vmatrix} 1 & 0 & 0 \\ 0 & 1 & 0 \\ 0 & 0 & 1 \end{vmatrix}$$

$$G_V = \begin{bmatrix} 0 & 0 & -27500.0 \end{bmatrix}^T$$

$$T_\omega^F = \begin{vmatrix} 0 & X_q & 0 \\ Y_p & 0 & Y_r \\ 0 & Z_q & 0 \end{vmatrix}$$ nominal engine and fan mass flow rate

$$T_V^F = \begin{vmatrix} X_u & 0 & 0 \\ 0 & Y_v & 0 \\ 0 & 0 & Z_w \end{vmatrix}$$ nominal

$$T_\omega^M = \begin{vmatrix} L_p & 0 & L_r \\ 0 & M_q & 0 \\ N_p & 0 & N_r \end{vmatrix}$$ nominal

$$T_V^M = \begin{vmatrix} 0 & L_v & 0 \\ M_u & 0 & M_w \\ 0 & N_v & 0 \end{vmatrix}$$ nominal

$$T_{\omega}^{F} = \begin{vmatrix} 0 & 44.43 & 0 \\ -44.43 & 0 & -334.557 \\ 0 & 334.557 & 0 \end{vmatrix}$$

$$T_{V}^{F} = \begin{vmatrix} -56.3 & 0 & 0 \\ 0 & -56.3 & 0 \\ 0 & 0 & -56.3 \end{vmatrix}$$

$$T_{\omega}^{M} = \begin{vmatrix} -2193.0 & 0 & -496.0 \\ 0 & -7673.3097 & 0 \\ -496.0 & 0 & -9777.6188 \end{vmatrix}$$

$$T_{V}^{M} = \begin{vmatrix} 0 & -44.43 & 0 \\ 44.43 & 0 & 334.557 \\ 0 & -334.557 & 0 \end{vmatrix}$$

$$I_M = \left| \begin{array}{ccc} I_Z/I_1 & 0 & I_{XZ}/I_1 \\ 0 & 1/I_Y & 0 \\ I_{XZ}/I_1 & 0 & I_X/I_1 \end{array} \right|$$

nominal weight, fan, and engine rates

$$I_A = \left| \begin{array}{ccc} 0 & (I_{XZ}I_{\Omega X} - I_Z I_{\Omega Z})/I_1 & 0 \\ -I_{\Omega Z}/I_Y & 0 & -I_{\Omega X}/I_Y \\ 0 & (I_X I_{\Omega X} - I_{XZ} I_{\Omega Z})/I_1 & 0 \end{array} \right|$$

nominal

$$I_M = \left| \begin{array}{ccc} 4.62911 \times 10^{-5} & 0 & 1.95333 \times 10^{-6} \\ 0 & 1.8595 \times 10^{-5} & 0 \\ 1.95333 \times 10^{-6} & 0 & 1.49462 \times 10^{-5} \end{array} \right|$$

$$I_A = \left| \begin{array}{ccc} 0 & -0.1255 & 0 \\ 0.0944 & 0 & 0.1041 \\ 0 & 0.8273 & 0 \end{array} \right|$$

$$T_{\omega}^{\theta} = \begin{vmatrix} 0 & 0 & \sec\theta \\ 0 & 1 & 0 \\ 1 & 0 & \tan\theta \end{vmatrix}$$

$$= \begin{vmatrix} 0 & 0 & 1 \\ 0 & 1 & 0 \\ 1 & 0 & 0 \end{vmatrix}$$

$$A_U = \begin{vmatrix} -\lambda_x & 0 & 0 & 0 & 0 & 0 \\ 0 & -\lambda_y & 0 & 0 & 0 & 0 \\ 0 & 0 & -\lambda_z & 0 & 0 & 0 \\ 0 & 0 & 0 & -\lambda_\phi & 0 & 0 \\ 0 & 0 & 0 & 0 & -\lambda_\theta & 0 \\ 0 & 0 & 0 & 0 & 0 & -\lambda_\psi \end{vmatrix}$$

$$= 0_{6x6}$$

$$B_T = \begin{vmatrix} 0 & \alpha_Y & 0 & 0 & 0 & \alpha_\psi \\ 0 & \alpha_Y & 0 & 0 & 0 & \alpha_\psi \\ 0 & \alpha_Y & 0 & 0 & 0 & \alpha_{\psi 3} \\ \theta_X & 0 & 0 & 0 & 0 & 0 \\ \theta_X & 0 & 0 & 0 & 0 & 0 \\ \theta_X & 0 & 0 & 0 & 0 & 0 \\ 0 & 0 & -F_{GV} & F_{GR} & -F_{GP} & 0 \\ 0 & 0 & -F_{GV} & -F_{GR} & -F_{GP} & 0 \\ 0 & 0 & -F_{GV3} & 0 & F_{GP3} & 0 \end{vmatrix}$$

$$= \begin{vmatrix} 0 & -1 & 0 & 0 & 0 & 1 \\ 0 & -1 & 0 & 0 & 0 & 1 \\ 0 & -1 & 0 & 0 & 0 & -1.9302 \\ -1 & 0 & 0 & 0 & 0 & 0 \\ -1 & 0 & 0 & 0 & 0 & 0 \\ -1 & 0 & 0 & 0 & 0 & 0 \\ 0 & 0 & -9057.5 & 9057.5 & -9057.5 & 0 \\ 0 & 0 & -9057.5 & -9057.5 & -9057.5 & 0 \\ 0 & 0 & -9385.1 & 0 & 18114.9 & 0 \end{vmatrix}$$

$$B_F = \begin{vmatrix} 0 & 0 & 0 & -F_{GN1}\cos\theta & 0 & 0 & \sin\theta & 0 & 0 \\ 0 & 0 & 0 & 0 & -F_{GN2}\cos\theta & 0 & 0 & \sin\theta & 0 \\ 0 & 0 & 0 & 0 & 0 & -F_{GN3}\cos\theta & 0 & 0 & \sin\theta \\ F_{GN1} & 0 & 0 & 0 & 0 & 0 & 0 & 0 & 0 \\ 0 & F_{GN2} & 0 & 0 & 0 & 0 & 0 & 0 & 0 \\ 0 & 0 & F_{GN3} & 0 & 0 & 0 & 0 & 0 & 0 \\ 0 & 0 & 0 & -F_{GN1}\sin\theta & 0 & 0 & -\sin\theta & 0 & 0 \\ 0 & 0 & 0 & 0 & -F_{GN2}\sin\theta & 0 & 0 & -\sin\theta & 0 \\ 0 & 0 & 0 & 0 & 0 & -F_{GN3}\sin\theta & 0 & 0 & -\sin\theta \end{vmatrix}$$

$$= \begin{vmatrix} 0 & 0 & 0 & -9057.5 & 0 & 0 & 0 & 0 & 0 \\ 0 & 0 & 0 & 0 & -9057.5 & 0 & 0 & 0 & 0 \\ 0 & 0 & 0 & 0 & 0 & -9381.1 & 0 & 0 & 0 \\ -9057.5 & 0 & 0 & 0 & 0 & 0 & 0 & 0 & 0 \\ 0 & -9057.5 & 0 & 0 & 0 & 0 & 0 & 0 & 0 \\ 0 & 0 & -9057.5 & 0 & 0 & 0 & 0 & 0 & 0 \\ 0 & 0 & 0 & 0 & 0 & 0 & -1 & 0 & 0 \\ 0 & 0 & 0 & 0 & 0 & 0 & 0 & -1 & 0 \\ 0 & 0 & 0 & 0 & 0 & 0 & 0 & 0 & -1 \end{vmatrix}$$

$$T_F^F = \begin{vmatrix} 1\,1\,1 & 0\,0\,0 & 0\,0\,0 \\ 0\,0\,0 & 1\,1\,1 & 0\,0\,0 \\ 0\,0\,0 & 0\,0\,0 & 1\,1\,1 \end{vmatrix}$$

$$T_F^M = \begin{vmatrix} 0 & 0 & 0 & -Z_{TLC} & -Z_{TLC} & Z_{TL} & -Y_{TLC} & Y_{TLC} & 0 \\ Z_{TLC} & Z_{TLC} & Z_{TL} & 0 & 0 & 0 & -X_{TLC} & -X_{TLC} & -X_{TL} \\ Y_{TLC} & -Y_{TLC} & 0 & X_{TLC} & X_{TLC} & X_{TL} & 0 & 0 & 0 \end{vmatrix}$$

$$= \begin{vmatrix} 0 & 0 & 0 & -3.1200 & -3.1200 & -3.7400 & -5.4800 & 5.4800 & 0 \\ 3.1200 & 3.1200 & 3.7400 & 0 & 0 & 0 & 10.170 & 10.170 & -19.630 \\ 5.4800 & -5.4800 & 0 & -10.1700 & -10.1700 & 19.630 & 0 & 0 & 0 \end{vmatrix}$$

APPENDIX 2.4.3.2

DERIVATION OF RAM DRAG FORCE AND MOMENT EXPRESSIONS

Ram drag forces and moments are those caused by the change in linear momentum given to the air flow at fan and engine inlets because the aircraft is translating and rotating. (The momentum change due to acceleration of air in the fans that generate nominal control thrusts is accounted for in the rigid body dynamical equations.) Below, a short derivation of the ram drag force and moment equation is given. Note that these equations are for the forces and moments $\underline{f}_{RBF}$ and $\underline{m}_{RBF}$ acting on the air. The complementary ones $\underline{f}_{RB}$ and $\underline{m}_{RB}$ acting on the aircraft are in the opposite directions. The final equations are summarized first.

$$-\underline{f}_{RB} = \underline{f}_{RBF} = \dot{M}_R \underline{v}_B - \dot{M}_R \underline{R}_{cm}^{\cdot} \times \underline{\omega}_B \qquad \text{(A2.4.3.2.1)}$$

$$-\underline{m}_{RB} = \underline{m}_{RBF} = \dot{M}_R \underline{R}_{cm} \times \underline{v}_B + \dot{I}_M \underline{\omega}_B \qquad \text{(A2.4.3.2.2)}$$

where $\dot{M}_R = \sum_i \dot{m}_i$; $\quad \underline{R}_{cm}^{\cdot} = \sum_i \dot{m}_i \underline{r}_i / \dot{M}_R$

$$\dot{I}_M = \sum_i \dot{m}_i \begin{vmatrix} (r_{yi}^2 + r_{zi}^2) & -r_{xi}r_{yi} & -r_{xi}r_{zi} \\ -r_{yi}r_{xi} & (r_{xi}^2 + r_{zi}^2) & -r_{yi}r_{zi} \\ -r_{zi}r_{xi} & -r_{zi}r_{yi} & (r_{xi}^2 + r_{yi}^2) \end{vmatrix}$$

In these equations, $\dot{m}_i$ is the airmass flow through fan or engine i and

and $\underline{r}_i$ is the position of that fan or engine inlet with respect to the aircraft center of mass.

To begin the ram drag force derivation, Newton's Law (or the principle of linear momentum conservation) is written in the earth frame for a mass m_i:

$$\underline{f}_{Ei} = \frac{d}{dt}\underline{P}_{Ei} = \frac{d}{dt}(m_i\underline{v}_{Ei}) = \dot{m}_i\underline{v}_{Ei} + m_i\dot{\underline{v}}_{Ei} \qquad \text{(A2.4.3.2.3)}$$

For a rigid body, $\dot{m}_i = 0$; however, the engines and fans are not rigid bodies since there is mass flow $\dot{m}$ through them. (The rotating parts are considered as contributing internal angular momentum in the aircraft moment equation.) The $\dot{m}_i\underline{v}_{Ei}$ term is nonzero and is refered to as the ram drag force.

$$\underline{f}_{REFi} = \dot{m}_i\underline{v}_{Ei} \qquad \text{(A2.4.3.2.4)}$$

This is the expression used for the ith fan or engine inlet. In body coordinates, were $\underline{r}_i$ is the location of the ith inlet, the force is:

$$\underline{f}_{RBFi} = \dot{m}_i(\underline{v}_B + \underline{\omega}_B \times \underline{r}_i) \qquad \text{(A2.4.3.2.5)}$$

Summing over all the inlets gives equation (A2.4.3.2.1) again:

$$\underline{f}_{RBF} = \dot{M}_R\underline{v}_B - \dot{M}_R\dot{\underline{R}}_{cm} \times \underline{\omega}_B \qquad \text{(A2.4.3.2.6)}$$

The conservation of angular momentum can also take into account the air mass flows. A torque or moment $\underline{m}_i$ on a small mass m_i at distance $\underline{r}_i$ from the center of rotation (assumed to be the center of mass here) is

related to the rate of change of the particle's linear momentum by:

$$\underline{m}_{E_i} = \underline{r}_{E_i} \times \frac{d\underline{p}_E}{dt}_i \qquad \text{(A2.4.3.2.7)}$$

The ram drag component of $d\underline{p}_{E_i}/dt$ is again $\dot{m}_i \underline{v}_{E_i}$. Thus for the air inlet i:

$$\underline{m}_{RBFi} = \underline{r}_{Bi} \times m_i(\underline{v}_B + \underline{\omega}_B \times \underline{r}_i) \qquad \text{(A2.4.3.2.8)}$$

Summing over all the inlets gives

$$\underline{m}_{RBF} = M_R \underline{R}_{cm} \times \underline{v}_B + \sum_i \dot{m}_i \underline{r}_i \times (\underline{\omega}_B \times \underline{r}_i) \qquad \text{(A2.4.3.2.9)}$$

or introducing $\dot{I}_M$:

$$\underline{m}_{RBF} = \dot{M}_R \underline{R}_{cm} \times \underline{v}_B + \dot{I}_M \underline{\omega}_B \qquad \text{(A2.4.3.2.10)}$$

which is the last of the two equations describing ram drag effects, equation (A2.4.3.2.2).

Although, in general, the $\dot{m}_i$ are time varying, they are considered constant in the aircraft model.

REFERENCES

1. Anderson, S.B., and Petersen, R.H., "How Good is Jet Lift VTOL Technology?", Astronautics and Aeronautics, Vol 15, #12, December 1977, pp. 38-42.

2. Deckert, W.H., "Moving V/STOL from Technology to System", Astronautics and Aeronautics, Vol 15, #12, December, 1977, pp. 26-27.

3. Few, D.D. and Edenborough, H.K., "Tilt-Proprotor Perspective", Astronautics and Aeronautics, Vol 15, #12, December, 1977, pp. 28-31.

4. Quigley, H.C., and Franklin, J.A., "Lift/Cruise Fan VTOL Aircraft", Astronautics and Aeronautics, Vol 15, #12, December 1977, pp. 32-37.

5. Roberts, L., and Anderson, S.B., "Toward a New V/STOL Generation", Astronautics and Aeronautics, Vol 15, #11, November, 1977, pp. 22-27.

6. American Institute of Aeronautics and Astronautics, AIAA/NASA Ames V/STOL Conference, Palo Alto, Calif., June, 1977: A Collection of Papers, American Institute of Aeronautics and Astronautics, 1977.

7. Merrick, V.K., and Gerdes, R.M., "Design and Evaluation of an Integrated Flight-Control System Concept for Manual IFR VTOL Operations", AIAA/NASA Ames V/STOL Conference, Palo Alto, Calif., June, 1977, Paper 77-601, 1977.

8. Bland, M.P., Fajar, B., and Konsewicz, R.K., "Mathematical Model for Lift/Cruise Fan V/STOL Aircraft Simulator Programming Data", NASA CR-151916, 1976.

9. Etkin, B., Dynamics of Atmospheric Flight, John Wiley and Sons, 1972.

10. Comstock, J.P., (Editor), Principles of Naval Architecture, (Revised Edition), The Society of Naval Architects and Marine Engineers, 1967.

11. Hoffman, D., "Analysis of Measured and Calculated Spectra", in: The Dynamics of Marine Vehicles and Structures in Waves, (Edited by Bishop, R.E.D., and Price, W.G.), Mechanical Engineering Publications, Ltd., London, 1975, pp. 8-18.

12. Dalgell, J., (Chairman), "Report of the Seakeeping Committee" in: 14th International Towing Tank Conference Proceedings, National Research Council of Canada, Vol 4, 1975.

13. Hildebrand, F.B., Advanced Calculus for Applications (Second Edition), Prentice-Hall, 1976.

14. Skelton, G.B., "Investigation of the Effects of Gusts on V/STOL Craft in Transition and Hover", AFFDL-TR-68-85, 1968.

15. Blackman, R.V.B., (Editor), Jane's Fighting Ships: 1957-58, Jane's Fighting Ships Publishing Co., Ltd., 1957.

16. St. Dennis, M., and Pierson, W.J., "On the Motions of Ships in Confused Seas", Transactions of the Society of Naval Architects and Marine Engineers, Vol 61, 1953, pp. 280-357.

17. Lewis, E.V., and Dalzell, J.F., "Motion, Bending Moment and Shear Measurements on a Destroyer Model in Waves", Stevens Institute of Technology Experimental Towing Tank, Report 656, 1958.

18. Wachnik, Z.G., and Zarnick, E.E., "Ship Motions Prediction in Realistic Short-Crested Seas", Transactions of the Society of Naval Architects and Marine Engineers, Vol 73, 1965, pp. 100-134.

19. Gawn, R.W.L., "Rolling Experiments with Ships and Models in Still Water", Transactions of the Institution of Naval Architects, Vol LXXXII, 1940, pp. 44-68.

20. Salvesen, N., Tuck, E.O., and Faltensen, O., "Ship Motions and Sea Loads", Transactions of the Society of Naval Architects and Marine Engineers, Vol 78, 1970, pp. 250-287.

21. Cartwright, D.E. and Rydill, L.J., "The Rolling and Pitching of a Ship at Sea: A Direct Comparison Between Calculated and Recorded Motions of a Ship in Sea Waves", Transactions of the Institution of Naval Architects, 1957, pp. 100-135.

22. Keane, W., and Usechak, D., "Simulation of Helicopter Containership Loading", United States Army Electronics Command, ECOM-4062, 1973.

23. Kwakernaak, H., and Sivan, R., Linear Optimal Control Systems, John Wiley and Sons, 1972.

24. Bryson, A.E., Jr., and Ho. Y.-C., Applied Optimal Control, Halsted Press, 1975.

25. Gelb, A., Applied Optimal Estimation, MIT Press, 1974.

26. Selby, S.M., (Editor), CRC Standard Mathematical Tables, (Twenty-First Edition), The Chemical Rubber Co., 1973.

27. Aiken, E.W., Personal communication, February, 1979.

28. Greif, R.K., Personal communication, February 1979.

29. Athans, M., and Falb, P.L., Optimal Control, McGraw-Hill, 1966.

30. Bracewell, R., The Fourier Transform and its Applications, McGraw-Hill, 1965.

31. Anderson, S.B.,"A Review of the Importance of Stability and Control in Aircraft Safety", a seminar at the Laboratory for Information and Decision Systems, Massachusetts Institute of Technology, October 1978.

End of Document